



The
University
Of
Sheffield.

Metabolite analysis of *Escherichia coli* in response to changes in oxygen levels

**A thesis submitted in part fulfilment for the degree of
Doctor of Philosophy.**

**Department of Molecular Biology and Biotechnology,
The University of Sheffield.**

Nur Adeela binti Yasid

September 2013

Abstract

E. coli is a versatile bacterium that has three metabolic modes: aerobic, anaerobic and fermentation. The major environmental factor that controls the switching between these metabolic modes is oxygen availability. *E. coli* in the intestinal tract is completely anaerobic but certain parts of the intestinal tract close to the gut are microaerobic. The change from anaerobic to aerobic or microaerobic is very rapid and leads to major metabolic change. The changes have been characterized by using NMR. A quenching technique has been developed by using ethanol/NaCl to cool the cells very rapidly after removal from the chemostat to inactivate the metabolic activity. The measurement error from most sources is small with acceptable error from extraction of intracellular metabolites. The technique is being used to studying the transition from anaerobic to aerobic at different levels of oxygen. Changes in the major intracellular and extracellular metabolites have been measured, where the metabolic activity inside the cells showed not much change. The metabolic profile of pyruvate that goes up and down in response to the switch led to the study of movement of pyruvate inside the cells. Tagging of the *pykF* gene with GFP and 3xFLAG tag (in particular) indicated that the localisation of the PykF protein changes from cytoplasm to cell membrane. This explained why the concentration of pyruvate is low inside the cells, suggesting that the pyruvate is transported out directly when oxygen is introduced.

Acknowledgements

Praises to Allah for giving me guidance in life and strength to complete the thesis and also, peace be upon the beloved Prophet Muhammad.

I would like to thank my supervisor, Professor Mike Williamson, for his invaluable help, encouragement and direction throughout the duration of this project and also to Professor Jeff Green for letting me work in his lab and for many helpful discussions and advice.

I gratefully acknowledge both the Ministry of Higher Education Malaysia and Universiti Putra Malaysia for the PhD scholarship.

I would like to thank all members of the NMR group and F10 lab for their help and support with my work. In particular, I would like to thank Dr Matthew Rolfe, Dr Wendy Trotter and Dr Andrea Hounslow.

I am grateful to the Department of Molecular Biology and Biotechnology for providing the facilities to carry out this project. I would also like to thank Dr Chris Hill and Dr Darren Robinson from the Department of Biomedical Science for their help with performing transmission electron microscopy and fluorescence microscopy analysis, respectively.

Finally, I would like to thank all my family members, especially my husband Mohd Shahrul Ezhar, kids: Nuha, Adam and Hana, my parents and parents-in-law, who always support me and pray for my success in life and hereafter.

List of Abbreviations

ATP	Adenosine triphosphate
FNR	Fumarate nitrate reductase
GFP	Green fluorescence protein
LB	Lennox broth
LN ₂	Liquid nitrogen
μM	micromolar
mM	millimolar
ms	Millisecond
MS	Mass spectrometry
NADH	Nicotinamide adenine dinucleotide
NMR	Nuclear magnetic resonance
NTA	Nitriloacetic acid
OD	Optical density
PBS	Phosphate buffer saline
PDHC	Pyruvate dehydrogenase complex
PEP	Phosphoenolpyruvate
PFL	Pyruvate formate lyase
pyk	Pyruvate kinase
PAGE	Polyacrylamide gel electrophoresis
SDS	Sodium dodecyl phosphate
TEM	Transmission electron microscopy
TSP	Trimethylsilylpropionate

1.4.6	Pyruvate kinase of <i>E. coli</i>	44
1.4.7	Oxygen-dependent regulation of <i>E. coli</i> metabolism	45
1.5	Research Aims	48
2.0	Materials and methods	50
2.1	Media and chemical suppliers	50
2.2	Strains and plasmids	50
2.3	Growth and media conditions	51
2.3.1	Rich media	51
2.3.2	Evans defined medium	51
2.3.3	Growth of <i>E. coli</i>	53
2.3.4	Measurement of bacterial growth	53
2.3.5	Storage of strains	53
2.4	Metabolite analysis and measurement	54
2.4.1	Bacteria and growth conditions	54
2.4.2	Sampling method	54
2.4.2.1	Extracellular metabolites	54
2.4.2.2	Intracellular metabolites (Quenching method)	56
2.4.2.3	Unquenched method	57
2.4.3	Intracellular metabolite extraction	57
2.4.4	Metabolite analysis by NMR	58
2.4.4.1	Sample preparation	58
2.4.4.2	NMR analysis	58
2.4.5	Pyruvate assay	60
2.4.6	Pyruvate kinase enzyme assay	61
2.5	DNA methods	62
2.5.1	Quantification and purity determination of nucleic acids	62
2.5.2	Agarose gels	63
2.5.3	Extraction and purification of DNA from the agarose gels	63
2.5.4	Purification of DNA	64
2.5.5	Digestion of DNA with restriction enzymes	64

2.6	Gene deletion using the Lambda-Red system	64
2.6.1	Primer design	64
2.6.2	Polymerase chain reaction (PCR)	67
2.6.3	Preparation of linear DNA	68
2.6.3.1	pykF-3xFlag	68
2.6.3.2	pykF-GFP	68
2.6.4	Preparation and transformation of electrically competent cells	69
2.6.5	PCR verification	70
2.7	Transduction of <i>E. coli</i> DNA by P1vir1 phage	70
2.7.1	Preparation of lysate	71
2.7.2	Transduction by P1 phage	72
2.7.3	Confirmation of lysogeny via streak testing	72
2.8	Protein methods	73
2.8.1	SDS-PAGE	73
2.8.2	Western blot	75
2.8.2.1	Transfer of proteins to a nitrocellulose membrane	75
2.8.2.2	Blocking the gel and antibody binding	75
2.9	Fluorescence microscopy	77
2.9.1	Poly-L-Lysine slides preparation	77
2.9.2	Sample preparation	77
2.9.3	Image processing	78
2.10	Transmission electron microscopy analysis and gold-labeling	78
3.0	Rapid sampling and quantitation of metabolites	80
3.1	Introduction	80
3.2	Quenching method	81
3.3	Measurement reproducibility	86
3.4	Measurement of intracellular metabolite concentration	89
3.4.1	Measurement based on internal standard	90
3.4.2	Measurement based on cell volume	91

3.4.3	Comparison of intracellular metabolite concentrations Calculated based on internal standard and cell volume	92
3.5	Identification of metabolites	94
3.6	Discussion	99
4.0	Analysis of <i>E. coli</i> metabolites at different levels of oxygenation	104
4.1	Introduction	104
4.2	Results	105
4.2.1	Metabolic profile of cells grown under anaerobic and aerobic steady-state culture	105
4.2.2	Steady-state metabolite analysis at different level of oxygenation	111
4.2.3	Metabolite changes during transition from anaerobic to aerobic growth	114
4.2.3.1	Extracellular metabolite	114
4.2.3.2	Intracellular metabolite	123
4.2.4	Pyruvate assay	128
4.2.5	Detection of unknown peak	131
4.3	Discussion	136
5.0	Metabolite channelling	142
5.1	Introduction	142
5.2	Results	145
5.2.1	Pyruvate kinase (PK) enzyme assay	145
5.2.2	Creation of mutants by linear transformation	148
5.2.3	Functionality of the tags	156
5.2.3.1	Western blotting	156
5.2.3.2	Fluorescence microscopy (GFP tag)	158
5.2.3.3	Transmission electron microscopy (TEM)	160
5.3	Discussion	163

6.0	General discussion and conclusion	168
7.0	References	172

CHAPTER 1

INTRODUCTION

1.0 Introduction

1.1 Metabolomics

Metabolomics can be defined as a comprehensive and quantitative analysis of all metabolites in a biological system. Nicholson *et al.* (1999) have made a distinction between metabolomics and metabonomics, the latter representing also the time dependence of metabolite concentrations. Comprehensive analysis of the metabolome, which is the complete set of metabolites in an organism or cell, covers the identification and quantification of all intracellular and extracellular metabolites. This large-scale analysis of metabolites is an important addition to extensive studies of DNA sequences (genome), mRNA (transcriptome) and proteins (proteome) (Figure 1.1).

What can happen

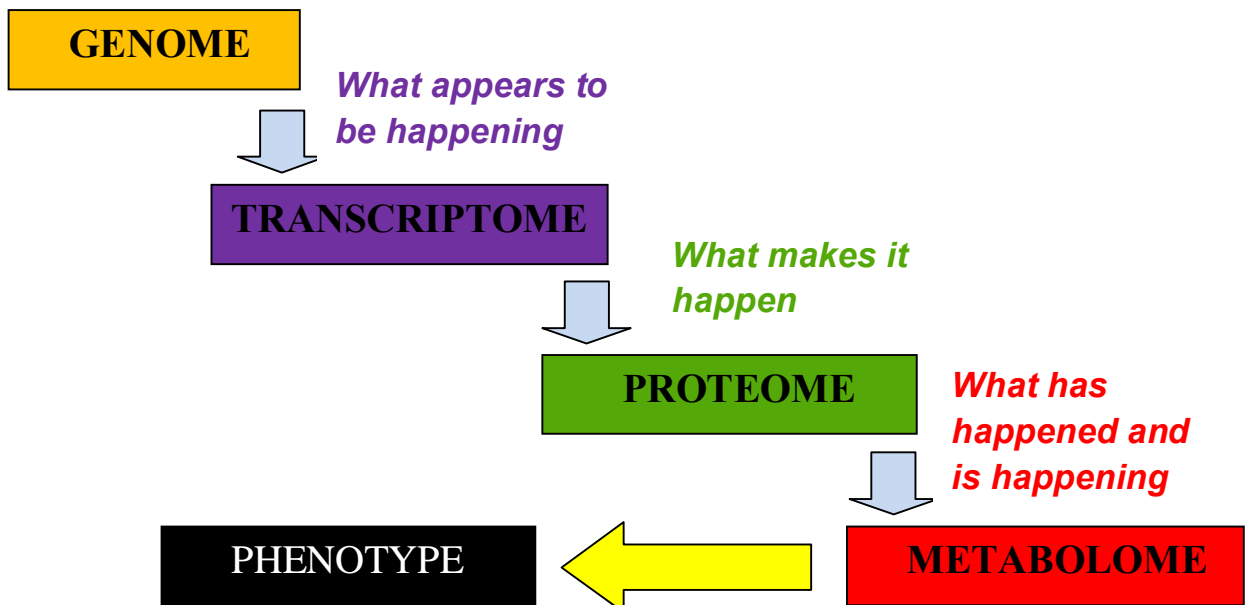


Figure 1.1: The 'Omics' cascade. Information flow in the cell. Adapted from Dettmer *et al.* (2007).

The term 'metabolome' is generally used to represent the molecules of low molecular mass (usually less than 1,000 Da) present in a biological sample. The most common samples studied are body fluids such as blood and urine, where often the aim is to identify biomarkers for disease. Both samples are relatively easy to collect and each biofluids is unique in the type of information it has to offer. However, samples can be taken from any biological system, including faecal extract, breast milk, amniotic fluid, umbilical cord blood and various cells and tissues. It has been estimated that the number of metabolites present in microbial metabolomes based on genome information ranges from 241 for a simple bacterium, like *Mycoplasma pneumoniae*, to 794 for the well-studied *Escherichia coli* (Goodacre *et al.*, 2004). But in practise, this number is likely to be a factor of two or three times higher, considering that many unknown functions remain present in every genome. In other words, in prokaryotes, the metabolome is estimated to consist of at least 1000 metabolites. In eukaryotic metabolomes, the number is very much larger, partly because the human body contains ten times more bacterial cells than human cells, and therefore contains many 'bacterial' metabolites as well as human metabolites (Nicholson and Wilson, 2003). Wishart *et al.* (2009) reported the estimated number of metabolites present in the human metabolome is around 7800. This number is incomplete as it does not include many lipids, drugs and food nutrients, thus it is expected that the number will increase significantly. The metabolome may consist of amino acids, lipids, carbohydrates, alcohols and natural compounds (such as antibiotics, pigments and cofactors) (Wishart *et al.*, 2013; Durot *et al.*, 2009). Metabolites differ widely in their chemical and physical properties, and also in their concentrations in the cell: in bacteria, the concentrations of different metabolites range from nM (ie, roughly one molecule per cell) to 100 mM, a dynamic range of 10^8 . Thus, it is difficult to say exactly how large the metabolome is for any organism, but it is estimated to be lower than the number of genes and proteins.

The concentrations of metabolites in the cell change in response to changes in enzyme concentrations and activities, and change much more rapidly than do the concentrations of enzymes or RNA. For example, it is estimated that the concentrations of glycolytic intermediates in yeast can change by a factor of two within one second (Dekoning and

Vandam, 1992). Thus, measurements of the concentrations of metabolites provide a good measure of cell metabolism, and hence identify the response of a cell or tissue to genetic or environmental changes, much more rapidly and precisely than do changes in proteome or transcriptome. Recently, studies of the metabolome have been increasing rapidly in popularity, for this reason (Hellerstein, 2004; Bundy *et al.*, 2007b; Trotter *et al.*, 2011; Yukihiro *et al.*, 2010). The challenges in metabolomic studies come because there are large variations in the chemical nature of the metabolites, their molecular weight, and their concentrations, which in eukaryotes can vary over nine orders of magnitude (pM-mM). The fact that metabolite concentrations can change very rapidly also introduces big problems. Finally, in cell metabolism, one metabolite can be involved in many pathways, meaning that after the concentrations of metabolites have been measured, it is not easy to relate these changes to changes in specific metabolic pathways. Thus, metabolomics presents challenges both in the collection of data and in their analysis.

Metabolomics studies show biological changes resulting from environmental perturbations (e.g changes in diet, drug consumption or development of disease), genetic and gut microbiota pressure. Numerous novel metabolic pathways and metabolites that have not been identified by other biochemical experiments are being discovered which can lead to further investigations. Metabolomics has a very big potential to be an important tool for early diagnosis of disease, predictor of treatment response or drug development. The quick response of metabolome to any changes make this 'omics' a very promising field in future. Metabolomic applications can be seen in three broad areas; clinical, biomedical and environmental. The clinical application of metabolomics is very important as this technique would help to increase the understanding of health in humans and the significant impact has been demonstrated by a high number of publications. Urine is a primary sample that enables noninvasive monitoring of any changes inside the body. Lindon *et al.* (1999) described an interesting study of transplant patients to differentiate between patients undergoing graft rejection and those suffering from cyclosporin toxicity, which marked the transition between traditional clinical and clinical metabolomics applications. NMR coupled with a recognition technique was used to monitor urine (collected from patients that were

given cyclosporin) and the result clearly could differentiate between patients undergoing graft rejection and taking cyclosporin. In the past 20 years, human inborn errors of metabolism have been studied using NMR (Holmes *et al.*, 1997; Lindon *et al.*, 1999) and more detailed study has been carried out on methods to identify inborn errors of metabolism by Constantinou *et al.* (2004). The relationship between serum metabolic profiles and hypertension has been investigated by Brindle *et al.* (2003) and Grainger (2006) looking at the severity of coronary heart disease.

There have also been rapid advances in biomedical applications. Cancer has been a popular subject as all researchers are trying to find more information about the metabolism of the disease. Griffin and Shockcor (2004) have profiled the metabolites of cancer cells in order to understand tumor development and progression. Early stage diagnosis of cancer is very important because the survival percentage is higher than when it is diagnosed late. Research carried out by Tiziani *et al.* (2009) has analysed blood serum by using NMR and managed to identify changes in system metabolic responses to cancer. Research in gut microflora in metabolism started many years ago (Coates, 1975; Gonthier *et al.*, 2003; Dumas *et al.*, 2006). Understanding the relationship between gut microbiota and host helps in developing an approach to improve health and fight the disease. A recent study by Nicholson *et al.* (2012) has characterised the metabolic interactions between host and gut microbiota. They are looking at the biological statistic that links microbes and the metabolites that are produced. Other recently reported research on host-microbe interactions includes a systems-level characterisation of a host-microbe metabolic symbiosis in the mammalian gut (Heinken *et al.* 2013) and uses metabolomic approaches to characterise metabolic interactions between the host and its commensal microbes (Xie *et al.* 2013).

The application of metabolomics technology has made significant impact into the environmental field. Environmental metabolomics basically looks at the interactions of living organisms with their environment. Metabolomics has many advantages as it can provide an

insight into an organism's response to disease, toxicity or genetic manipulation. Previously, it has been applied to both the terrestrial (Bundy *et al.*, 2007a) and aquatic environments (Viant *et al.* 2003; Rosenblum *et al.*, 2006). A review by Lin *et al.* (2006) mentioned several applications in biomarker development and risk assessment of toxicant exposure, disease diagnosis and metabolic response to environmental stressors. Viant (2008) described the advanced technologies being used in environmental metabolomics. His group also reported a first international NMR-based environmental metabolomics comparison in 2009 to evaluate the accuracy and precision of ^1H NMR measurements, based on these factors; data collection, data processing and multivariate analysis. The literatures mentioned above demonstrates that metabolomics research is increasing in number and it can be applied in many other unexpected area that can benefit and improve our life.

Methods for analysis of metabolites require several different analytical techniques, because of the problems described above of the range of chemical composition and concentrations involved. At the transcriptome and proteome level, high-throughput methods are already in use and the development of more comprehensive analysis methods is currently rising very fast compared to metabolomics analysis methods (Kaderbhai *et al.*, 2003). Fiehn (2002) described four approaches in metabolomics; target analysis, metabolite profiling, metabolomics and metabolic fingerprinting. Target analysis includes identification and quantification of known metabolites in the sample. Metabolite profiling, on the other hand, aims to do rapid analysis of a larger set of compounds, with the objective to identify unknown metabolites that characterize given samples. This approach has been applied widely; to plants (Bolling and Fiehn, 2005), microbes (Fischer and Sauer, 2003), urine (Kind *et al.*, 2007) and plasma samples (Dumas *et al.*, 2006), in order to identify and quantify unknown compounds. Metabolic fingerprinting is looking into a large set of intracellular metabolites that has been detected by a selected technique. Metabolomics can be performed as a linker between genotype and phenotype (Fiehn, 2002) and is widely used in many fields of research, including microbes and plants. Metabolomics data sets offer a more complete view on how cells function, thus bringing new solutions for biotechnology.

Since metabolomics links molecular biology with chemistry and physics, electronic databases are very important in metabolomics research. Similar to other 'omics' discipline, quality databases could help in the interpretation and understanding of many complex biological processes. There are many types of databases available; (i) metabolic pathway databases, e.g KEGG database, BioCyc database and Reactome database; (ii) compound-specific databases, e.g Lipid Maps, KEGG Glycan, DrugBank, ChEBI and PubChem; (iii) spectral databases, e.g Biological Magnetic Resonance Bank (BMRB), Madison Metabolomics Consortium Database (MMCD), MassBank and Metlin and (iv) organism-specific databases, e.g Biochemical Genetic and Genomics (BiGG), SYSTONOMAS and Human Metabolome Database (HMDB). These electronic resources contain information on a wide range of organisms.

1.2 Microbial metabolomics

Microbes are widely used in biotechnology, in fields such as fermentation, foods and biomass fuel production. They are ideal organisms to carry out systems biology studies because they are easy to manipulate and have important roles in life, and have simpler metabolomes than higher organisms. For example, the Sauer group have been actively involved in investigating the regulation of metabolic fluxes in microbes. Their work included analysis of metabolic fluxes on riboflavin-producing *Bacillus subtilis* (Sauer *et al.*, 1997) and, studies on metabolic integration (Sauer, 2006), and established a protocol for ¹³C-based metabolic flux analysis (Zamboni *et al.*, 2009). They have modelled bacterial metabolism to understand systems biology, thus providing valuable information on the regulatory network, multiple pathways and metabolic fluxes (Gerosa and Sauer, 2011).

The aim of microbial metabolomics generally is to obtain biological information to facilitate the understanding of microbial interactions and cellular functions. In general it requires knowledge of both extracellular and intracellular metabolites. Metabolite concentrations of

intracellular metabolites become very significant in microbial metabolomics, as they play vital roles in regulating microbial metabolism. Any attempt at modelling the rates of metabolic systems requires a detailed knowledge of concentrations. The level of most intracellular metabolites lies below 1 mM (Bennett *et al.*, 2009; Holms, 1996), thus presenting a big challenge in determining intracellular metabolite concentrations. Microbial cells usually are grown in liquid culture to relatively low titres, limiting the detection of metabolites present at low concentrations, since intracellular volumes take up no more than 3% of the total sample volume (Russell and Cook, 1995). Therefore the standard procedure for analysing intracellular metabolites is to separate the cells from the medium before analysing cellular contents, for example by centrifugation. It is essential to quench cellular metabolism rapidly, immediately after sampling, since the turnover rates of many metabolites are on the subsecond scale. For example, cytosolic glucose is converted at approximately 1.0 mM s^{-1} , and cytosolic ATP at approximately 1.5 mM s^{-1} (de Koning and van Dam, 1992). Therefore, the quenching step in metabolite analysis must be done within a very short time (<1 s) to ensure all the biochemical reactions will be stopped immediately after sampling.

Microbial metabolomics can be performed in a number of different ways, depending on the data of interest. This then determines the type of fermentation experiment, the method of sampling and the analysis of data. Lowry *et al.* (1971) analysed *E. coli* metabolites during logarithmic growth on a variety of carbon and nitrogen sources, to assess the regulatory role of various metabolites. The *E. coli* metabolome has been investigated extensively using qualitative analysis (Simao *et al.*, 2005; Dwivedi *et al.*, 2010). Metabolomics offers not only qualitative data but also quantitative data of intracellular metabolites that can provide the information needed to model the metabolic network operating under *in vivo* conditions. Many scientific researchers have described models for the central metabolism of different organisms, such as *Saccharomyces cerevisiae* (Dobson *et al.*, 2010), *Escherichia coli* (Usuda *et al.*, 2010), *Aspergillus niger* (Andersen *et al.*, 2008) and *Lactococcus lactis* (Oliveira *et al.*, 2005). Models have also been described from metabolome measurements for biosynthetic pathways leading to shikimate in *Streptococcus pneumoniae*, L-phenylalanine and L-

threonine in *E. coli*, and L-valine and L-lysine in *Corynebacterium glutamicum* (Chassagnole *et al.*, 2001a; Magnus *et al.*, 2006; Noble *et al.*, 2006; Yang *et al.*, 1999).

For quantitative analysis, it is important to define the physiological state of the biological system used for the measurements; in particular using a well-controlled steady-state culture. A steady-state chemostat is commonly used to cultivate microorganisms, e.g. *E. coli*, with the aim to fix the specific growth rate while varying a culture condition (see Section 1.4.2). The steps necessary for quantification of intracellular metabolites can be summarized as follows: harvesting the sample, quenching of metabolism in the sample, determination of intracellular volume, extraction of metabolites, and finally the quantitative analysis of metabolites (Weuster-Botz and de Graaf, 1996). Each step has a very important role in obtaining an accurate picture about microbial metabolism.

1.3 Methods for Metabolomics

Several robust and reliable rapid sampling instruments have been developed and various quenching and separation procedures have been proposed and applied in the past several years. As mentioned above, it is important to start from a well-defined steady state. However it is also useful to be able to measure the time dependence of metabolic changes, because this provides the data which allows modelling of the rates of metabolic reactions. In general in microbial systems, the rates can be very rapid, making it important to be able to sample and quench very rapidly. Such systems are described in the following sections. In our case, rapid quenching is also important, but rapid sampling is not so critical, because the changes that we will be interested in are happening on a slower timescale.

1.3.1 Rapid sampling

To understand microbial metabolism, quantitative information on both extracellular and intracellular concentrations is required, which can be achieved through rapid sampling. Generally, analysis of intermediary metabolites, such as glycolytic intermediates and sugar phosphates, is complicated by their short time constants caused by high exchange rates and low pool sizes (de Koning and van Dam, 1992; Weibel *et al.*, 1974). Due to this, rapid sampling techniques have been developed so that collected samples represent *in vivo* conditions as closely as possible.

There are many manually operated devices for rapid sampling from bioreactors that have become popular in the past several years. Theobald *et al.* (1993) described a simple sampling technique which took only 2 to 5 s intervals between samples that consists of a homemade sample port coupled to the bioreactor. It used a sampling tube containing the quenching solution under vacuum that provokes a rapid displacement of the sample from the bioreactor into the tube. Iversen (1981) designed a sampling valve with a minimal dead space. However, the disadvantage of these systems is that they have a limitation on sampling frequency. Weuster-Botz (1997) proposed a better idea to perform all steps (sampling, quenching and extraction of metabolite) in a continuous way. He used a long tube connected to the bioreactor to fix the highly dynamic metabolite patterns, resulting from an immediate disturbance of the culture in the bioreactor. Automated sampling devices were developed a few years later to improve the sampling device that was proposed by Theobald *et al.* (1993) with a better sampling reproducibility. Schaefer *et al.* (1999) therefore developed sampling tubes that were fixed in transport racks with a maximum sampling frequency of 4.5 samples s^{-1} to achieve much shorter intervals between samples. Lange *et al.* (2001) also invented a new system that consists of a submerged capillary port that is placed inside a stainless steel cylinder to fit a standard bioreactor and silicon tubing that connects to a waste container and to the sampler tube adapter.

Another sampling device was based on the stopped-flow technique combined with a modified rapid-freezing method, proposed by Buziol *et al.* (2002). The device serves as a mixing chamber, where the sample was directed to a sampling tube containing liquid nitrogen (-196°C), which acts as a quenching liquid. This device helps the culture to remain at a steady state because the organisms are stimulated by the glucose in the mixing chamber. It also has a short time span between glucose stimulus and first sample that is less than 100 ms. Another group that applied this stopped-flow technique is Dekoning and Vandam (1992). They incubated starved yeast cells in a quench apparatus to measure the changes of glycolytic intermediates after adding a pulse of glucose within a time frame of 15-5000 ms. Visser *et al.* (2002) developed a rapid sampling and perturbation device (BioScope) which is a mini plug-flow reactor that can be coupled to the steady-state bioreactor. The system was equipped with 11 sample ports, including one sample port before the mixing chamber where the perturbing agent was mixed with the culture broth. The newest development is reported by Schaub *et al.* (2006) who used a coiled single tube heat exchanger connected to the bioreactor to produce a continuous sampling, quenching and extraction procedure.

1.3.2 Quenching

Many intracellular metabolites are characterized by a rapid turnover and sometimes low pool sizes. In this situation, the aim of quenching is to inactivate the intracellular enzymes so that the metabolite profile is frozen. The most commonly used method for rapid quenching of microbial metabolic activity in culture samples is achieved by instant change of sample temperature or pH, or by rapid addition of organic solvents, accomplished by mixing the cell sample with an appropriate quenching solution. In general, removal of the extracellular metabolites present in the broth is performed by centrifugation of the quenching solution to obtain a cell pellet. Centrifugation is often performed at temperatures below -20 °C in order to make sure no conversion of metabolites occurs. The cells occupy a smaller volume than the medium, and therefore for accurate measurement of intracellular metabolites it is

important to separate the cells from the medium before analysis. However, the centrifugation must be done quickly to reduce the risk of metabolic change: centrifugation at too low a temperature runs the risk that ice crystals may form and damage the cell membrane, leading to leakage of intracellular contents.

The most popular quenching method is based on cold aqueous 60% (v/v) methanol at temperatures of -40 or -50 °C (Buchholz *et al.*, 2001; de Koning and van Dam, 1992; Schaefer *et al.*, 1999), and has been widely used for *E. coli* and *S. cerevisiae*. For example, Dekoning and Vandam (1992) have used this to measure glycolytic and other low molecular weight metabolites in yeast cells. However, this method was found to be not very suitable for prokaryotic microbes, resulting in loss of intracellular compounds (Bolten *et al.*, 2007; Wittmann *et al.*, 2004). The leakage of metabolites during quenching is likely to be dependent on cell wall and membrane structure. Even for yeast cells that are thought to be more robust, leakage of metabolites during quenching has been observed to occur. Canelas *et al.* (2008) have quantified metabolite leakage during cold methanol quenching of the yeast *S. cerevisiae*, by determining the levels of a large range of metabolites in total broth and different sample fractions, using isotope dilution mass spectrometry (IDMS). They confirmed that leakage does occur during quenching in pure methanol. The impact of the cold shock phenomenon, whereby the decrease in temperature results in an increase of the permeability of the cell membrane, has led to suggestions that this method is not appropriate. Release of metabolites after rapid cooling to 0°C has been observed by Taymaz-Nikerel *et al.* (2009) for *E. coli*. Bolten *et al.* (2007) found that the cold methanol quenching method could result in either higher or lower concentrations compared with filtration. Since the filtration procedure took nearly 30 s per sample, this method also does not appear to be suitable for steady-state measurements of metabolites with short turnover times. Alternative methods that have been used for quenching of *E. coli* include rapid freezing of the sample in liquid nitrogen (Chassagnole *et al.*, 2002b) and rapid heating of the broth (Schaub *et al.*, 2006). Rapid quenching in liquid nitrogen requires thawing of frozen sample followed by separation of the cells from the medium by centrifugation. It is likely that ice crystals may damage the cell membranes during the freezing, thus leading to

metabolite leakage and hence inaccurate quantification of the metabolites. The direct spraying of cell samples into perchloric acid also inactivates metabolism and extracts metabolites simultaneously (Theobald *et al.*, 1993; Weuster-Botz, 1997), though it has disadvantages as discussed in the next section.

Recently, several attempts have been made to develop new quenching procedures, with the aim to minimize the metabolite leakage. Villas-Boas and Bruheim (2007) have proposed a quenching method using a cold glycerol-saline solution as a promising quenching agent for yeast and bacteria. They have shown that metabolite levels were much higher than when samples were quenched with the cold methanol solution, and therefore presumably there was less leakage due to damage to the cell wall. However, a disadvantage of this method is that it is impossible to get rid of the glycerol that sticks to the pellets; washing with water leads to loss of intracellular metabolites. A new quenching method has therefore been developed by (Spura *et al.*, 2009), where they used 40% ethanol and 0.8% (w/v) sodium chloride as a quenching solution. This method has been tested on Gram positive and Gram negative prokaryotes, as well as eukaryotes. Ethanol was used instead of methanol to prevent damage of the cell membrane, and in a further effort to reduce membrane damage, the concentration of alcohol was reduced. The sodium chloride is used to produce an isotonic solution that should not result in osmotic shock. More than 80% of identified metabolites showed higher relative concentrations in the ethanol quenching compared with the methanol quenching, and therefore presumably less loss of metabolites. This method appears to be the most reproducible, stable and fast for bacterial cells. It has therefore been implemented, to check if it can be used as a routine method for analysis of chemostat cultures. Various quenching procedures are summarized in Table 1.1.

Quenching agent	Temperature	Microorganisms	References
EtOH/H ₂ O	-23°C	<i>S. cerevisiae</i>	Villas-Boas and Bruheim (2007)
60% (v/v) MeOH/H ₂ O	-40°C	Yeast	de Koning and van Dam (1992)
60% (v/v) MeOH/H ₂ O	-40°C	<i>S. cerevisiae</i>	Villas-Boas <i>et al.</i> (2005a)
60% (v/v) MeOH/H ₂ O	-50°C	<i>E. coli</i>	Schaefer <i>et al.</i> (1999)
60% (v/v) MeOH/H ₂ O	-50°C	<i>E. coli</i>	Buchholz <i>et al.</i> (2001)
60% (v/v) MeOH/H ₂ O	-58°C	<i>C. glutamicum</i>	Wittmann <i>et al.</i> (2004)
			Bolten <i>et al.</i> (2007)
40% (v/v) EtOH/NaCl (0.8%) (w/v)	-30°C	<i>E. coli</i>	Spura <i>et al.</i> (2009)
Liquid nitrogen	-150°C	<i>E. coli</i>	Chassagnole <i>et al.</i> (2002b)

Table 1.1: Comparison of quenching agents used for microbial metabolites

1.3.3 Extraction methods for intracellular metabolites

Once metabolism has been arrested by quenching, the metabolites need to be extracted from the cells. The best extracting agent should extract as many intracellular metabolites as possible with minimal degradation and no chemical or enzymatic modification of the targeted metabolites. Sample cells are homogenized, sonicated or freeze-thawed in the presence of aqueous and/or organic solvents in order to break up the cells to release the metabolic compounds (Khoo and Al-Rubeai, 2009). The mixture of cell debris and extracted metabolite is then centrifuged to separate the liquid containing the desired metabolites. It is important to remove the extracellular metabolites first for proper quantification of the intracellular metabolites. Although generally the concentration of extracellular metabolites is much lower than intracellular concentrations, the amount present in the supernatant may still be very significant because the volume of the supernatant is two orders of magnitude larger than the total cell volume. This has been proved by Bolten *et al.* (2007), where they found significant amounts of several central metabolites and amino acids present in the cell culture filtrate.

The broken cells may need to be subjected to further separation to extract the metabolites. The most commonly used extraction method is perchloric acid (Chassagnole *et al.*, 2002b; Kayser *et al.*, 2005; Schaefer *et al.*, 1999). One disadvantage of perchloric acid extraction is that it is only suitable for nucleotides and water-soluble metabolites. Because of the pH extreme involved, perchloric acid extraction may cause a destruction of compounds like pyruvate, NAD, NADH⁺, phosphorylated deoxyadenosine sugars and indole compounds (Gonzalez *et al.*, 1997). Maharjan and Ferenci (2003) have concluded that the use of cold methanol is much preferred because of its simplicity and because it allowed more components to be extracted. Since the extraction is carried out at -40°C, chemical and enzymatic changes in metabolites are likely to be minimized. An additional advantage is that cold methanol extraction can be used for other organisms including eukaryotes and mammalian cells as a general tool for quantification of metabolites. Fajjes *et al.* (2007) have

made a similar observation and suggested that factors like handling and temperature should be carefully controlled during the procedure. Rabinowitz and Kimball (2007) have proposed cold acidic solvent mixtures containing acetonitrile for extraction of *E. coli* metabolites especially for nucleotide triphosphates. By contrast, Hiller *et al.* (2007) claimed that buffered hot water (30 mM triethanolamine (TEA), pH 7.5, 95°C) produced more reliable results for *E. coli* compared to buffered ethanol, unbuffered hot water or perchloric acid. However, treatment by water at 95° could lead to loss of volatile and reactive compounds, and has not been pursued further here. Based on this analysis, we have concluded that cold ethanol/saline followed by methanol extraction is the most promising method. In Chapter 3, we present some refinements of the method aimed at improving its reproducibility.

1.3.4 Determination of metabolite concentration

1.3.4.1 Traditional methods

Traditionally, quantitative analysis of extracellular and intracellular metabolites has been carried out using enzyme-based assays (Hajjaj *et al.*, 1998; Theobald *et al.*, 1993). This method has the advantage of being very specific, but the main disadvantage lies in the relatively large sample needed for quantification, and by the fact that each metabolite must be assayed separately. Nowadays, many analytical techniques have been applied, including gas chromatography (GC), thin-layer chromatography (TLC), mass spectrometry (MS), high-performance liquid chromatography (HPLC), nuclear magnetic resonance (NMR) and laser induced fluorescence (LIF) detection. All these methods can be used in measuring metabolite concentration, but they differ in selectivity and sensitivity, and in the need for pre-treatment of the sample. They also differ in the speed of the method and the ease of subsequent analysis.

1.3.4.2 System wide methods

1.3.4.2.1 Nuclear magnetic resonance (NMR) spectroscopy

1.3.4.2.1.1 Overview of NMR

NMR spectroscopy is one of the leading technologies used to characterize a chemical structure and has been used extensively for metabolite profiling (Griffin, 2003; Lindon *et al.*, 2000). NMR was first developed in 1946 by a research group in the USA (Purcell *et al.*, 1946) and was the subject of the Nobel Prize for Physics in 1952. Chemical shift (the observation that the resonance frequency of a nucleus is affected by its chemical environment) was discovered in 1950 and later it was observed that a nucleus could influence the resonance of another through the phenomenon of *J*-coupling through chemical bonds. Later, the chemical shift and spin-spin couplings have been proved to be related to chemical structure. The signal to noise ratio in NMR was significantly improved in 1970 through the introduction of Fourier transformation (FT) of the time-domain response resulting in a frequency domain spectrum. Richard R. Ernst, who pioneered this work, has received the Nobel Prize for Chemistry in 1991 for his contribution to the development in methodology of high resolution nuclear magnetic resonance spectroscopy.

Recent advances in NMR techniques, software for analysis and spectroscopic libraries of metabolites have enlarged the potential to identify new metabolites. NMR provides a rich information set for metabolic analysis, because the intensities of NMR signals are linearly proportional to concentration. Most NMR analyses use ^1H NMR for detection of metabolites, meaning that any compounds containing protons can be observed by NMR. NMR can thus detect almost any metabolite present at sufficient concentrations. It is also non-destructive, non-biased, requires little or no separation and needs no chemical

derivatization. NMR is particularly appropriate for compounds that are less tractable for GC-MS or LC-MS analysis, e.g. sugars, amines, volatile ketones and relatively non-reactive compounds. The disadvantage of NMR spectroscopy is its lack of sensitivity, with a lower limit of detection of about 1-5 μM . Large sample sizes ($\sim 500 \mu\text{l}$) are typical though it is possible to use much smaller volumes (example 35 μl), permitting sensitive detection on more concentrated samples, not usually a problem since metabolites are usually soluble. The strong solvent signal (for example of $^1\text{H}_2\text{O}$) must be suppressed in some way to avoid saturation of the analogue-to-digital converter of Fourier-transform (FT) spectrometers. To avoid a large water signal, D_2O can be used instead of H_2O (Gaines *et al.*, 1996) or the water signal can be suppressed with suitable pulse sequences (Hore, 1989). The sensitivity of NMR has markedly improved with the introduction of higher field magnets (up to 900 MHz), cryogenically cooled probes and small-volume microprobes (Ehrmann *et al.*, 2007; Robosky *et al.*, 2007).

Although several other important nuclides, e.g. ^{31}P , ^{13}C and ^{15}N can be detected by NMR, proton (^1H) remains the most widely used to understand metabolic and physiological processes. It is the most sensitive nucleus, it is present at 99.98% natural abundance, and it is present in almost all carbon-containing biological molecules, substrates and products. ^1H NMR spectra can be obtained in a few minutes and contain quantitative information on all metabolites simultaneously, making it a good high-throughput method. In ^1H NMR spectra, metabolite signals are confined to a narrow bandwidth of roughly 10 ppm. In principle, this could lead to overlap of signals, but in practice, this is seldom a problem. ^{13}C is present at 1.1% abundance, and has a gyromagnetic ratio 25% that of ^1H , which makes it considerably less sensitive. However, the signals are better resolved. Fluorine (^{19}F) is less used compared to ^1H and ^{13}C since it is present in only about 10% of pharmaceutical compounds, even though it is 100% abundance. Phosphorus (^{31}P) is one of the routine NMR nuclei that are less sensitive than ^1H but more sensitive than ^{13}C . It has an isotopic abundance of 100% and is found in many metabolites, which are not only at high concentration in the cell but also of importance for cell energetics (eg ATP: Table 1.2). Brown *et al.* (1977) applied ^{31}P NMR to measure the *in vivo* exchange rates between inorganic phosphate (Pi) and the terminal

phosphate of ATP (ATP γ) in suspensions of aerobic *E. coli* cells. Finally, ^{15}N is useful because nitrogen is present in a large number of metabolites, but isotopically enriched samples are almost essential for heteronuclear NMR because of its low natural abundance and low sensitivity.

Quantification of complex biological samples by NMR is not straightforward. The problem with analyzing complex spectra is there are hundreds or thousands of signals, which may often be overlapped. There are two approaches in collecting, processing and interpreting metabolomic NMR data. These are called quantitative and chemometric methods (Figure 1.2). In quantitative metabolomics, compounds are identified and quantified absolutely by comparing the NMR spectrum of the sample with a spectral reference of pure compounds (Weljie *et al.*, 2006). By contrast, in chemometric analysis, peaks are not identified initially. The statistical differences between their spectral pattern and intensities are used to identify special features, and are treated by a variety of approaches (Winning *et al.*, 2008) which may or may not involve identification of the metabolites involved. There are a few approaches for chemometrics that are routinely used, such as Principal Component Analysis (PCA), Soft Independent Modeling of Class Analogy (SIMCA) and Orthogonal Partial Least Squares (OPLS). By comparison to chemometric methods, the quantitative method allows precise compound quantification, does not require spectral alignment or binning, and permits immediate interpretation of metabolic pathways as we can get both compound identities and concentrations from this method (Weljie *et al.*, 2006; Wishart, 2008). It does however require much more individual interpretation of each spectrum. In general, there are five main steps in quantitative spectral analysis: zero filling and line broadening, chemical shift referencing, phasing, baseline correction and possibly line-shape correction. These are not unlike the steps used to process most small-molecule NMR spectra.

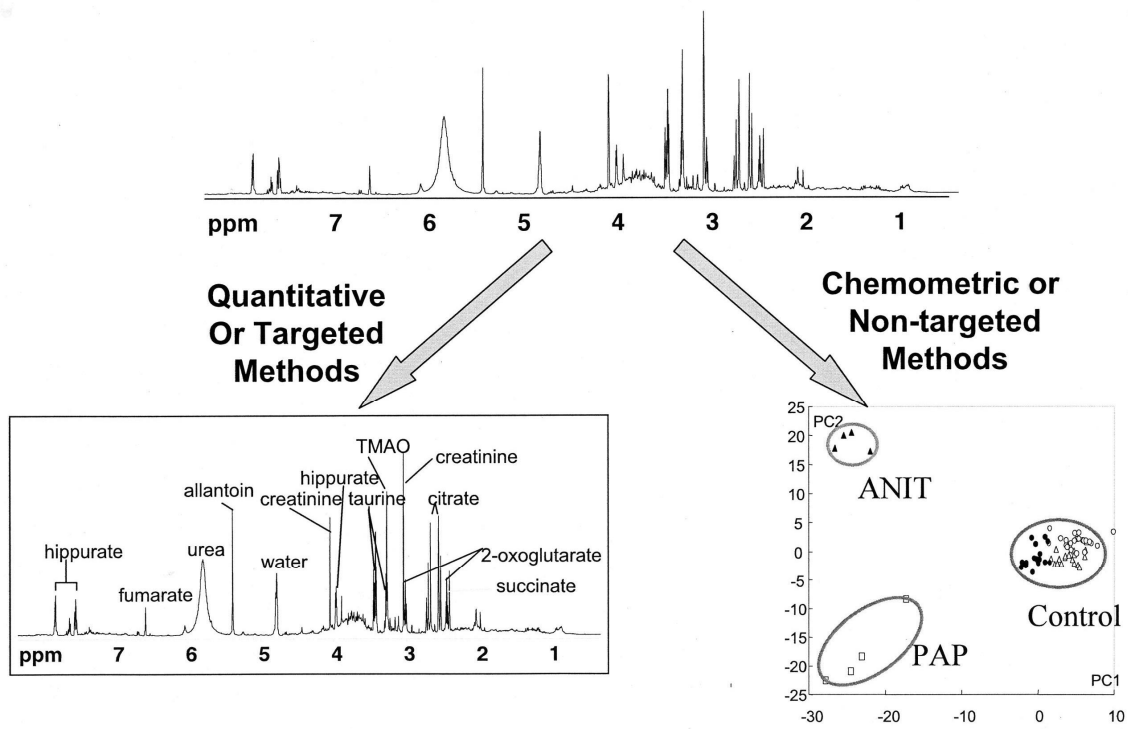


Figure 1.2: Schematic diagram of two routes to metabolomic analysis; quantitative and chemometric methods. Adapted from Wishart *et al.* (2001)

1.3.4.2.1.2 The principles of NMR

The NMR spectrometer consists of various pieces of equipment that provide the capability of various experiments. The basic spectrometer consists of a receiver, a transmitter, a probe, a magnet and a computer (Figure 1.3). During the NMR experiment, the computer instructs the transmitter to issue a radio frequency (rf) pulse to the probe. This rf pulse excites the spins in the sample. A sample consisting of many nuclear spins has a macroscopic magnetisation, which behaves like a small magnet. When the sample is excited by a radiofrequency (rf) field, the nuclear magnetisation is rotated. Usually, the rf field is turned off after the magnetisation has rotated 90° , after which the magnetisation rotates around the applied magnetic field axis. The oscillating magnetic field creates a current in a coil placed around the sample. The frequency of the oscillation is detected as a Free Induction Decay or FID, and converted to a frequency in a spectrum using a Fourier transform.

NMR is the observation of the spin of a nucleus, which generates a magnetic field. When an external magnetic field (B_0) is present, the nuclei align themselves either with or against the field of the external magnet (Figure 1.4b). Without an external applied magnetic field, the nuclear spins are random in directions (Figure 1.4a). The energy difference between the two states (ΔE) depends on the applied field. The greater the strength of the applied magnetic field, the larger the energy difference between the two spin states (Figure 1.5). The resulting spin-magnet has a magnetic moment (μ) proportional to the spin. Spin quantum number (I) is related to the atomic and mass number of the nucleus. Some nuclei have integral spins (e.g. $I = 1, 2, 3$), some have fractional spins (e.g. $I = 1/2, 3/2, 5/2$) and a few have no spin (e.g. ^{12}C , ^{16}O , ^{32}S).

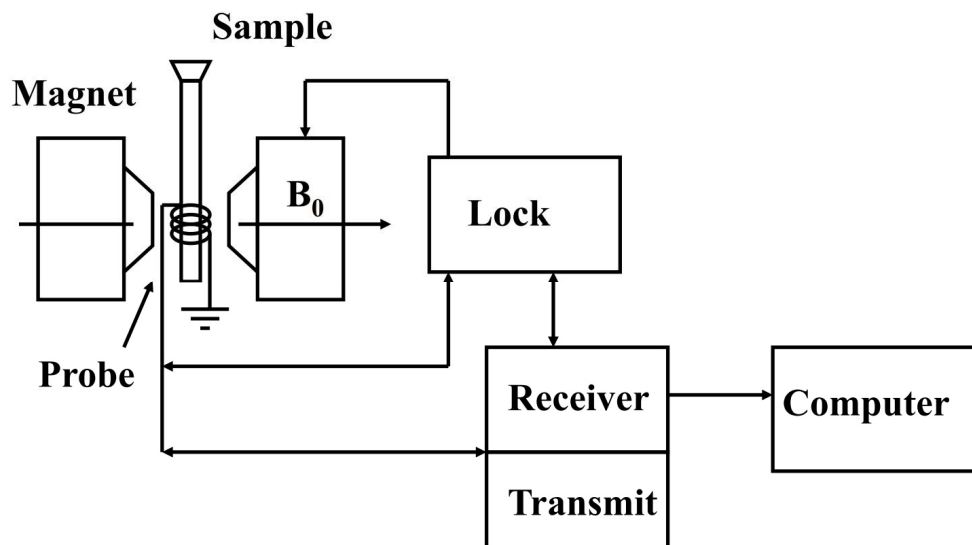


Figure 1.3: Essential parts of an NMR spectrometer. The computer instructs the transmitter to issue a radio frequency (rf) pulse to the probe. The rf pulse excites the spins in the sample. Then the computer instructs the receiver to turn on to receive the rf energy that being radiated from the spins.

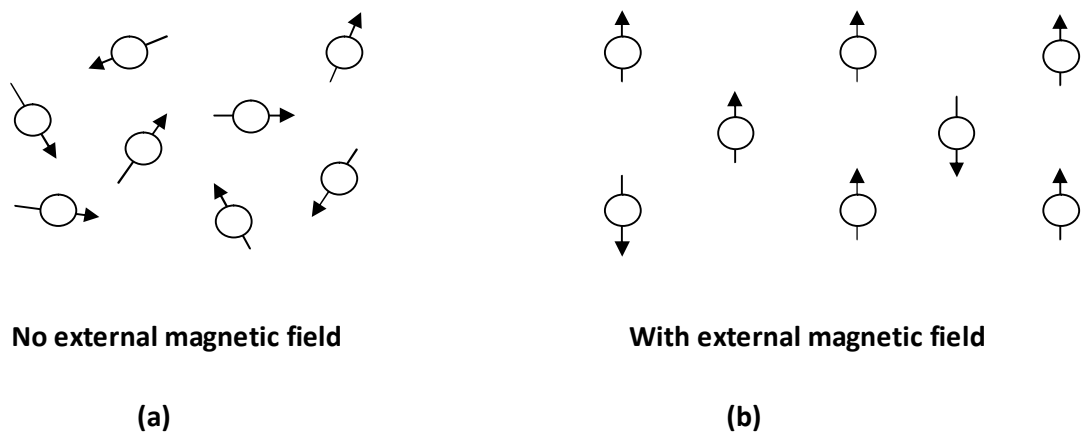


Figure 1.4: Two schematic representations of alignment in magnetic fields. In the absence of magnetic field (a), the nuclei are randomly oriented but when a field is applied (b), they line up parallel to the applied field either spin aligned or spin opposed.

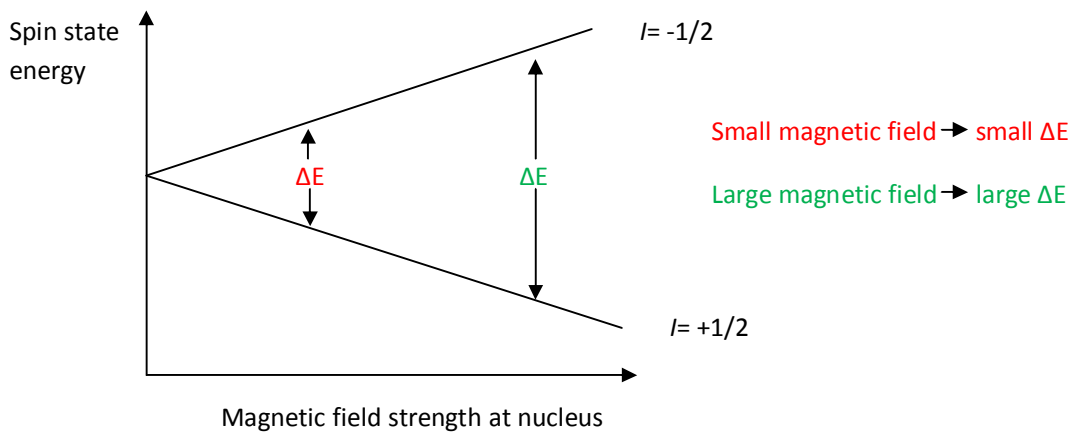


Figure 1.5: ΔE influenced by magnetic field strength at nucleus.

Nuclei in different locations in a molecule experience different local magnetic fields. These are measured as the difference between the resonance frequency of the nucleus and a standard, relative to the standard. This quantity is reported in ppm and given the symbol delta, δ . Important factors involved in chemical shift are electron density or electronegativity of neighbouring groups and anisotropic magnetic field effects. One of the first spectra recorded that reveal the NMR chemical shift is the proton spectrum of ethanol. Trends in chemical shift are explained based on the degree of shielding or deshielding. When a signal is found with a higher chemical shift, the nucleus is more shielded and when the chemical shift is low, the nucleus is more shielded. In NMR spectroscopy, the most common standards used are either tetramethylsilane (TMS) or trimethylsilyl propionate (TSP), which are defined to be at 0 ppm. Spin couplings through bonds are observed in NMR. This effect can cause splitting of the signal for each type of nucleus into two or more lines. The size of the splitting (J) is independent of the magnetic field and is therefore measured as an absolute frequency (Hertz). Relaxation times (T_1 and T_2) describe how rapidly magnetisation returns to equilibrium (in the z and xy directions respectively) and are important for proper interpretation of NMR spectra, but they can vary greatly depending on the structure of the molecule. For example, when relaxation is very fast, NMR lines will be broad and the signal harder to detect.

Figure 1.6 shows the most basic and common pulse sequence used in Fourier transform-NMR experiments. This sequence is used for routine ^1H and ^{13}C acquisitions. The radio pulse excites the nuclei, which then precess during the acquisition time, giving an NMR signal in the form of an exponentially decaying sine wave. This decaying sine wave is known as the free-induction decay (FID). The radio pulse has a characteristic frequency, called the spectrometer frequency (SF), which is dependent upon the nucleus and the magnetic field strength of the spectrometer used. The radio pulse also has a width and it is most commonly described in terms of a flip angle in degrees. As shown in Figure 1.7, this is because of its effect on the nuclear spins. The amount of rotation is dependent on the power and width of the pulse in microseconds (μw). Maximum signal is obtained with a 90° pulse. Thus, the 90° pulse width is the amount of time the pulse of energy is applied to the

particular sample in order to flip all the spins into the X-Y plane. The nuclear spins are no longer at equilibrium and will return to equilibrium along the Z-axis. In Figure 1.6a, the decaying sine wave represents this process of Free Induction Decay (FID), which is a plot of induced voltage as a function of time. The time to acquire the FID is called the acquisition time (at). The signal acquired is digitised; the spectrometer represents the FID by a series of points along the FID curve. Fourier transforming the FID produces a spectrum which gives intensity as a function of frequency. The frequency domain spectrum has two important parameters associated with it, the frequency and the spectral width. There are many variations on this simple pulse sequence. A common one, used for most of the spectra shown here, adds a frequency-selective pulse before the 90° pulse, to suppress the intense signal from the water (Figure 1.6b).

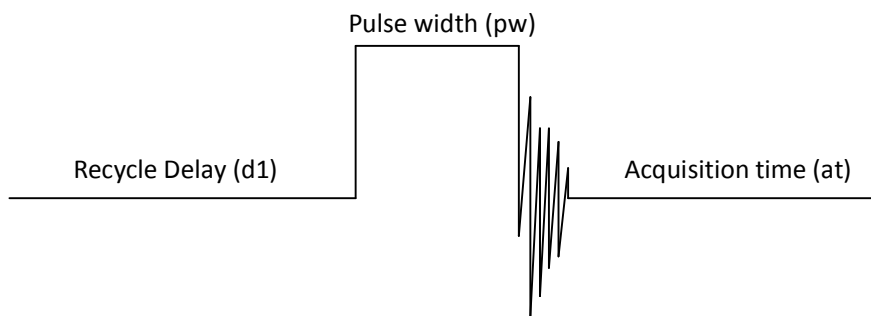


Figure 1.6(a): Schematic presentation of one cycle of a simple one-pulse NMR.

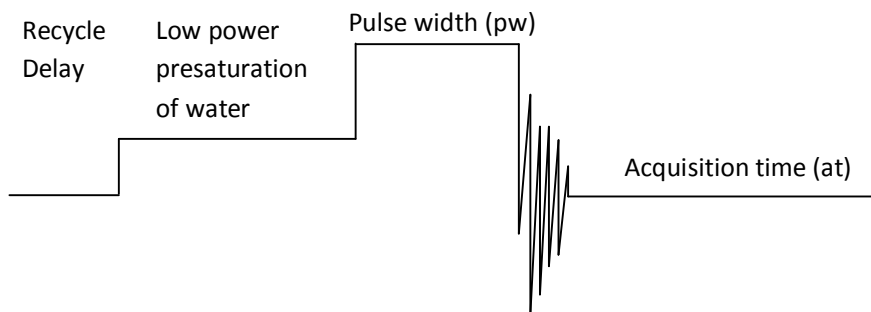


Figure 1.6(b): A simple 1D single-pulse experiment including a long low-power pulse on resonance with the water signal, to suppress the intense water signal.

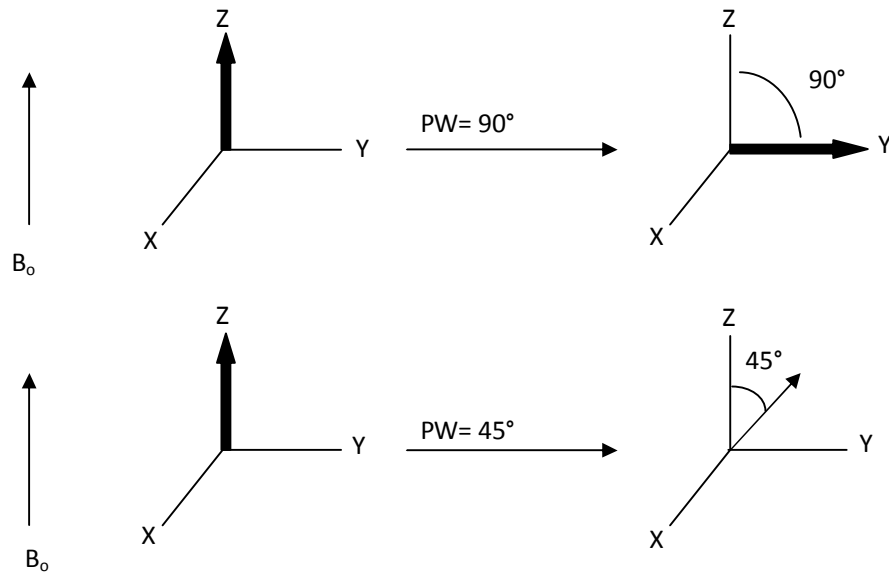


Figure 1.7: The average nuclear spin magnetisation (bold arrow) for an NMR sample placed in a magnetic field aligned along the Z-axis before and after application of a pulse.

1.3.4.2.1.3 ^1H NMR Studies of Metabolism

Developments in metabolomics are driven by brilliant analytical methods. ^1H NMR is an important experimental technique that allows high-throughput quantification of small molecules in biological system, known as metabolites (Nicholson *et al.*, 1999). The application of ^1H NMR includes to characterise, diagnose and understand the metabolic states, and is increasingly applied in biomedical research, toxicology, drug characterisation and in human nutritional research (Shockcor and Holmes, 2002; Stella *et al.*, 2006; Holmes *et al.*, 2006; Winnike *et al.*, 2009; Azaïs *et al.*, 2009; Jung *et al.*, 2011). In particular, NMR is widely used for identification and quantification of metabolites, in which biofluids like plasma and urine are the most commonly used samples (Nicholson *et al.*, 1999). Metabolites contain one or more protons and this/these proton(s) are detectable by ^1H NMR as a peak. The number of peaks generated by a metabolite is determined by the chemical structure of the molecule.

Currently, ^1H NMR is being actively applied in metabolomics; particularly in metabolite identification and profiling. The major challenges in ^1H NMR metabolic profiling are the assignment of metabolites from spectra due to huge data volumes and the presence of unknown metabolites. Many approaches have been introduced to facilitate ^1H NMR in performing metabolic profiling. Yeom *et al.* (2013) have used ^1H NMR and multivariate analysis, e.g PCA and OPLS to study the metabolic changes in biofilm-forming bacteria, *Acinetobacter baumannii* 1656-2. They have found that metabolites like acetate, pyruvate, succinate and glutamate were involved in the metabolism of biofilm formation. Other groups, e.g Barba *et al.* (2010) and Isern *et al.* (2013) used ^1H NMR together with spiking experiments (comparison to prepared standard) to identify and quantify metabolites from vitreous fluid of diabetic retinopathy patients and fermentation products in *Caldicellulosiruptor saccharolyticus*. Apart from the above mentioned method, scalar coupling between ^1H and ^{13}C can give more detailed identification of metabolites and structure determination (Misra and Bajpai, 2009). Metabolites can also be identified by

comparing the experimental chemical shift with the published chemical shift, which helps in identification of metabolites (Tulpan *et al.* 2011). It is common practice to add a reference compound to the sample such as trimethylsilyl propionate. This is useful to check for correct alignment and referencing of spectra. It also provides a useful guide to correct setup and recording of the experiments, because the linewidth of the reference should remain less than 1 Hz for all spectra. Nowadays, 2D NMR has been widely used in metabolomics to achieve better results. Some 2D NMR methods, e.g. ^{13}C - ^1H HSQC and homonuclear 2D spectra (^1H - ^1H NMR; ^{13}C - ^{13}C NMR) have been extensively used in metabolomics. In ^{13}C NMR, the chemical shift dispersion is greater and spin-spin interactions are removed by decoupling. This can be seen in research carried out by Kivero *et al.* (2008), Tredwell *et al.* (2011) and Zhang *et al.* (2012).

The combination of NMR analysis with an in-line chromatographic separation technique has become a highly practical analytical method. It eliminates much of the overlap problem in the ^1H spectrum. The best example for this method is LC-NMR. The extracts or mixtures can be fractionated before NMR spectra being recorded (Lindon and Nicholson, 1997). This approach has been applied in the analysis of complex mixtures that contain unknown components, metabolites in pharmaceuticals, natural products and synthetic polymers (Pasch *et al.*, 2008). LC-NMR has the ability to separate complex mixtures into individual components which made it as an important method in determination of structure of unknown compounds (Alsante *et al.* 2004). The highest sensitivity of LC-NMR is provided when all separated components are introduced into a flow-cell. Most LC-NMR operations used reversed-phase columns that caused problem to NMR measurement and it has been overcome by using other eluents and deuterated solvents. Optimisation of HPLC separation is important to be carried out in LC-NMR analysis (Patel *et al.* 2010).

Both MS and NMR techniques are limited by overlapping signals. In MS, the overlapping signals come from the fragmentation of the mass ion, whereas in NMR multiple signals arise directly from the same molecule. NMR is more quantitative than MS. In MS, preparing

samples is more time-consuming, where frequent calibration and variable retention times are needed. Thus, NMR plays an important role in metabolite analysis to enrich the metabolomics field.

1.3.4.2.2 Mass Spectrometry (MS)

Currently, mass spectrometry is widely employed for analysis of metabolites because it provides highly selective and sensitive methods for the detection of a wide range of metabolites. MS measures the mass (or more specifically the mass-to-charge ratio) of charged metabolites. In principle, a mass spectrometer generates multiple ions from the sample, then separates them according to their mass, and records the relative abundance of each ion type (Figure 1.8). Modern MS provides highly specific chemical information that is directly related to the chemical structure and allows detection and measurement of picomole to femtomole levels of many primary and secondary metabolites. These unique advantages make MS an important tool in metabolomics (Bedair and Sumner, 2008). There are many types of MS that differ in operation and performance, such as resolving power and mass accuracy. In the late 1980s, electrospray ionization (ESI) and matrix assisted laser desorption/ionization (MALDI) were developed, and since then have become popular in biomolecular research (Domon and Aebersold, 2006). In ESI, the solvent passing through the chromatographic column is channelled through a capillary charged with a high voltage, either positive or negative. Fourier transform ion cyclotron resonance (FT-ICRMS), orbitrap MS and multi-mass TOFMS are examples of mass analyzers with different resolving power that have been used in metabolomics. Coupling chromatography to MS offers an excellent solution to complex mixture analyses.

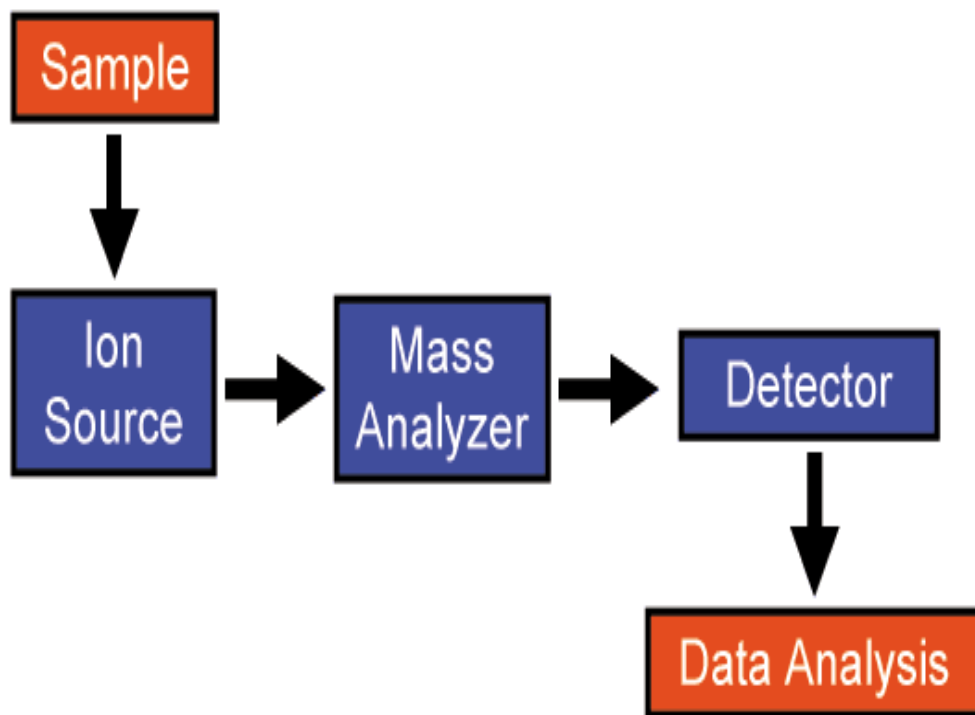


Figure 1.8: Schematic presentation of the basic principle of a mass spectrometer. The first step in the mass spectrometric analysis of compounds is the production of gas phase ions of the compound. This molecular ion may undergo fragmentation, depending on how much energy it had when it went into the gas phase. The ions are separated in the mass spectrometer according to their mass-to-charge-ratio and are detected in proportion to their abundance. A mass spectrum of the molecule is thus produced.

Currently, there are three chromatography techniques that have commonly been incorporated into MS based metabolomics, which are gas chromatography (GC), liquid chromatography (LC) and capillary electrophoresis (CE). Chromatographic separation of metabolites prior to MS analyses has several advantages: it allows for more accurate quantification of individual metabolites, better separation of isomers, reduction of matrix and ionization suppression (Figure 1.9) (Villas-Boas *et al.*, 2005b). In GC, the mobile phase carrying the metabolite is gaseous. This is why it is limited to volatile compounds and compounds that can be made volatile through derivatization. The disadvantage of GC is that the derivatization makes the querying of compounds from metabolite databases more difficult (Halket *et al.*, 2005). Nowadays, LC is often preferred to GC. In LC, the solutes are carried and eluted by a liquid mobile phase. High performance liquid chromatography (HPLC) with solid columns of porous stationary phase for trapping the metabolites is popular in metabolomics, because of improved separation and smaller solvent volumes. The stationary phase of the column separates metabolites based either on the size of particles, affinity of the solutes to the stationary phase or ion exchange (Wilson *et al.*, 2005). The two columns used in this study are a C4 column and C18 column. The C18 column is based on hydrophobic interactions between the solutes and the eluent molecules. It is based on an 18-carbon hydrocarbon attached to silica which works as a stationary phase, as the solvent elutes the compounds according to their hydrophobicity. The column is an example of reverse-phase chromatography (Dettmer *et al.*, 2007). The C4 column is less hydrophobic and therefore more suitable for more polar compounds. Desorption electrospray ionization (DESI) has been demonstrated to be robust in the identification of unlabeled and labelled metabolites in *E. coli* extracts (Jackson *et al.*, 2008). Another high sensitivity instrument that is available for the quantification of extracellular and intracellular metabolites is LC-ESI-MS, which can analyze down to a detection limit of 8 fmol (Carmella *et al.*, 2005). A recent technique applied is capillary electrophoresis-mass spectrometry (CE-MS) (Ramautar *et al.*, 2009).

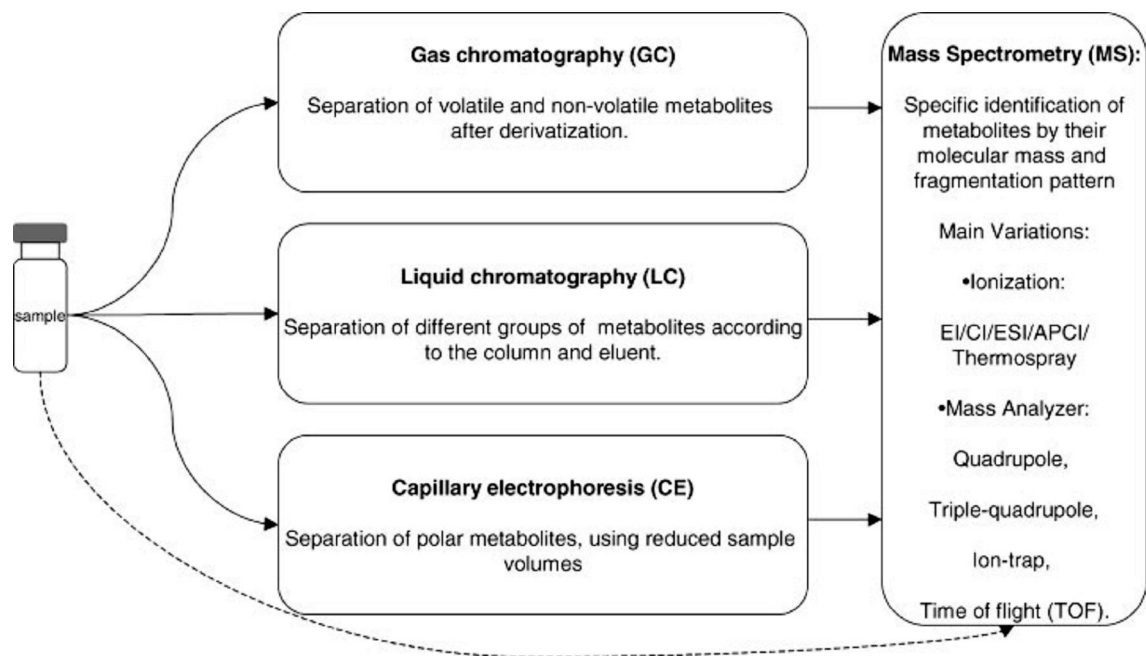


Figure 1.9: Three predominant chromatographic techniques have been incorporated in mass spectrometry (MS) analysis of metabolites. The sample can be directly analyzed by MS (dashed arrow), or it can be first resolved with different on-line separation techniques (full arrows). Adapted from Villas-Boas *et al.* (2005b).

1.4 *Escherichia coli*

Escherichia coli is a Gram-negative and non-spore forming rod bacterium. This bacterium is part of the large bacterial family, *Enterobacteriaceae*, most of which are harmless enteric bacteria and facultative anaerobes. They are part of the normal intestinal microflora found in the intestines of humans and animals. They also can be found in water and, soil or are parasites on a variety of animals and plants. Apart from *E. coli*, *Enterobacter* also colonize the gastrointestinal tract (Hooper and Gordon, 2001). They are beneficial to the human body by keeping the intestinal tract free from harmful bacterial infections, and help in digestion and in the absorption of many necessary vitamins, like vitamins B₁₂ and K (Kaper *et al.*, 2004). Other genera within the family such as *Salmonella*, *Klebsiella* and *Shigella* are human intestinal pathogens. When they spread throughout the body, they can cause diseases like diarrhoea, urinary tract infections and meningitis (Nataro and Kaper, 1998). Diarrhoea is a major health problem in the world with over two million deaths arising each year (Kosek *et al.*, 2003).

E. coli is one of the most important model organisms that have been studied. The first complete DNA sequence of an *E. coli* K12 genome was published in 1997 (Blattner *et al.*, 1997). Today it is commonly used in industry as a cloning host in recombinant DNA technology. Genes can be introduced into the microbes using plasmids which permit high level expression of protein and this protein may be mass produced in industrial fermentation processes. It is also useful as an indicator bacterium for resistance in pathogenic bacteria (von Baum and Marre, 2005). This bacterium is easy to grow, can be manipulating genetically and has simple nutritional and cultivation technique requirements. It also can ferment glucose and metabolically convert it into anabolites that are used to build up the cell (Kaper *et al.*, 2004). This versatile bacterium can live in the presence and absence of oxygen. Under anaerobic conditions, it can grow by fermentation, which produces acids and gas as end products, or anaerobic respiration where they use molecules such as nitrite, nitrate or fumarate as the final electron acceptor for respiratory electron

transport processes (Lupp and Finlay, 2005). This allows *E. coli* to adapt to both the anaerobic environment inside the intestine and external aerobic environments (Hooper and Gordon, 2001).

1.4.1 Growth of bacteria

The methods for growth of bacterial cultures can be classified into two main groups, which are called batch and continuous culture. Batch culture can be described as a growth occurring in a fixed volume of culture medium that is continuously being altered by the metabolism of the growing organisms until it is no longer suitable for growth. During the early stages of exponential growth in batch culture conditions may remain relatively stable, but as the cell number increases drastic change in the chemical composition of the medium occurs. A continuous culture is a flow system of constant volume to which medium is added continuously and from which continuous removal of any overflow can occur. Once such a system is in equilibrium, cell number and nutrient status remains constant and the system is said to be in a steady state. Comparing to continuous culture, nutrient concentration can affect both the growth rate and the growth yield of bacteria in a batch culture. At very low concentrations of a given nutrient, the growth rate is reduced; probably because that nutrient cannot be transported into the cell fast enough to satisfy metabolic demand. At moderate or higher levels of this nutrient, growth rates may not be affected while cell yield continues to increase.

1.4.2 Chemostat culture

The most common type of continuous culture device used for producing biomass for global metabolic studies is a chemostat. A chemostat is a bioreactor to which fresh medium is continuously added, while culture liquid is continuously removed. It provides a reproducible

environment and populations of cells in physiological steady state since the parameters, such as growth rate, dissolved oxygen and nutrient concentrations can be kept constant. The chemostat was developed by Monod (1950) and Novick and Szilard (1950) and permits control of both the population density and the growth rate of the culture. Two elements are used to control a chemostat: the dilution rate and the concentration of a limiting nutrient, which most commonly is the carbon source. However, other limiting nutrients (nitrogen and phosphorus) have been used as well (Kovárová-Kovar and Egli, 1998; Visser *et al.*, 2002). In a chemostat, culture growth rate and yield can be controlled independently of each other. Growth rate can be controlled by adjusting the dilution rate while growth yield can be controlled by varying the concentration of the nutrient present in a limiting amount. Steady state relationships in a chemostat are shown in Figure 1.10. The organism cannot grow fast enough at high dilution rates to keep up with the dilution. The culture is thus washed out of the chemostat. At very low dilution rates, a large fraction of the cells may die of starvation because the limiting nutrient is not being added fast enough to permit the maintenance of cellular metabolism. The cell density in the chemostat is controlled by the level of the limiting nutrient. The cell density will increase when the concentration of the nutrient in the fresh medium is high. In a chemostat, a population may be maintained in the exponential growth phase for long periods. It is a stable and reproducible system, a big advantage of the chemostat. Prolonged chemostat cultivation also leads to evolutionary adaptation of the cells to the culture conditions (Steiner and Sauer, 2003; Wick *et al.*, 2001).

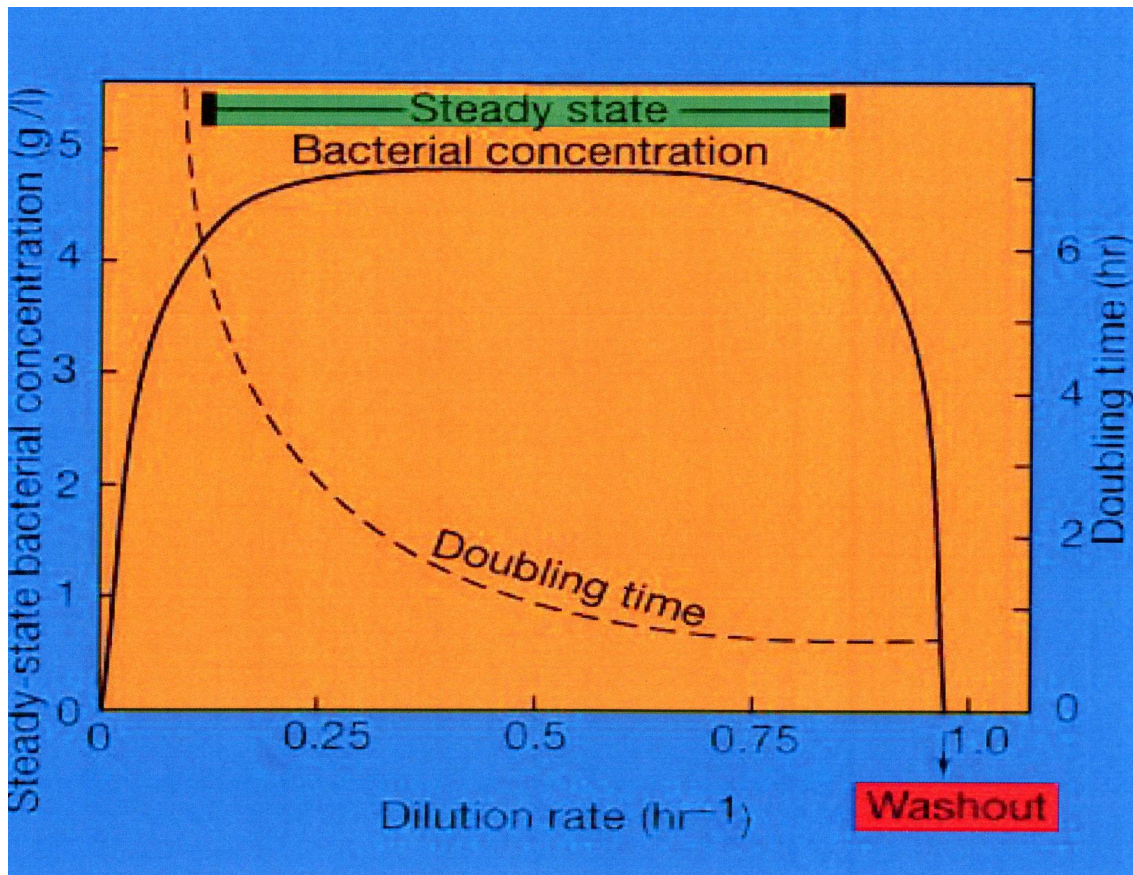
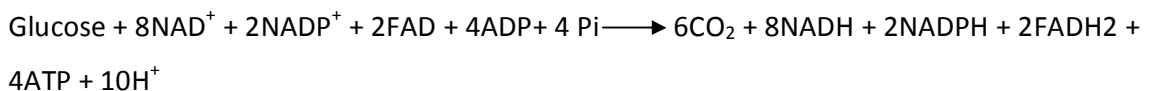


Figure 1.10: Effect of dilution rate in chemostat bacterial growth. Because the mass of bacteria remains constant in a chemostat, growth of the culture is linear, not exponential. Hence the time required to add a volume of liquid equal to the capacity of the chemostat is the doubling time.

1.4.3 The metabolic modes of *E. coli*

E. coli is a versatile bacterium that can sense and respond to oxygen availability in its environment and use different metabolic pathways to produce energy for growth. It prefers to grow aerobically, because the energy produced from substrates such as glucose is much greater in the presence of oxygen. In the middle of the gut, there is almost no oxygen and it has to grow anaerobically. However, close to the gut wall, the environment is microaerobic. *E. coli* is capable of changing its metabolic mode very rapidly as it encounters different growth conditions.

Pyruvate is the key intermediate in carbohydrate metabolism because it is the switch point between respiratory and fermentative metabolism. When oxygen is available, maximal energy is generated when a growth substrate such as glucose is completely oxidised. Therefore, aerobic respiration is the most productive and preferred metabolic mode (Guest *et al.*, 1996). Pyruvate produced by glycolysis is oxidatively decarboxylated by the pyruvate dehydrogenase complex (PDHC) to acetyl coenzyme A (Acetyl-CoA), carbon dioxide (CO₂) and NADH (Figure 1.10A). The *E. coli* PDHC consists of three subunits, pyruvate dehydrogenase (E1), acetyltransferase (E2) and dihydrolipoamide dehydrogenase (E3). In *E. coli* the complete oxidation of 1 mole of glucose in glycolysis and the TCA cycle generates 10 moles of NAD(P)H and 2 moles of FADH₂:



The reducing equivalents produced enter an electron transport chain and are used in the reduction of O₂ to H₂O. This creates proton gradients to generate energy with 34 ATP per mole of glucose. This irreversible PDHC reaction shows that it is important to prevent

unnecessary destruction of pyruvate. Within the complex, only the E1 reaction is irreversible. This means that the E1 reaction is the focus of the control steps.

Two alternative metabolic modes are achievable when no oxygen is present. Anaerobic respiration will take place if other electron acceptors, such as nitrates, sulfates, fumarate or trimethylamine N-oxide (TMAO) are available (Patschkowski *et al.*, 2000) (Figure 1.10B). During anaerobic respiration and fermentation, the role of pyruvate dehydrogenase complex (PDHC) is played by pyruvate formate lyase (PFL), the citric acid cycle (CAC) is repressed and the metabolic flow in the C4 section of the CAC is reversed. PFL converts pyruvate to acetyl CoA and formate; the formate produced cannot be used by the cell and it is secreted out of the cell. The preference for PFL has been demonstrated with several bacteria under carbon limitation conditions imposed either in a chemostat or in the presence of a poor carbon source (Melchiorsen *et al.*, 2001). Fumarate is reduced to succinate by fumarate reductase and some energy is conserved during this step. The energy produced is less than that achieved by aerobic respiration because the substrate (glucose) is only partially oxidized. Fermentation is the process by which cells release energy under anaerobic conditions, in the absence of any terminal electron acceptor. This involves the utilisation of carbon and energy sources to produce more reduced products. Energy is conserved by substrate level phosphorylation and formation of the overflow metabolites (acetate, ethanol, formate, succinate) to maintain the redox balance, which are secreted from the cell. However, in comparison, anaerobic respiration is more productive than fermentation (Figure 1.11).

E. coli is able to adapt its metabolism to maximise energy production under different redox conditions. Although PDHC is essential for maintaining cellular redox balance in an aerobic cell, no PDHC-based fermentation has been demonstrated in *E. coli* or other bacteria growing anaerobically. A very high sensitivity of PDHC towards NADH inhibition is related to the absence of PDHC activity under anaerobic conditions. The metabolic pathways used by

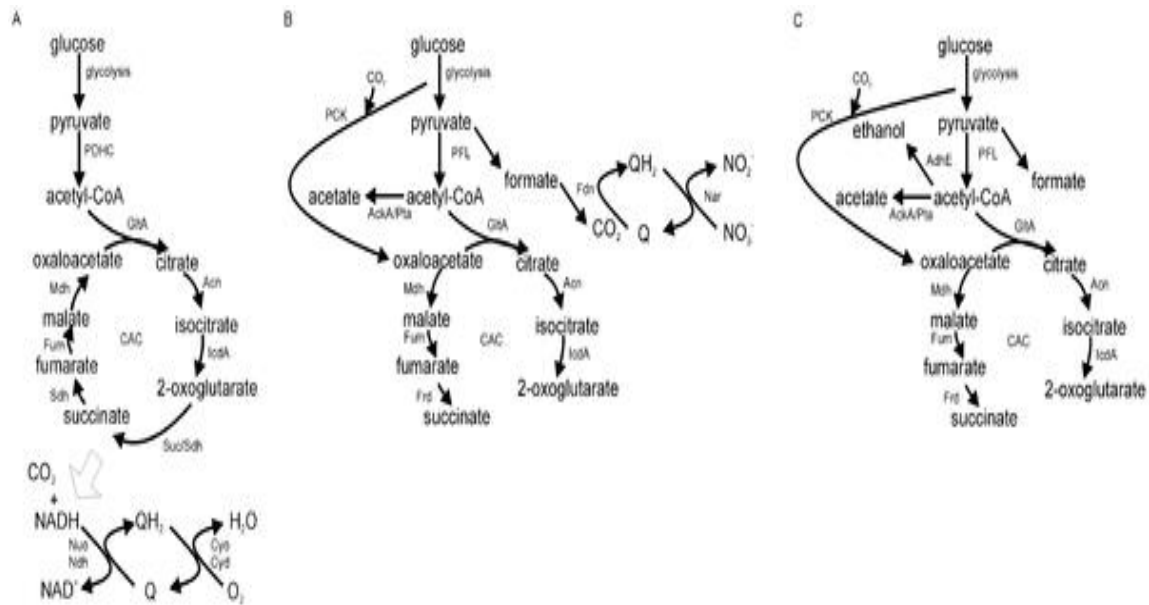


Figure 1.11: The metabolic modes of *Escherichia coli*. The main pathways of energy metabolism of *E. coli* growing under (A) aerobic respiration, (B) anaerobic respiration and (C) fermentation are shown in the above diagram. Under aerobic conditions, glucose is completely oxidized to CO₂ and water. Under anaerobic conditions, glucose is partially oxidized to CO₂ and acetate in the presence of an alternative electron acceptor such as nitrate. Under anaerobic fermentative conditions, glucose is converted to acetate, ethanol and formate and energy is conserved by substrate-level phosphorylation rather than oxidative phosphorylation. The enzyme activities responsible for each step are indicated: AckA, acetate kinase; Acn, aconitase B; AdhE, alcohol dehydrogenase; Cyo, cytochrome *bo* oxidase; Cyd, cytochrome *bd* oxidase; Fdn, formate dehydrogenase-N; Fum, fumarase (A, B, C); GltA, citrate synthase; lcdA, isocitrate dehydrogenase; Mdh, malate dehydrogenase; Nar, nitrate reductase; Nuo, NADH dehydrogenase I; Ndh, NADH dehydrogenase II; PCK, phosphoenolpyruvate carboxykinase; PDHC, pyruvate dehydrogenase complex; PFL, pyruvate formate lyase; Pta, phosphotransacetylase; Sdh, succinate dehydrogenase; Suc, 2-oxoglutarate dehydrogenase/succinyl-CoA synthetase (Trotter *et al.*, 2011).

E. coli are dependent on the nature of the growth substrate, oxygen availability and also the availability of any alternative electron acceptors, with aerobic respiration preferred to anaerobic respiration, with both preferred to fermentation. The ability of *E. coli* to adopt different metabolic modes is based on a number of redox-responsive regulatory mechanisms that manage this successful coordination (Green and Paget, 2004). Ultimately, this metabolic hierarchy is rooted in and maintained by altered patterns of gene expression.

1.4.4 Composition of the core *E. coli* metabolome

Knowledge of concentrations of extracellular and intracellular metabolites is important for quantitative analysis of the metabolic networks of microorganisms. Together with information about kinetic properties of the enzymes involved in specific pathways, information about the intermediary metabolites is of fundamental importance for characterization of the microbial metabolism through kinetic modelling. No single platform that allows a reliable analysis of a complete microbial metabolome has been described.

Most reports of the effects of oxygen on *E. coli* are at transcription level and compare aerobic and anaerobic cultures (Partridge *et al.*, 2007; Partridge *et al.*, 2006; Sauer *et al.*, 1999). Thus, there is relatively little information at metabolite level either on the steady state or during adaptation to changes in oxygen availability. In 2007, van der Werf and group have developed an analytical platform that allows the detection of all metabolites present in microbial metabolomes, known as in silico metabolomes (van der Werf *et al.* 2007). A total of 176 different metabolites were detected when applying this platform to mid-logarithmic *E. coli* cells, of which 61 metabolites currently are not present in the EcoCyc database (Keseler *et al.*, 2005). Quantification of intracellular metabolites in glucose-fed, exponentially growing *E. coli* was achieved by Bennett *et al.* (2009). They used liquid chromatography-tandem mass spectrometry to quantify 103 metabolites adding up to a total intracellular metabolite pool of approximately 300 mM. The intracellular metabolome

can be divided into a few groups: amino acids, nucleotides, central carbon intermediates and redox cofactors and glutathione. Glutamate was the most abundant compound, followed by glutathione, fructose-1,6-bisphosphate and ATP. Nearly 80% of the total molar concentration of the measured metabolites consists of the ten most abundant compounds (Table 1.2). For extracellular metabolites, (Trotter *et al.*, 2011) measured the concentration of extracellular metabolome of anaerobic steady state cultures by ¹H NMR. The results showed the presence of formate, acetate, ethanol, lactate and succinate, with formate dominating the extracellular volume, with the highest concentration (~35.1 mM), followed by acetate (~18.7 mM), ethanol (~9.7 mM), succinate (~5.4 mM) and lactate (~0.1 mM).

Metabolite	moles/l
Glutamate	9.6×10^{-2}
Glutathione	1.7×10^{-2}
Fructose-1,6-bisphosphate	1.5×10^{-2}
ATP	9.6×10^{-3}
UDP-N-acetyl-glucosamine	9.2×10^{-3}
Hexose-P	8.8×10^{-3}
UTP	8.3×10^{-3}
GTP	4.9×10^{-3}
dTTP	4.6×10^{-3}
Aspartate	4.2×10^{-3}

Table 1.2: Ten most abundant intracellular metabolites in glucose-fed, exponentially growing *E. coli* (Bennett *et al.*, 2009).

1.4.5 Pyruvate transport system and pyruvate levels in *E. coli*

Pyruvate is a key intermediate in catabolic and biosynthetic reactions and is the end product of glycolysis. There are two metabolic routes (glycolysis and pentose phosphate pathway) that can deliver this compound but the main pathway to synthesize pyruvate is by activation of pyruvate kinase, which catalyzes the final step of glycolysis: conversion of phosphoenolpyruvate (PEP) and adenosine diphosphate (ADP) to produce pyruvate and adenosine triphosphate (ATP). Pyruvate can also be synthesized from gluconate through the Entner-Doudoroff pathway (Eisenberg and Dobrogosz, 1967), and from PEP by the phosphotransferase transport system (PTS or PT system), coupled with glucose transport (Flores *et al.*, 2004). Pyruvate is the first non-phosphorylated intermediate in the glycolytic pathway and plays a central role in metabolism (Ponce *et al.*, 1995; Steiner *et al.*, 1998). There are specific transport systems that have been suggested for the glycolytic intermediates, e.g pyruvate, lactate, glycolate, phosphoenolpyruvate and lactate. All cells must have a pyruvate transport system, as defect in this system caused repression of gluconeogenic enzymes under some growth conditions (Wills *et al.* 1986). Studies by Martin and Konings (1973) concluded that pyruvate and lactate may share the same transport system, from inhibition studies on the uptake of lactate and succinate in membrane vesicles of *E. coli*.

Studies of the pyruvate transport system in *E. coli* have been carried out by Lang *et al.* (1987) and they found out that this energy requiring process is reduced when treated with an energy poison. Accumulation of pyruvate reached steady state at about 20 min, and after 10 min the concentration of pyruvate was calculated to be 8.1 mM and the external concentration was 0.05 mM, assuming that the fluid volume of the cell was 2.7 $\mu\text{l}/\text{mg}$ (dry weight) and the accumulated pyruvate was not significantly metabolized. This is consistent with an active transport process, where pyruvate is taken up against the concentration gradient. The K_m for pyruvate uptake was 19 μM in cells grown to the mid-log or stationary phase. Under normal conditions, the intracellular levels of an intermediate pyruvate are higher than the extracellular levels (Moses and Sharp, 1972). When exogenous pyruvate was added to the feed medium, both intracellular and extracellular pyruvate pool levels were

increased (Yang *et al.*, 2001). The pyruvate level that they measured (7 to 14 mM) was similar to the level reported by Lowry *et al.* (1971) and Snoep *et al.* (1992) (10 mM to 100 mM).

Pyruvate can also be metabolised by lactate dehydrogenase (LDH) to produce lactate, in the process regenerating NAD^+ from NADH. This reaction is important for redox balance in anaerobic growth. Pyruvate is thus a key metabolic control point even in anaerobic cells.

1.4.6 Pyruvate Kinase of *E. coli*

Pyruvate kinase plays an important role in pyruvate synthesis. It catalyzes the conversion of PEP and ADP to pyruvate and ATP in the glycolytic pathway. The reaction catalyzed by pyruvate kinase is irreversible *in vivo* and appears to be a control point for the regulation of glycolytic flux (Pertierra and Cooper, 1977). Several mechanisms exist to control pyruvate kinase activity. *E. coli* and *Salmonella typhimurium* possess two types of pyruvate kinase, of which one is inducible and activated by fructose-1,6-diphosphate, and the other is constitutive and activated by AMP. Pyruvate kinase is inhibited by ATP, acetyl-CoA and alanine. The phosphorylated form of pyruvate kinase is more strongly inhibited by ATP and alanine and has a higher K_m for phosphoenolpyruvate (PEP). Pyruvate kinase in tetrameric form (in the presence of Fructose-1,6-biphosphate) has high affinity for the substrate and is associated within the glycolytic enzyme complex (Jurica *et al.*, 1998).

There are two pyruvate kinase isoenzymes in *E. coli*, PykA and PykF, encoded by the *pykA* and *pykF* genes. PykF is the dominant activity when growth occurs aerobically on glucose. The specific activity of *pykF* is 15-fold higher than that of *pykA* (Ponce *et al.*, 1995; Siddiquee *et al.*, 2004). Many studies have been carried out to look at the function of PykF and PykA in metabolism. Single pyruvate kinase gene mutants under phosphotransferase system-inducing (PTS+) conditions lead to a slight decrease in bacterial growth on glucose (Ponce *et al.*, 1995). Studies by Ponce *et al.* (1998) and Zhu *et al.* (2001) showed that double knockout of *pykF* and *pykA* produced much less acetate than the wild type. It also demonstrates 25%

reduction in growth rate, indicating that the isoenzymes are not essential for growth on glucose. PEP inhibits phosphofructokinase and the imported glucose to hexose monophosphate (HMP) pathway is and also converted directly to oxaloacetate via PEP carboxylase (Cunningham *et al.*, 2009).

1.4.7 Oxygen-dependent regulation of the *E. coli* metabolism

Many environmental factors significantly affect microbial growth. The major ones however are temperature, oxygen, pH and osmotic effects. Studies on the adaptation of bacteria that lead to changes in metabolism have been growing rapidly. Oxygen tension is one of the most important environmental factors that can trigger major changes in gene expression and metabolite levels. Bacteria can respond to both excess oxygen and oxygen starvation, and remarkably they can survive and grow well when starved of oxygen. Oxygen availability plays a critical role in controlling the transcription of genes encoding these processes, ensuring that their expression is tightly regulated by growth conditions. All this adaptive process is coordinated by a group of global regulators.

Much progress has been made in recent years in analyzing sensing and regulation systems for the rapid response to availability of oxygen and the presence of other electron acceptors (Lin and Iuchi, 1991; Uden *et al.*, 1995). The adaptive responses are coordinated by a group of global regulators, of which the main ones are FNR (fumarate, nitrate reduction) and the two-component Arc (anoxic redox control) system. The Arc two-component system of *Escherichia coli* consists of ArcB and ArcA to repress aerobic respiration. ArcA is a cytosolic response regulator and ArcB is a transmembrane histidine kinase protein which senses unfavourable respiratory conditions. ArcB is activated during the transition from aerobic to microaerobic growth, and remains in the activated state during anaerobic growth. ArcB contains three catalytic domains: an N-terminal transmitter domain (H1), a central receiver domain and a C-terminal secondary transmitter domain (H2). ArcB is autophosphorylated at

the expense of ATP and the phosphoryl group is then transferred to ArcA by a His-Asp-His phosphorelay, which then becomes functional (Georgellis *et al.*, 1999). ArcA generally behaves as an anaerobic repressor, and represses the synthesis of some enzymes, such as CAC enzymes and pyruvate dehydrogenase, but at the same time it activates the expression of other enzymes such as cytochrome d oxidase and enzymes involved in fermentative metabolism (Iuchi and Lin, 1988).

On the other hand, the FNR system induces the expression of genes (such as pyruvate formate lyase, formate dehydrogenase, and fumarate reductase) under anaerobic conditions, which permit growing *E. coli* to transfer electrons to alternative terminal acceptors (Lin and Iuchi, 1991), while it represses the respiratory chain genes such as cytochrome *bd* (*cyd*) and cytochrome *bo* (*cyo*). The FNR protein is located in the cytoplasm and contains a $[4\text{Fe-4S}]^{2+}$ cluster that serves as a redox sensor (Unden *et al.*, 2002). This cluster is assembled into FNR during its biosynthesis under anaerobic conditions. This assembly results in simultaneous FNR dimerization and activity of specific DNA binding and transcription regulation. The $[4\text{Fe-4S}]^{2+}$ cluster is very sensitive to oxygen, and can be rapidly oxidized to $[2\text{Fe-2S}]^{2+}$ when oxygen is present (Kiley and Beinert, 1998). FNR dimer then dissociates and is no longer active in DNA specific binding and transcriptional regulation (Ralph *et al.*, 2001) (Figure 1.12). The concentration of the FNR protein is similar in both aerobic and anaerobic conditions (Sutton *et al.*, 2004).

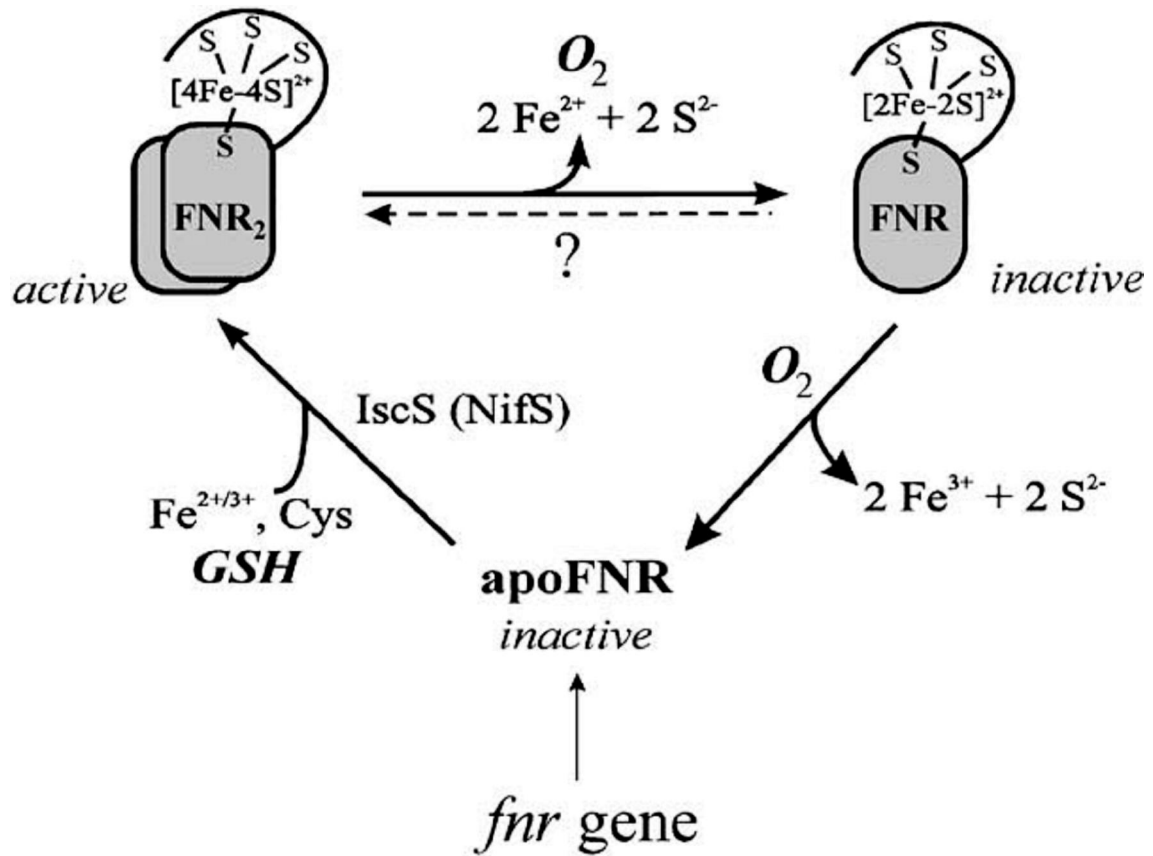


Figure 1.12: Different forms of FNR and their interconversion induced by oxygen as oxidizing agent and glutathione as reducing agent. Adapted from Uden *et al.* (2002).

1.5 Research Aims

The main purposes of this thesis were to analyse the metabolite changes of *E. coli* during the transition from anaerobic to aerobic, in order to understand the adaptation process to the new environment using a metabolomics approach. Even though *E. coli* is the best characterised organism, metabolic activity information is still poorly characterised. Understanding the rapid adjustments required in the metabolic network for cells to cope with these conditions may give significant information on the cellular function in the organism. This transition and the ability to survive in the new environment require significant reprogramming of the metabolic pathway. As discussed, the biggest challenge in this study is to determine the intracellular metabolite concentration, since the turnover rates are on a subsecond scale. In order to obtain reliable data, a rapid quenching method was developed and its error was measured, to assure data reflect the changes happening inside the cells. Pyruvate is a key junction in metabolism, for which the general hypothesis is that pyruvate responds the most to the new environment introduced to the cells. The experiments described in this thesis were carried out to examine this hypothesis using metabolomics, molecular biology and biochemical approaches.

CHAPTER 2

MATERIALS AND METHODS

2.0 Materials and Methods

2.1 Media and chemicals suppliers

All chemicals were obtained from BDH, GIBCO, Oxoid or Sigma-Aldrich, UK. Antibiotics were purchased from Sigma-Aldrich. Gases were supplied by BOC (UK), restriction enzymes; DNA ligase and DNA polymerase were bought from Promega, Roche or New England Biolabs (NEB). Oligonucleotides were ordered from Sigma-Genosys (UK). Water was always deionised and distilled.

2.2 Strains and plasmids

Bacterial strains and plasmids used throughout this study are detailed as below.

Table 2.1: List of bacterial strains and plasmid

Strain/Plasmid	Relevant characteristics	Source or reference
MG1655	<i>F-λ- ilvG- rfb-50 rph-1</i>	(Blattner <i>et al.</i> , 1997)
pGFP3.1mut3.1	Ampicillin resistance, <i>gfpmut3.1</i>	Clontech
pKD4	Template plasmid Amp ^R , FRT-flanked Kan	(Datsenko and Wanner, 2000)
pSIM18		(Chan <i>et al.</i> , 2007)

2.3 Growth media and conditions

2.3.1 Rich media

Escherichia coli were grown in sterile Luria-Bertani (LB) broth medium (Miller, 1972)

Recipe (per litre)	
LB broth	Tryptone (10g), Yeast extract (5 g), NaCl (10 g)
LB agar	Tryptone (10 g), Yeast extract (5 g), NaCl (10 g), Bacteriological agar (15 g)

Medium was sterilised by autoclaving. Once cooled to 50°C appropriate antibiotics were added to LB agar and the molten agar was poured into Petri dishes and allowed to set. Plates were stored at 4°C and used within four weeks. Antibiotics used include 20 mM glucose, ampicillin (100 µg/ml), IPTG (100 µg/ml), kanamycin (50 µg/ml) and hygromycin (150 µg/ml).

2.3.2 Evans defined medium

When a defined medium was necessary *E. coli* was grown in Evans medium (Evans *et al.*, 1970). The following components were added as indicated from stock solutions of the specified concentration.

	Stock concentration	Volume added
NaH ₂ PO ₄	2 M	5 ml l ⁻¹
KCl	2 M	5 ml l ⁻¹
MgCl ₂	0.25 M	5 ml l ⁻¹
Na ₂ SO ₄	0.4 M	5 ml l ⁻¹
CaCl ₂	0.0004 M	5 ml l ⁻¹
NH ₄ Cl	4 M	25 ml l ⁻¹
Nitrilotriacetic acid	-	0.38 g l ⁻¹
Trace element solution	-	5 ml l ⁻¹

Components were added in the order listed above and the solution was made up to the required volume with dH₂O with the final mix adjusted to a pH of 6.9 with 1 M KOH.

Trace element solution	
ZnO	1.03 g l ⁻¹
FeCl ₃ .6H ₂ O	13.5 g l ⁻¹
MnCl ₂ .4H ₂ O	5 g l ⁻¹
CuCl ₂ .2H ₂ O	0.43 g l ⁻¹
CoCl ₂ .6H ₂ O	1.19 g l ⁻¹
H ₃ BO ₃	0.16 g l ⁻¹
Na ₂ MoO ₄ .H ₂ O	0.01 g l ⁻¹

HCl (37%, 20 ml l⁻¹) was added to lower the acidity of the trace element solution, which helps keep the other metal ions in solution. Media were supplemented with various carbon sources prior to use.

2.3.3 Growth of *E. coli*

Aerobically grown *E. coli* strains were typically cultured in 250 ml flasks, with shaking at 250 rpm in volumes of 5-50 ml of medium. Cultures were usually grown for 16 h at 37°C.

2.3.4 Measurement of bacterial growth

Bacterial growth was monitored by determining the optical density at 600 nm (OD₆₀₀) with 1 ml samples using a spectrophotometer. Samples with an OD₆₀₀ greater than 0.8 were diluted 1:10 prior to determination of the OD₆₀₀.

2.3.5 Storage of strains

Strains were maintained for up to one month on solid media at 4°C. For long-term storage bacterial strains were stored as glycerol stocks. Bacterial cells from 5 ml overnight cultures of the strains to be stored were collected by centrifugation and resuspended in 1.25 ml LB broth and 1 ml 80% (v/v) sterile glycerol. Appropriate antibiotics were included and strains stored at -80°C, where they are viable for up to five years.

2.4 Metabolite analysis and measurement

2.4.1 Bacteria and growth conditions

E. coli strain MG1655 was grown in a 1 L capacity Labfors 3 chemostat (Infors) (Figure 2.1) at 37°C with stirring at 400 rpm. The pH was maintained at 7.0 by automatic titration with sterile 1 M potassium hydroxide (KOH) or 1 M sulphuric acid (H₂SO₄). Carbon-limited Evans medium (section 2.3.2) (Evans *et al.*, 1970) was used with 20 mM glucose as the carbon source. 5 ml of overnight culture was inoculated into the media vessel and the cells were left to grow overnight in the chemostat as a batch culture. Steady state was achieved by feeding growth medium at a dilution rate of 0.2 h⁻¹ for 4-5 vessel volumes. Anaerobic cultures were maintained by sparging with N₂ (95%) and CO₂ (5%) at 0.4 L min⁻¹. Dissolved oxygen levels were monitored by using a TruDO Dissolved Oxygen Sensor (Finesse). The change to micro-aerobic conditions was controlled by Iris software, which switching the gas mix ratio of N₂ and CO₂ to air to maintain the dissolved O₂ tension in the culture at 5% (~10 µM).

2.4.2 Sampling method

2.4.2.1 Extracellular metabolites

1 ml samples were collected from the chemostat and centrifuged at 14000 rpm in a microfuge for 1 min at 20°C. The 900 µl of clear supernatant was transferred into a clean tube and stored at -20°C for future analysis.

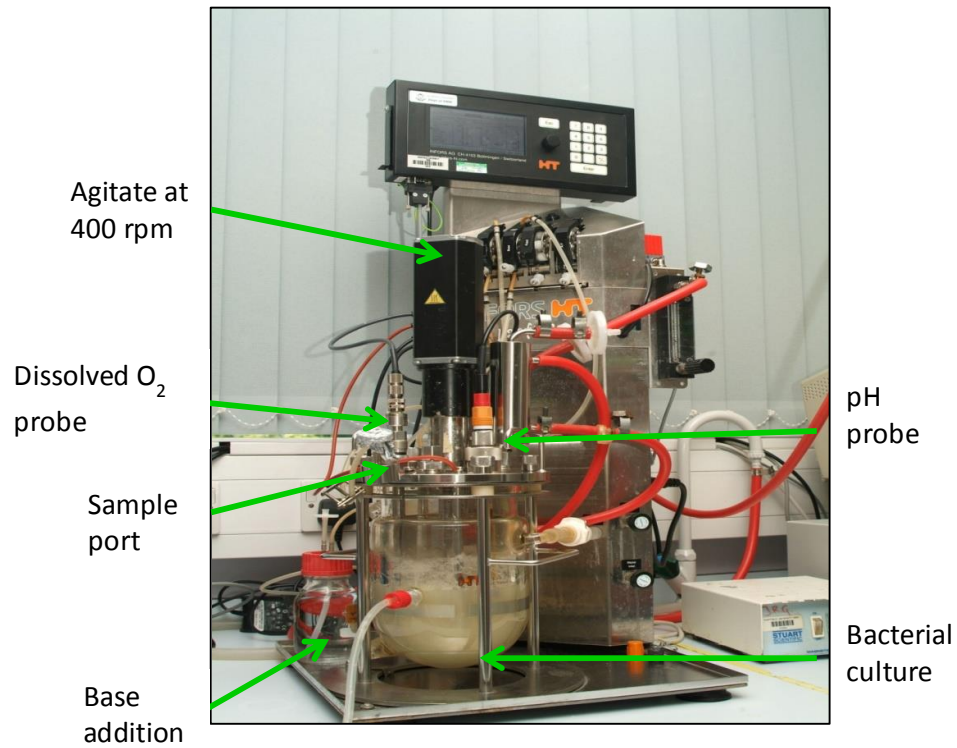


Figure 2.1: Chemostat used to grow the bacterial culture. Growth occurs at a constant rate where all the parameters remain constant.

2.4.2.2 Intracellular metabolites (Quenching method)

This quenching technique is based on the ethanol and sodium chloride (NaCl) method of Spura *et al.* (2009) and has been adapted as described in Chapter 3. Samples (20 ml) collected from chemostat are transferred into a 50 ml falcon tube containing 20 ml of quenching solution (40% ethanol v/v + 0.8% NaCl w/v), which had been precooled to -35°C by placing in an insulated bath containing isopropanol that had been cooled by addition of dry ice (Figure 2.2). The sample mixture was then mixed instantly by inversion, producing a cell suspension at approximately 0°C and left to cool down to -5°C in the -35°C isopropanol bath over the course of 2-3 minutes (Figure 2.2). The cells are stirred all the time at this stage, using the thermometer. Then the cells were centrifuged at $3940 \times g$ at -11°C for 5 min in a precooled centrifuge (Beckman Avanti HP-25I, JLA-10.500) and the supernatant was removed by aspiration, ready for metabolite extraction.

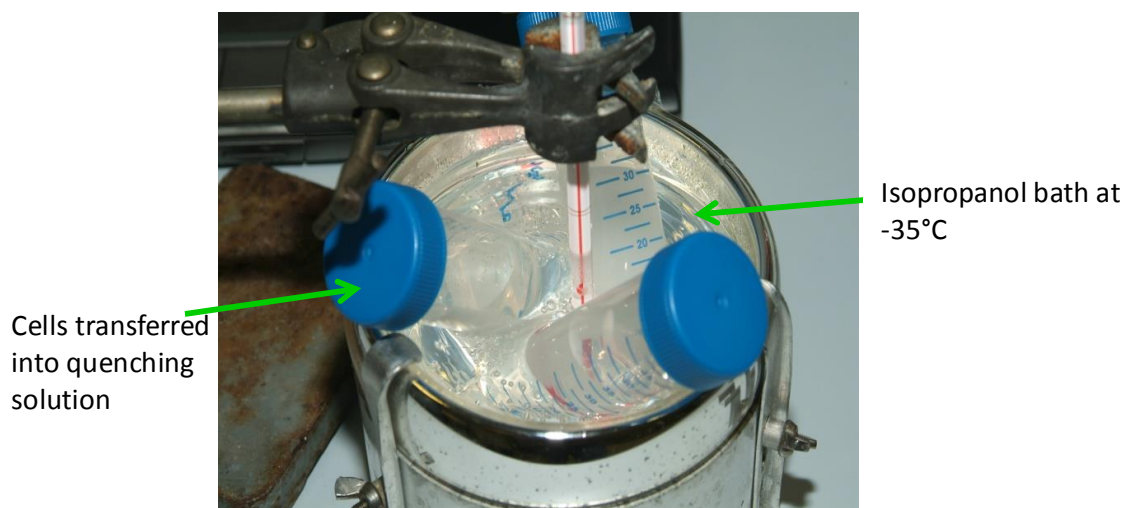


Figure 2.2: Cold ethanol-sodium chloride quenching

2.4.2.3 Unquenched method

Samples (20 ml) were removed from the chemostat and immediately centrifuged at 5000 *g* at 4°C for 5 min. The supernatant was aspirated off and the pellet immediately frozen in liquid N₂. Then metabolite extraction was carried out as in section 2.3.3.

2.4.3 Intracellular metabolite extraction

Extraction of metabolites from the cell pellets was performed with the cold methanol method of Faijes *et al.* (2007). After centrifugation, cells were air dried using a vacuum pump before putting into liquid nitrogen (LN₂). Then, 500 µl cold methanol (precooled to -80°C in the -80°C freezer) was added to the cells. The suspension was vortexed, and the cells were freeze-thawed three times in LN₂ before being centrifuged again. The supernatant was transferred into an Eppendorf tube and the freeze-thawing and centrifugation step was repeated once again. The final supernatant was transferred to the same tube as before. The final supernatant was concentrated for 5-6 hrs by using a cell concentrator. The pellet obtained was stored at -20°C awaiting further analysis.

2.4.4 Metabolite analysis by NMR

2.4.4.1 Sample preparation

For extracellular metabolite analysis, the supernatant fractions from section 2.4.2.1 were analysed in a volume of 500 μl containing 450 μl sample, 50 μl D_2O and 1 mM trimethylsilylpropionate (TSP) (as 5 μl of a 100 mM stock). For intracellular samples, the pellet was resuspended in 500 μl D_2O , and 100 μM of TSP (as 5 μl of a 10 mM stock). All samples were analysed in 5 mm diameter NMR tubes. All samples prepared contained D_2O for locking on the deuterium frequency and TSP that served as a chemical shift and concentration reference.

2.4.4.2 NMR analysis

The spectra were acquired on a Bruker DRX-500 spectrometer operating at 500 MHz and 298 K (Figure 2.3). The H_2O signal was reduced by pre-saturation for 2 s applied during the recycle time. A spectral width of 6,256 Hz was excited using a 90° pulse. 128 scans (extracellular sample) and 1024 scans (intracellular sample) were used following 4 dummy scans, for a total experiment time of 10 min for extracellular samples and 1 hr for intracellular samples. For extracellular samples, a pulse program was used that included a Hahn echo delay before acquisition, in order to give a flatter baseline. Manual and computer shimming was performed for each sample and FIDs were processed by multiplication by an exponential function equivalent to 1.0 Hz line broadening prior to Fourier transformation. Spectra were processed and peaks quantified by integration by using the Bruker software Topspin. Chemical shifts and concentration were calculated by referencing to TSP. For ethanol, acetyl aspartate and lactate, signal used for quantification as follows: ethanol (both

of the signal were used); acetyl aspartate (only the methyl signal used) and lactate (the methyl signal used, the other signal is overlapped).



Figure 2.3: Bruker 500 MHz NMR spectrometer, equipped with a TXI 5 mm triple resonance high resolution probe with z gradient.

2.4.5 Pyruvate assay

Intracellular pyruvate concentration was measured using the Enzychrome™ Pyruvate Assay Kit (Bioassay Systems). Cells collected from the chemostat were quenched and extracted as described in sections 2.4.2.2 and 2.4.3. A pyruvate standard curve was prepared by mixing 10 µl of 25 mM standard with 490 µl of distilled water. Then the standard was diluted in distilled water into a 96-well plate to obtain a range of pyruvate concentrations as shown below.

No	Standard + H ₂ O	Vol (µl)	Pyruvate (µM)
1	100µL + 0µL	100	500
2	80µL + 20µL	100	400
3	60µL + 40µL	100	300
4	40µL + 60µL	100	200
5	30µL + 70µL	100	150
6	20µL + 80µL	100	100
7	10µL + 90µL	100	50
8	0µL + 100µL	100	0

10 µl volumes of samples and standards were transferred into separate wells of the 96-well plate. Then, 90 µl Working Reagent (prepared by mixing Enzyme Mix and Dye Reagent in a ratio of 94:1 (v/v) were transferred into each assay well and mixed by tapping the plate. The mixtures were incubated for 30 min at room temperature before the OD₅₇₀ was taken in a plate reader. The blank OD was subtracted from the standard OD values and the OD values were plotted against the standard concentration to generate a standard curve. The slope was determined using linear regression fitting. The pyruvate concentration of sample was calculated using the formula below. OD_{sample} and OD_{H₂O} are optical density values of the sample and water.

$$\text{Concentration of pyruvate} = \frac{\text{OD}_{\text{sample}} - \text{OD}_{\text{H2O}}}{\text{Slope}} \quad (\mu\text{M})$$

2.4.6 Pyruvate kinase enzyme assay

Pyruvate kinase activity during the transition from anaerobic to aerobic was measured using the Pyruvate Kinase Activity Assay Kit (BioVision). Supernatant and pellet samples was collected at different time point, quenched and sonicated followed by use of a kit. A pyruvate standard curve was prepared by mixing 10 μl of 100 nmol/ μl standard with 990 μl of Assay Buffer. The dilution of the standard was prepared by adjusting volume of 0, 2, 4, 6, 8 and 10 μl of the diluted standard to 50 μl /well with Assay Buffer to generate 0, 2, 4, 6, 8 and 10 nmol/well of the Pyruvate Standard. Then, sample was prepared by mixing enough reagents for the number of standard and assays to be performed as shown below:

	Pyruvate kinase measurement	Background control
Assay Buffer	44 μl	46 μl
Substrate mix	2 μl	----
Enzyme mix	2 μl	2 μl
OxiRed TM Probe	2 μl	2 μl

50 μl of the reaction mix was added to each well containing the pyruvate standard, samples and control and mixed well. The OD₅₇₀ was taken at T1 to read A1, and the samples was incubated for 10-20 min at 25°C before taking the reading at T2, to read A2. The pyruvate standard curve was plotted. The pyruvate kinase activity can be calculated using the formula below.

$$\text{PK activity} = \frac{B}{(T2-T1) \times V} \times \text{Sample Dilution Factor} = \text{nmol/min/ml} = \text{mU/mL}$$

where: B is the pyruvate amount from pyruvate standard curve (in nmol)

T1 is the time of the first reading (A1) (in min)

T2 is the time of the second reading (A2) (in min)

V is the sample volume added into the reaction well (in ml)

2.5 DNA methods

Plasmid DNA was isolated from 5 ml overnight cultures using QIAGEN miniprep kits according to the manufacturer's instructions. Typically, 10 to 15 µg plasmid was recovered for 5 ml cells.

2.5.1 Quantification and purity determination of nucleic acids

Concentration of DNA and RNA were measured spectroscopically using an Eppendorf BioPhotometer. Samples of nucleic acid solutions (100 µl) were read in an Eppendorf UVette and the BioPhotometer was used to calculate nucleic acid concentrations using set-programmed values. The BioPhotometer also measured the purity of the sample by calculating the A_{260}/A_{280} ratio. A ratio of 1.8 indicated a sample of high purity.

2.5.2 Agarose gels

Agarose gel electrophoresis was used for the analysis and purification of DNA. Gels were made to 1-2% agarose, depending on the size of DNA fragments to be separated, and made up in 1X TAE buffer (see below). The agarose was dissolved by heating and once cooled to approximately 50°C, 0.5 µg/ml of ethidium bromide (to enable DNA visualization under UV light) was added. Generally 10 µl of DNA sample including 3 µl loading buffer (Fermentas) was loaded per lane and run alongside the appropriate markers. This was generally Hyperladder I. Electrophoresis was carried out at 100 V for up to 1 h in Bio-Rad electrophoresis apparatus.

50X TAE	
242 g	Tris
57.1 ml	Glacial acetic acid
100 ml	50 mM EDTA pH 8
Made up to 1 litre with dH ₂ O	

2.5.3 Extraction and purification of DNA from the agarose gel

DNA fragments within agarose gels were visualised under UV light and excised using a clean scalpel blade. DNA was then purified from the gel fragments using the QIAGEN Gel Extraction kit, following the manufacturer's instructions.

2.5.4 Purification of DNA

When necessary, DNA samples were purified using a Qiagen PCR purification kit, according to manufacturer's instructions.

2.5.5 Digestion of DNA with restriction enzymes

Restriction digests were performed in a reaction volume of 50 μ l, 10 units of enzyme and the appropriate buffer to a final 1x concentration. BSA was added when required. Reactions were incubated for 1 h at 37°C. Reactions were stopped by heat inactivation or by separation of fragments by agarose gel electrophoresis and subsequent purification (section 2.4.2 and 2.4.3).

2.6 Gene deletion using the Lambda-Red system

Gene knockout mutants of *E. coli* were created using a linear transformation protocol adapted from the method of Datsenko and Wanner (2000) to introduce a kanamycin cassette into the genes of interest. Two mutants were created: pykF-3xFLAG and pykF-GFP by using a 2-step PCR reaction.

2.6.1 Primer design

Oligonucleotide primers were designed manually to amplify the kanamycin cassette from the plasmid pKD4; such that a 3xFLAG-tag or GFP coding sequence was added at the 5' end of the kanamycin cassette. The primers also added 40 bp sequences at the 5' and 3' ends of

the PCR product that was complementary to adjoining 40-bp sequences at the 3' end of the *pykF* gene, so that the resultant PCR products would add a 3xFLAG-tag or GFP sequence plus a kanamycin cassette at the C-terminal end of *pykF*. This necessitated the use of two assembly PCR reactions. Primers used in creation of *pykF*-3xFLAG and *pykF*-GFP mutants were presented below in Table 2.2 and 2.3.

Table 2.2: Primers for use in creation of *pykF*-3XFLAG mutant

Primer	Description
<p>pykF_3xFLAG_PCR1F</p> <p>TTACAAAGATCACGACGGCGATTATAAAGACCATGATAT CGATTATAAAGATGACGACGATAAATAAatttgcttGTGTA GGCTGGAGCTGCTTC</p>	<p>The sequence in blue corresponds to the sequence of the FLAG-tag; the sequence in red is a stop codon; the lower case sequence is a linker; and the sequence in green is the start of the kanamycin resistance cassette sequence</p>
<p>pykF-3xFLAG_PCR1R</p> <p>AAAGCGCCCATCAGGGCGCTTCGATATACAAATTAATTC ACATATGAATATCCTCCTTTAG</p>	<p>The sequence in green is complementary to the end of the kanamycin cassette; the sequence in black is complementary to the sequence immediately 3' of the end of the <i>pykF</i> gene.</p>
<p>pykF-3xFLAG_PCR2F</p> <p>ACCGAGCGGCACTACTAACACCGCATCTGTTACGTCCT GGATTACAAAGATCACGACGG</p>	<p>The sequence in red is the last 40 bases at the 3' end of the <i>pykF</i> gene; the sequence in blue is the start of the FLAG-tag, including an extra GA sequence</p>
<p>pykF-3xFLAG_PCR2R</p> <p>AAAGCGCCCATCAGGGCGA</p>	<p>This is identical to the start of PCR1R. In other words, this merely re-amplifies the same sequence</p>

Table 2.3: Primers for use in creation of *pykF*-GFP mutant

Primer	Description
<p>pykF-GFP_PCR1F</p> <p>ACCGAGCGGCACTACTAACACCGCATCTGTTACGTCCT GCGTAAAGGAGAAGAACTT</p>	<p>The sequence in red is the 3' end of the <i>pykF</i> gene; the sequence in blue is the 5' end of the GFP gene</p>
<p>pykF-GFP_PCR1R</p> <p>GAAGCAGCTCCAGCCTACACTTATTTGTATAGTTCATCCA</p>	<p>The sequence in blue is complementary to the 3' end of GFP. The region in black is complementary to the 5' end of the kanamycin cassette</p>
<p>pykF-GFP_PCR2R</p> <p>GCGCCCATCAGGGCGCTTCGATATACAAATTAATTCACA ACATATGAATATCCTCCTTAG</p>	<p>The region in blue is complementary to the 3' intergenic region of <i>pykF</i>, and the region in black is complementary to the 3' end of the kanamycin cassette</p>

2.6.2 Polymerase chain reaction (PCR)

A Techne TC-312 thermocycler and Extensor Hi-Fidelity DNA polymerase (Abgene) were generally used in PCR reactions. The standard conditions for a 50 μ l PCR reactions were:

25 μ l Extensor Hi-Fi Master Mix*

4 μ l 10 pmol/ μ l forward primer

4 μ l 10 pmol/ μ l reverse primer

4 μ l Template DNA

13 μ l sterile dH₂O

*Extensor Hi-Fidelity PCR master mix contains Taq DNA polymerase (1.25 U per reaction volume), dNTPs (350 μ M each) and MgCl₂ (2.25 mM) in Extensor Reaction Buffer.

Amplification conditions used for pykF-3xFLAG and pykF-GFP were as below:

Step	pykF-3xFLAG			pykF-GFP		
	Temp	Time	Cycle	Temp	Time	Cycle
Initial denaturation	95°C	15 min	1	94°C	3 min	1
Denaturation	94°C	45 sec		94°C	30 sec	
Annealing	55°C	1 min	35	55°C	30 sec	35
Extension	72°C	2.5 min		68°C	2 min 45 sec	
Final extension	72°C	10 min	1	68°C	10 min	1

2.6.3 Preparation of linear DNA

2.6.3.1 *pykF*-3xFLAG

The first PCR reaction (section 2.6.2) was carried out to amplify the kanamycin cassette from pKD4 using primers that add a 3xFLAG tag and a stop codon upstream of the kanamycin cassette and a 40 bp region of homology to the 3' intergenic region of *pykF* downstream of the cassette. The PCR product was visualized by agarose gel electrophoresis (section 2.5.2) and purified using a PCR purification kit (section 2.5.3). The template DNA (pKD4 plasmid) was then removed by digestion by *Dpn* I (section 2.5.5), which digests methylated DNA, and the PCR product was repurified. Then, the second PCR was performed using the product from PCR 1 as a template. A 40 bp sequence corresponding to the final 40 3' bases of *pykF* was added upstream (stop codon removed), and the downstream end was reamplified without change, before the PCR product was visualized by agarose gel electrophoresis and purified.

2.6.3.2 *pykF*-GFP

In the first PCR reaction, the coding sequence of GFPmut3.1 was amplified and a 40 bp region was added in front of the GFP gene corresponding the 3' end of *pykF* (the *pykF* stop codon was removed). A stop codon and a 20 bp sequence was added by the reverse primer to the end of GFP to allow amplification of the kanamycin cassette from pKD4 (in the next PCR). The PCR product was confirmed as the correct size by agarose gel electrophoresis (section 2.5.2) and gel purified (2.5.3) to remove template. The purified product was then used as a forward primer to amplify the kanamycin cassette in the second PCR reaction. A 40 bp sequence was added downstream of the kanamycin cassette by the PCR2R primer, complementary to the 3' intergenic region of *pykF*. A final PCR was carried out to complete

the whole 2.3 kbp product efficiently and provide sufficient yield for transformation. The final product was visualized by agarose gel electrophoresis and purified.

2.6.4 Preparation and transformation of electrically competent cells

An overnight culture of SL1344pSIM18 was set up in 5 ml of hygromycin LB (LB plus 150 $\mu\text{g ml}^{-1}$ hygromycin) and grown at 30°C in a shaker. Then 4 ml of overnight culture was pipetted into 100 ml of hygromycin LB and grown to an OD_{600} of 0.3. The culture was split into 2 x 50 ml Falcon tubes before a heat shock step was performed in a 42°C water bath for 15 min and then the culture was cooled immediately in an ice-bath for 10 min. Cells were centrifuged at 4°C for 10 min at 4000 rpm. The pellet was resuspended in 45 ml of ice-cold water and the cells were spun down again. The supernatant was discarded and the pellet was again resuspended in 45 ml of ice-cold water before centrifugation and resuspension in 1.5 ml of ice-cold sterile water. The cells were transferred into Eppendorf tubes and washed 5 times with 1.5 ml of ice-cold water, with the cells centrifuged each time at 10000 rpm at 4°C for 2 min. The supernatant was decanted and the pellet was resuspended in 120 μl of ice-cold water. The competent cells were split into 40 μl aliquots, and used immediately.

Competent cells were transformed by the addition of 3 μg of DNA to 40 μl aliquots of cells in an ice-cold electroporation cuvette and pulsed at 1800 V in a Hybaid Cell Shock Electroporator. LB medium (1 ml) was added to the cuvette and then the solution was transferred into a fresh tube. The suspension was incubated at 37°C for 2 hours and then centrifuged at 8000 rpm for 4 min. The pellet was resuspended in 100 μl of LB broth and spread onto LB agar plates (section 2.3.1) containing 50 μgml^{-1} kanamycin. Plates were then incubated overnight at 37°C and colonies were checked by PCR (section 2.6.5).

2.6.5 PCR verification

A colony was picked using a sterile pipette tip into 50 μ l dH₂O and vortexed before heating at 100°C for 10 min. Then the mixture was centrifuged at 14000 rpm for 1 min. Aliquots (4 μ l) of the supernatant were added to the standard components for a 50 μ l PCR reaction (Section 2.6.2). Reactions were then incubated in a Techne TC-312 thermocycler using a programme as in Section 2.6.2. Samples (10 μ l) of the resulting PCR products were visualized after electrophoresis on an agarose gel (Section 2.5.2) with appropriate markers.

Primers for use in PCR verification of recombinant clones

pykF_CheckF	TGGCACACAAAGGTGACG
-------------	--------------------

pykF_CheckR	GGATGCTTCCATCGGATT
-------------	--------------------

These amplify outside of our gene fusion from which we expected to see bigger bands.

2.7 Transduction of *E. coli* DNA by P1vir1 phage

P1 transduction was used to move the gene fusion into a fresh MG1655 background. This removed the possibility of secondary metabolism, caused by λ -red mediated recombination and removed pSIM18 contamination of the strain.

2.7.1 Preparation of lysate

A colony from a verified plate was picked and grown overnight in 5 ml LB broth with 5 mM CaCl₂. P1 phage stock was diluted with phage dilution buffer (10⁻³, 10⁻⁴, 10⁻⁵, 10⁻⁶ dilutions) in sterile Eppendorf tubes. Donor cells (100 µl) were mixed with 50 µl of each of the diluted P1 phage suspensions and incubated for 20 min at 37°C. Suspensions were then added to 3 ml molten LB-agar soft top agar (0.65 % (w/v) containing 1% glucose and 2.5 mM CaCl₂ pre-warmed to 50°C in 4 inch glass tubes, and mixed thoroughly before pouring evenly into prewarmed phage lysate plates. The soft-top layer was allowed to set before incubation at 37°C overnight. The plates were collected the next day and plaques were counted across the dilution series. Then 5 ml of phage dilution buffer was overlaid on the soft-top layer of the plate that was nearly confluent and incubated at 4°C for 5 h, with gentle agitation. After 5 h, the LB broth together with the soft top layer was collected into a falcon tube, and vortexed before centrifugation for 15 min at 6000 rpm. The supernatant was filter sterilized with a 45 µm filter into a sterilized glass universal, containing water, together with a few drops of chloroform to prevent bacterial growth, and stored at 4°C.

Phage dilution buffer	
Tris base	1.35 g
MgSO ₄ .7H ₂ O	2.73 g
CaCl ₂ .2H ₂ O	0.82 g
NaCl	3.24 g

*pH 7.5, autoclaved

2.7.2 Transduction by P1 phage

P1 phage lysate from 2.6.1 was serially diluted (10^0 - 10^{-2}) in phage dilution buffer and 100 μ l aliquots were mixed with 100 μ l recipient cells in sterile Eppendorf tubes and incubated at 37°C for 15 min. The mixture was then plated into LB agar plates containing kanamycin (50 μ g ml^{-1}) supplemented with 125 μ M sodium pyrophosphate and grown for 16 h at 37°C. Sodium pyrophosphate binds Ca^{2+} to stop phage infection on the plates. Resistant colonies were purified by streaking out twice on fresh LB agar plates plus kanamycin to ensure a monoculture.

2.7.3 Confirmation of lysogeny via streak testing

Cross streaking was carried out to distinguish the true lysogens from pseudo-lysogens where the P1 phage shall infect the recipient cell. Each strain was cross-streaked across lines of wild-type phage P1. Successful transduction will be susceptible to wild-type P1. Pseudo-lysogens will be susceptible to P1. A sterile pipette was used to dribble a thin, continuous line of phage P1 across the surface of each of LB plates. Another sterile pipette was used to repeat this procedure using a stock of P1 WT. The phage was allowed to dry completely for 5-10 mins. Then a sterile pipette was used to pick isolated colonies of the possible transductants and inoculate them as a single streak across the phage stripe. The cross-streak plate was incubated at 37°C.

2.8 Protein Methods

2.8.1 SDS-PAGE

SDS-PAGE analysis was carried out as described by Laemmli (1970) using the BioRad Mini Protean 3 system as described in the manufacturer's instructions. The glass plates were cleaned with ethanol and locked into the clamping assembly and secured firmly to ensure no leakage from the base. A resolving gel mixture (10 ml) of 10% acrylamide was prepared and poured between the plates. Water saturated butanol (100 μ l) was then layered over the gel, which was then allowed to set. After this time the butanol was removed before a prepared stacking gel mix was poured up to the plate's rim and a comb inserted to produce the wells for sample loading. After the stacking gel had set, the comb was removed, wells rinsed thoroughly and the assembled apparatus was placed into the running tank with appropriate running buffer (see below). Protein samples (15 μ l) were denatured prior to loading by the addition of 10 μ l 3x loading buffer (see below) and boiling for 5 min. Samples were loaded and the gel was run at 200 V for the necessary duration with prestained size markers loaded to allow estimation of protein molecular weight and visualize successful bands. Following electrophoresis the gel was stained in Coomassie Blue stain for 4 h then in destain for 16-20 h.

Table 2.4: Composition of SDS-PAGE for 10% gel

Solution	Resolving gels	Stacking gels
H ₂ O	4 ml	2.7 ml
30% acrylamide	3.3 ml	0.67 ml
1.5 M Tris pH 8.8	2.5 ml	0.5 ml
10% SDS	0.1 ml	0.04 ml
10% APS	0.1 ml	0.04 ml
TEMED	0.004 ml	0.004 ml

1x SDS-PAGE running bufferGlycine 14.4 g l⁻¹Tris 3 g l⁻¹SDS 1 g l⁻¹

*Adjust to pH 8.3

3x SDS-loading buffer

Glycerol 20% (v/v)

Tris-HCl (pH 6.8) 100 mM

SDS 4% (v/v)

Bromophenol blue 0.02% (v/v)

 β -mercaptoethanol 200 mM1x Coomassie blue stain

Methanol 20% (v/v)

Acetic acid 7.5% (v/v)

Coomassie blue 0.1% (w/v)

Destain (500 ml)

200 ml Methanol 40% (v/v)

50 ml Acetic acid 10% (v/v)

250 ml Water 50% (v/v)

2.8.2 Western blot

2.8.2.1 Transfer of proteins to a nitrocellulose membrane

Protein under investigation was first separated by SDS-PAGE (Section 2.8.1) and then transferred to Immuno-Blot™ PVDF membrane (BioRad) using a BioRad Transblot Electrophoretic Transfer Cell in accordance with the manufacturer's instructions. The membrane, gel, filter paper and sponge were soaked in the transfer buffer (see below) for 10-20 min. The plastic clamp was opened in a large bowl, where the soaked sponge was added onto the negative side, followed by soaked filter paper, membrane, soaked filter paper and finally the soaked sponge. The clamp was closed and placed into the half-full blotting tank, before adding the pre-cooled Bio-Ice cooling unit to ensure the apparatus does not overheat as it transfers. A small magnetic stirrer was added before the lid was placed on the tank and the gel was run at 100 V for 1 h.

2.8.2.2 Blocking the gel and antibody binding

The membrane was removed from the blotting tank once blotted. 50 ml of Blocking solution (5% Marvel in PBS-Tween) was added to the membrane in a 9 cm by 9 cm square petri dish and left overnight at 4°C with gentle shaking. Next day, the Primary antibody-Binding solution was prepared by adding 15 µl of primary antibody (Anti-Flag, Sigma) to a 15 ml of Binding solution (1:10000 dilution) and briefly mixed. The Blocking solution was then removed and the Binding solution was placed onto the membrane and left to shake for 1 h at room temperature. The primary antibody binding solution was tipped off and the membrane was washed three times with PBS-Tween (PBS with 0.05% Tween-20). Each wash was left for 15 mins on a shaker before being drained off 2 µl secondary antibody (ECL-Peroxidase labelled anti-rabbit antibody) was added to 50 ml of Binding solution (1:25000

dilution), mixed briefly and transferred onto the membrane after the wash solution was removed. After 1 h (leave on the shaker), the secondary antibody binding solution was removed and the membrane was washed three times with PBS-Tween, with each wash being left for 15 min on the shaker. Then, the wash step was repeated with PBS twice. Just prior to the end of the washes, a working solution was prepared by mixing an equal volume (1:1) of the stable peroxide solution and the luminal/enhancer solution. The excess wash buffer was drained off from the washed membrane and they were placed, protein side up, on a sheet of SaranWrap. The mixed detection reagent was pipetted on to the membrane and incubated for 5 min at room temperature. During this 5 min, the reagents should cover the entire surface of the membrane. The excess detection reagent was drained off by holding the membrane with forceps and touching the edge against a tissue. The protein blot was placed side down onto a fresh piece of SaranWrap, and the blot was wrapped up (any air bubbles were gently removed using an absorbant tissue). Then, the wrapped blot, protein side up, was placed in an X-Ray film cassette. A sheet of autoradiography film was placed on top of the membrane. The cassette was closed and exposed for 10 second. This step was carried out in a dark-room, using red safelights. The film was removed and replaced with a second sheet of unexposed film. The first film was developed immediately. Second exposures can vary from 1 min to 1 h, depending on the appearance of the first film.

Transfer buffer (1 litre)

3.0 g Tris-base	25 mM
11.3 Glycine	150 mM
200 ml Methanol	20% (v/v)

2.9 Fluorescence microscopy

2.9.1 Poly-L-Lysine slides preparation

The slide was cleaned using 70% ethanol. Then 10 μ l of 0.01% poly-L-lysine (Sigma) was placed in the centre of the slide and left to air dry for 15 min at room temperature. A washing step was carried out next by depositing 100 μ l of dH₂O on top of the dried drop and removing again. This step was repeated three times and the slide was left to air dry at room temperature.

2.9.2 Sample preparation

To describe localization of protein inside the cell, GFP-expressing cells were examined under fluorescence microscopy. The cells were grown in the chemostat (section 2.4.1) until they reached steady state. The cells were sampled and mixed directly into quenching-fixing solution (40% ethanol; 15% paraformaldehyde; 0.8% saline; 25% glutaraldehyde) precooled to -35°C and left in a -35°C isopropanol bath with stirring to reach -5°C. Samples were kept cooled at 4°C in a shaker for 1 hr before being centrifuged at 13200 rpm for 2 min. Then the cells were washed with 1x PBS (137 mM NaCl; 2.7 mM KCl; 10 mM NaH₂PO₄; 2 mM KH₂PO₄) and centrifuged again. Supernatant was discarded and the process was repeated twice. Then, the cells were resuspended in an appropriate amount of GTE solution (50 mM glucose; 10 mM EDTA; 20 mM Tris pH7.5). 5 μ l of the cells were placed on top of a dried poly-lysine spot (section 2.9.1) and allowed to dry at room temperature. The dried spot was then washed with dH₂O by placing 10 μ l of water on top of it and the dH₂O was then discarded. The washing step was repeated twice before leaving to air dry. Then 10 μ l of dH₂O was used to mount the coverslip and the slides were sealed with DPX Mountant (Sigma).

2.9.3 Image processing

Fixed cells were imaged on standard microscope slides as described in section 2.9.1 and 2.9.2. The images were acquired on an Olympus BX61 upright microscope fitted with a 100x (NA 1.4) oil objective with help from Dr Darren Robinson from Light Microscopy Facility, University of Sheffield.

2.10 Transmission electron microscopy analysis and gold-labeling

This experiment was carried out with help from Dr Chris Hill from Electron Microscopy Unit, University of Sheffield. A purified pykF-3xFLAG construct was examined by transmission electron microscopy (TEM) followed by immunogold analysis. Sections were cut at approximately 85 nm thickness (Lowycriol Mono-step HM 20 Resin Agar Scientific, Stansted, England) onto fomvar coated nickel grids. The sections were rinse on distilled water drop for at least 10 min prior to staining. Then the sections were incubated in Tris buffered saline pH 7.4 containing 5% normal goat serum (Vector Labs, England) for 30 min. The sections were washed two times with TBS pH 7.4 (by drops), 4.5 min per wash. To gold-label, construct was incubated for 2 hr with Rabbit anti-FLAG (Sigma Aldrich), diluted 1:50 with TBS pH 7.4 containing 0.1% bovine serum albumen. After two washing steps (the first wash was done with TBS pH 7.4 while the second wash was done in TBS pH 8.2; 1 min for each wash), sample was incubated with 10 nm immunogold conjugated goat anti rabbit secondary antibody (Biocell, England) at 1:50 dilution in TBS pH 8.2 containing 0.1% bovine serum albumen for 30 mins. This incubation process was carried out in a darkened chamber. The grids then washed two times with distilled water (5 min for each wash). The sample was stained in 5% aqueous uranyl acetate for 2 min and washed in distilled water before being stained again in 0.5% alkaline lead citrate Ph 12 for 2 min. The sample was washed well after that with distilled water. Grids were imaged using FEI tecnai TEM at 80 Kv, and images were recorded using Gatan multiscan 600 digital camera.

CHAPTER 3

RAPID SAMPLING AND QUANTITATION METABOLITES

3.0 Rapid sampling and quantitation of metabolites

3.1 Introduction

Metabolome analysis has become an important tool for profiling biological systems. The study of the metabolome will provide useful information about biological processes since it represents the metabolic state of the microorganism. Although transcriptomics and proteomics provide a useful description of the RNA and proteins present in the cell, this is not a complete picture of cellular activity. A more complete description of the state of the cell can only be determined using metabolomics as well. There are many analytical techniques that have been used in metabolite analysis, in particular nuclear magnetic resonance (NMR) and mass spectrometry (Rui *et al.*, 2010; Smart *et al.*, 2010; Villas-Boas *et al.*, 2005b). Sampling, followed by separation of cells and medium, is an important step in the above methods.

The measurement of extracellular metabolites is straightforward, because the extracellular volume is much larger than the intracellular volume in typical culture densities, and therefore changes due to leakage from cells do not lead to significant changes in the concentrations of extracellular metabolites. Thus all that is necessary is to spin down cultures and remove cells.

Intracellular metabolite quantification is more difficult due to rapid turnover and small pool sizes. Thus, metabolic activity needs to be stopped as quickly as possible so that collected samples represent the *in vivo* conditions. This can best be achieved by rapidly decreasing the sample temperature to values below 0°C. The most popular method for quenching of microbial cells is rapid cooling by plunging the cells into cold methanol, where the bath temperature is kept below -20°C in order to cool the cells rapidly to close to 0°C (de Koning

and van Dam, 1992). After this, metabolism is stopped and the cells can be harvested by centrifugation prior to extraction with minimal further metabolic change. This approach was originally developed and applied for yeast, but has later also been used in studies of different bacteria (Buchholz *et al.*, 2001; Letisse and Lindley, 2000; Zhu and Shimizu, 2005).

This chapter describes work carried out to develop an effective and reproducible method for quenching *E. coli* cells, and for quantitating metabolite levels.

3.2 Quenching method

The major requirement of a reliable quenching method is that the sampling and quenching method is fast enough to stop the metabolism. This means that we should stop all metabolic activity inside the cells and prevent any further conversions of metabolites by enzymatic reactions. Quenching of metabolism should ideally be achieved within a second to get the samples to reflect the biological status of interest. For this, several methods have been proposed. One of these uses cold glycerol-saline solution (Villas-Boas and Bruheim, 2007). However this method is not suitable for our use because it is impossible to get rid of the glycerol that sticks to the pellets. A more suitable quenching technique has been described that uses ethanol and sodium chloride (NaCl) (Spura *et al.*, 2009). In this method, an isotonic solution containing 40% ethanol v/v + 0.8% NaCl w/v is cooled to -30°C, and 20 ml samples from the chemostat are added to 20 ml of cooling solution. The resulting mixture is thus instantly cooled to close to 0°C. This method gives a high concentration of metabolites, assumed to mean that it leads to a small amount of damage to the cell membrane and thus only a small amount of leakage of intracellular contents.

To verify the quenching efficiency, and to establish the best method, cells were sampled and quenched in various ways, and compared to cells that were sampled and centrifuged

without being quenched first. NMR spectra taken of cells grown in different ways showed that the most reliable way to compare them was to use cells grown aerobically or microaerobically. Typically, *E. coli* WT MG1655 was grown aerobically in a 1 L chemostat until it reached a steady state (section 2.4.1). Then the cultures were shifted to a microaerobic condition by being perturbed by the introduction of air at 5%. Cultures were sampled from the chemostat and immediately transferred into the precooled quenching solution, or analysed without quenching (sections 2.4.1-2.4.2.3). Incomplete quenching followed by centrifugation results in anaerobic metabolism occurring in the cells. This is evident from the presence of succinate at 2.4 ppm in the spectra of incompletely quenched cells (Figure 3.1). Other metabolite peaks like acetate are also higher in unquenched cells compared to quenched cells.

This technique cools the cells within 1-2 seconds to inactivate the metabolic activity. The temperature of the medium reached approximately 5°C following the method of Spura *et al.* (2009). In order to cool the cells further, different temperatures for the cooling solution were tried. Too low a temperature leads to a risk of freezing the cells, and the creation of ice crystals, which can rupture the cell membrane and lead to leakage of metabolites. To investigate whether this quenching method could lead to cell leakage, we analysed the extracellular (Figure 3.2a) and intracellular (Figure 3.2b) metabolites grown under anaerobic conditions to identify the metabolites that leaked during the quenching process. Use of a cooling solution at -40°C led to measurable leakage of cell contents. However, a bath at -35°C meant that no intracellular metabolites, such as those found in the glycolytic pathway, could be detected. On mixing, the medium was cooled immediately to 0°C. Interestingly, no glutamate was detected in the extracellular fraction, which was reassuring, as glutamate is a highly abundant intracellular metabolite (Bolten *et al.*, 2007).

In the method of Spura *et al.* (2009), samples are further cooled down to -5°C (and therefore further slow down the metabolism) before centrifugation to separate the pellet (intracellular) from the supernatant (extracellular) fractions. Several variations on this were

tried, of which the most successful was to essentially reproduce their method, by leaving the Falcon tube in the cold isopropanol bath for a further 2 minutes (approximately) until the temperature of the medium reached -5°C . Measurements of the reproducibility of the method were carried out, described below, and it was shown that it was essential to stir the medium during this cooling process in order to prevent local cold spots developing and potentially leading to ice crystals. Once the medium reached -5°C , it was transferred to an ice/salt mixture to keep it at -5°C until ready for centrifugation. Centrifugation was carried out using a centrifuge precooled to -11°C , using 5 min at 3940 *xg*. After removing supernatant, the centrifuge bottle is then placed immediately in LN_2 to quench metabolism completely, after which the cold methanol extraction method was used (section 2.4.3) before analysis by ^1H NMR (sections 2.4.4.1-2.4.4.2).

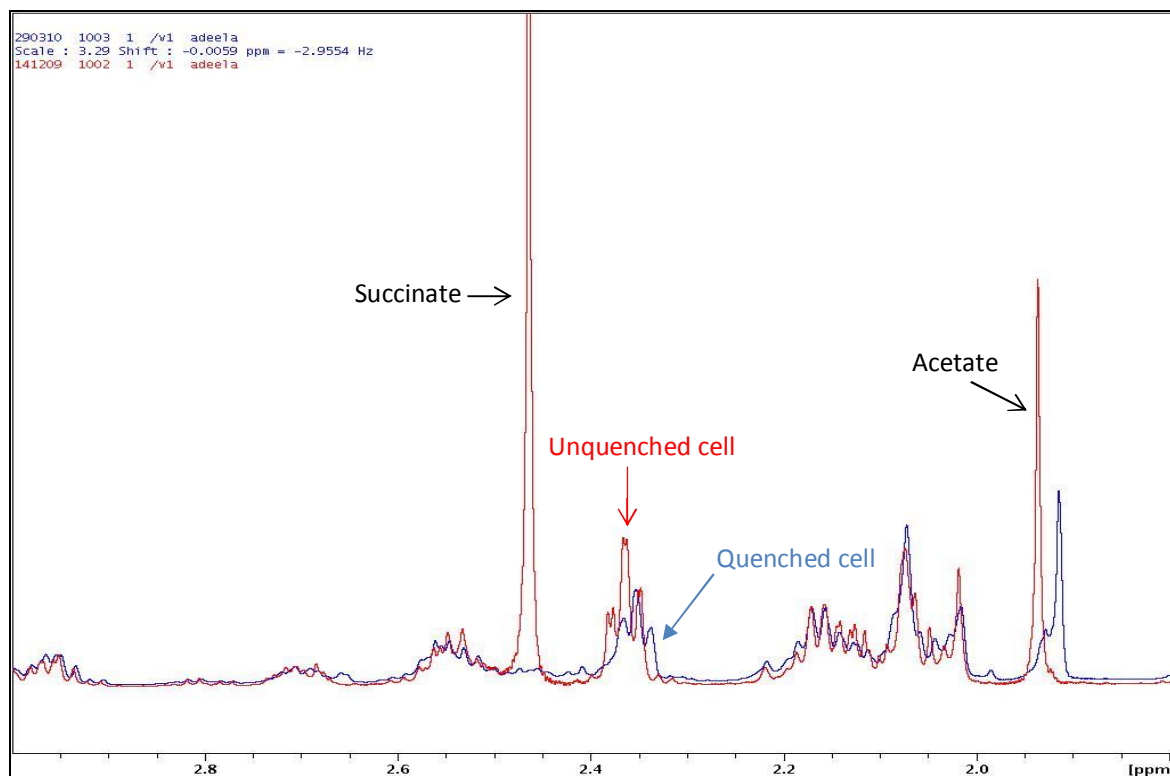
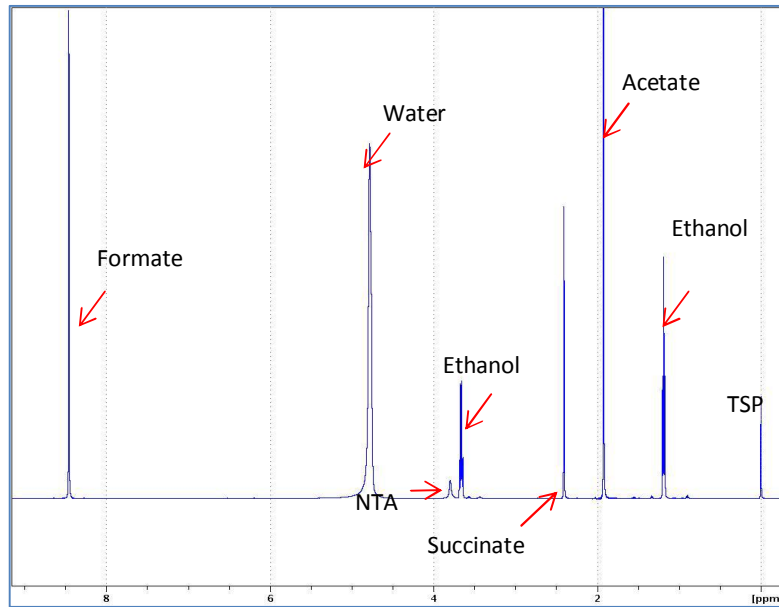
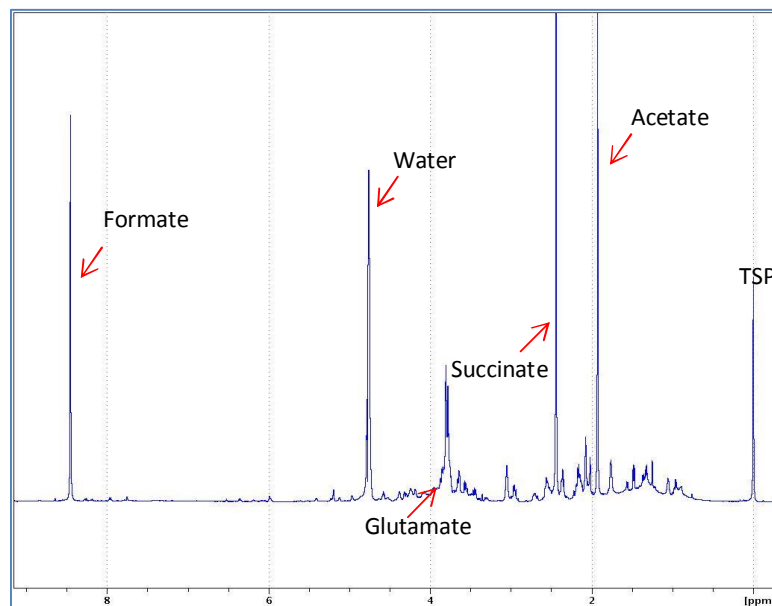


Figure 3.1: Comparison of NMR spectra of microaerobic *E. coli* WT MG1655 cells, quenched and unquenched. The unquenched cells are shown in red while the quenched cells are shown in blue. The succinate peak (2.4 ppm) was detected only in unquenched cells.



(a)



(b)

Figure 3.2: NMR spectra of (a) extracellular and (b) intracellular fractions obtained from *E. coli* WT MG1655 during anaerobic growth. Glutamate was detected only in intracellular fractions, suggesting that the metabolites remain in the cells during the rapid quenching.

3.3 Measurement reproducibility

A study was carried out to identify the magnitudes of errors from different sources during the measurement of metabolite concentrations by NMR. In order to obtain reproducible results, it is important to know how big the errors are, and to minimise the large ones. We have separated the errors into four types; integration, sampling, biological variation and quenching errors.

Integration error is the error in integrating the NMR signals, and can be estimated by repeated processing and integrating of the same FID (in our case, 5 times). Errors of this type have been analysed in detail in the past (Lindon and Ferrige, 1980) and these errors are usually small provided that the signal-to-noise ratio of the NMR spectra is adequate and peaks are reasonably sharp. The NMR lab in Sheffield typically processes spectra using a convolution difference method to remove the water signal from the spectrum (Craven and Waltho, 1995). However, this method has the effect of reducing the intensity of signals close in frequency to the water. All spectra here were therefore acquired and processed by simple presaturation of the solvent signal, and exponential multiplication of the FID before Fourier transformation. The Sheffield lab also typically processes spectra and analyses them using the program Felix (Felix NMR Inc, San Diego, CA). This program has the potential for a more automated approach to analysing spectra (for example, by baseline correction and setting integral limits in a standard way for all spectra). However, it proved to be much less reproducible than processing manually using Bruker software.

Sampling error is the error arising from independent sampling and handling of the same biological sample, and was measured by collecting several samples from the same culture at the same time and measuring them independently. The error obtained from this procedure should be the sum of integration and sampling errors. The error from this source was not expected to be large, and indeed is not (Table 3.1).

Biological variation error is the variation arising from the fact that different biological samples may be different, for example from variation in the genome, biological contamination, small changes in pH, temperature etc. This error is measured from steady-state cultures starting off from different starter cultures, and can be observed either in supernatant or intracellular samples.

Finally, quenching error is the error arising from the quenching procedure. It can only be observed on the intracellular samples, because in sampled cell suspensions the intracellular volume is much smaller than the supernatant, so small amounts of leakage or crossover from intracellular samples will only have a very small effect on supernatant measurements, whereas they will have a much larger effect on intracellular measurements. Quenching errors can be observed from measurement of intracellular metabolites obtained from repeated samples of the same steady-state culture (in which case the observed error is the sum of integration, sampling and quenching errors) or from measurement of intracellular metabolites from steady-state cultures in different growth runs (in which case the observed error is the sum of integration, sampling, quenching and biological variation errors). This error is expected to be the largest source of error in the measurements, because bacterial metabolic rates are fast, and the physical processes involved in quenching and extracting intracellular metabolites have lots of possibilities for variation to occur.

Measurements were performed on samples from chemostat cultures grown at microaerobic steady state. Table 3.1 presents a summary of the errors and shows that the errors from most sources are small except for quenching. The error for biological variation is calculated as 0 using supernatant and 4.5% using intracellular samples. It is reasonable to expect a larger variation using intracellular samples, because in a chemostat in which the medium is replaced at a rate of 0.2 h^{-1} , extracellular concentrations only change slowly with time and are effectively averages over time. By contrast, the intracellular concentration is more likely to vary. Nevertheless, an error from biological variation of zero is unlikely. We can therefore conclude that errors increase in the order integration < sampling < biological variation <

Table 3.1: The percentage of errors measured on samples from chemostat growths at microaerobic steady state. The biggest error is coming from quenching with 14%.

Error	% of errors (Total)*	% of errors (Individual)*
Integration	0.62	0.6
Sampling	1.8	1.2
Quenching	16.03	14.2
Biological variation (supernatant)	2.12	0
Biological variation (intracellular)	20.57	4.5

*The total error is the error as measured. However this total is usually the sum of several individual sources, as discussed above. The individual error is obtained by subtracting known individual errors: for example, the individual error for quenching is obtained by taking the total quenching error and subtracting the individual errors for integration and sampling.

quenching. This means that the process that we should worry about most is the quenching, because this is what gives rise to most of the error. An internal standard is used in a proton NMR experiment to provide a chemical shift reference, which represents the frequency difference relative to the reference proton, measured in ppm. TSP has been chosen as an internal standard because it is very stable and has a chemical shift of 0.00 ppm, which is a smaller chemical shift than that for any other metabolite. TSP has 9 equivalent protons which resonate at the same frequency and result in one intense signal. The relative intensity of signals in the NMR spectrum provides information on the concentration of the compound. When we integrate the signal, the area under the curve of each signal is proportional to the number of equivalent protons creating the signal. Accurate proportionality requires a long relaxation delay to avoid errors arising from different relaxation rates. In this study, relaxation delays of 3 seconds were used. Proportionality was further tested by running spectra of the major metabolites identified at known concentrations, and using this to correct the measured intensities.

In the present study, there are two different samples involved; extracellular and intracellular samples. The chemical shifts of extracellular metabolites are quite easy to measure compared to intracellular metabolites, where some signals are overlapped. We use TSP as an internal standard for the extracellular sample. The integrated signals were scaled to the TSP, so that peak intensities represent intensity relative to the TSP. The concentration of metabolites can be calculated by comparing the intensities of metabolite signals with the intensities of TSP and multiplying by the concentration of TSP used.

3.4 Measurement of intracellular metabolite concentration

The measurement of intracellular metabolite concentrations can be carried out based on one of two different calibration methods: relative to an internal standard of known concentration, or calculation based on knowledge of numbers of cells in the sample plus an

assumption about cell volume. It was a challenge to choose the right internal standard because it is necessary to identify a metabolite whose concentration is constant under both aerobic and anaerobic conditions. Further explanation about these two methods is reported in sections 3.4.1 and 3.4.2.

3.4.1 Measurement based on internal standard

For calibration of the concentration of intracellular metabolites, it is challenging to find a suitable internal standard to be used in measurement of metabolite concentration. Previously, TSP was used as an internal standard for both extracellular and intracellular metabolites, but this gives no absolute value for the concentration without further information. The reference for the intracellular sample must be able to present the changes happening inside the cells, of which the most suitable one must be located inside the cells. Based on this fact, glutamate was chosen as an internal standard. Glutamate is the most abundant compound in aerobically grown cells (Bennett *et al.*, 2009) and investigations have been carried out to look at the stability of the glutamate level inside the cells. The observations suggested that the concentration of glutamate does not change much during cell growth, which means that glutamate might be an appropriate internal standard.

In order to perform the measurement of metabolite concentration, a set of metabolite references with known concentration (100 mM) has been run in NMR and integrated. For extracellular samples, the measurement was done by comparing the intensities of metabolite signals with the intensities of a known concentration of TSP and multiplying by the concentration of TSP. For intracellular metabolites, the intensities of metabolite signals were compared with the intensities of known concentrations of glutamate and multiplied by the concentration of glutamate in the cells (~ 96 mM); (Bennett *et al.*, 2009). The formulas used in measuring the extracellular and intracellular metabolite concentrations are shown as below:

Extracellular sample

$$[\text{metabolite}] = \frac{\text{Metabolite sample} \times \text{TSP reference}}{\text{Metabolite reference} \times \text{TSP sample}} \times 100 \text{ mM}$$

Intracellular sample

$$[\text{metabolite}] = \frac{\text{Metabolite sample} \times \text{Glutamate reference}}{\text{Metabolite reference} \times \text{Glutamate sample}} \times 96 \text{ mM}$$

3.4.2 Measurement based on cell volume

Intracellular metabolite concentration can be calculated on the basis of cell volume. The cell volumes of *E. coli* were reported to be in a range from 0.5 to 4 μm^3 (Churchward *et al.*, 1981; Loferer-Krossbacher *et al.*, 1998), with the lower value being the more generally accepted one. Determination of cell volume is one of the biggest challenges to get an accurate measurement of intracellular metabolite concentration. For each metabolite, the intracellular concentration can be calculated as follows:

$$[\text{Metabolite}] \text{ Molar} = \frac{\left[\frac{\text{mmoles in NMR tube}}{\text{Cells in 20 ml}} \times 10^{12} \right]}{\text{Cell volume}} \times 10^{-15}$$

The mmoles of metabolite in NMR tube was calculated, and the amount of cells in 20 ml (volume of samples taken for analysis) was determined. The fmoles of metabolite per cells was calculated by dividing the mmoles of metabolite in the NMR tube with the amount of cells in 20 ml, and multiplied by 10^{15} . The concentration of metabolite was then calculated by dividing the fmoles of metabolite per cell by the total cell volume of 0.5 fL (Neidhart and Umbarger, 1996) and the result were further multiplied by 10^{-15} to get the concentration of metabolite in Molar. This total cell volume (0.5 fL) is an estimated number calculated based on volume of water per cell. The number could be changed as the cell varies depending upon growth rate, different medias, temperature and other factors.

3.4.3 Comparison of intracellular metabolite concentrations calculated based on internal standard and cell volume.

The concentration of intracellular metabolites is normally calculated on the basis of cell volume. This method is well established and has been used by researchers to measure intracellular concentration. Another method is to use an internal standard that is located and present in the cells, which is more direct but relies on knowing the concentration of an intracellular metabolite. Therefore we performed both calculations and compare the metabolite concentrations derived in Table 3.2.

The concentrations calculated based on internal standard are higher than the calculation based on cell volume, by a factor of 2-3. The relative concentrations are fairly constant: over all the values except for those at $t=0$, the ratio is 2.6 ± 0.9 . The result also demonstrates that the concentrations at 0 min are all roughly twice as big as for every other time point (ratio 5.2 ± 1.3). This can be explained by the observation that the glutamate concentration roughly doubles from 0 min to 30 and 60 minutes (based on the calculation using intracellular volume), meaning that the concentration of glutamate is not constant. These two methods therefore present a different pattern of numbers. We have decided to use a

Table 3.2: Comparison of intracellular metabolite concentrations calculated using two methods, based on (a) internal standard, (b) cell volume

Time	0 min		10 min		30 min		60 min		120 min	
Metabolite	(a)	(b)	(a)	(b)	(a)	(b)	(a)	(b)	(a)	(b)
Acetate	269.8	65.5	155.4	52.4	155.7	46.1	156.1	56.8	202.4	56.8
Formate	765.7	143.4	486.4	125.7	567.7	127.7	541.5	152.4	467.6	96.8
Succinate	234.7	71.0	120.3	50.4	129.2	46.3	101.8	45.8	70.2	23.0
Pyruvate	17.6	5.9	8.1	6.9	13.2	6.5	10.14	7.8	1.9	6.0
Lactate	35.8	12.8	28.0	13.9	26.1	10.7	23.9	12.5	31.9	12.4
Putrescine	39.6	13.4	39.7	18.7	43.8	16.7	36.9	18.1	37.1	14.6
Acetyl aspartate	37.2	13.4	25.9	12.7	29.2	11.8	36.6	19.3	34.1	13.2
Fumarate	1.0	0.3	1.0	0.4	3.5	1.0	4.0	1.4	2.8	0.7

The concentration unit is millimolar (mM)

calculation based on cell volume to measure the concentration of intracellular metabolites. The method chosen is far better established compared to the other one and we are lacking important information on the stability of glutamate inside the cells. Ratios of concentration between these two methods imply that metabolite concentration in anaerobic cells is bigger than in aerobic cells. This clarified that concentration of glutamate in the cells is not constant.

Analysis of the values calculated by method (b) shows that the values obtained at $t=0$ are consistently low. This can be seen most easily for lactate, putrescine and acetyl aspartate, which remain approximately constant from $t=10$ min onwards but are lower at $t=0$. The most obvious explanation for this observation is that the relationship between OD and intracellular volume is different for anaerobic and aerobic cells: for example either because aerobic cells have a larger volume than anaerobic cells, or because they scatter light less. Our observations of cells by electron microscopy and fluorescence microscopy (Chapter 5) do not suggest any gross changes in cell size after the introduction of oxygen, although it does appear that the size and shape of the periplasm is different following introduction of oxygen. It is also possible that aerobic growth causes the cells to scatter light differently. The calculated metabolite concentrations at $t=0$ have therefore been multiplied by 1.5 in the subsequent analysis in Chapter 4, to reflect this anomalous value.

3.5 Identification of metabolites

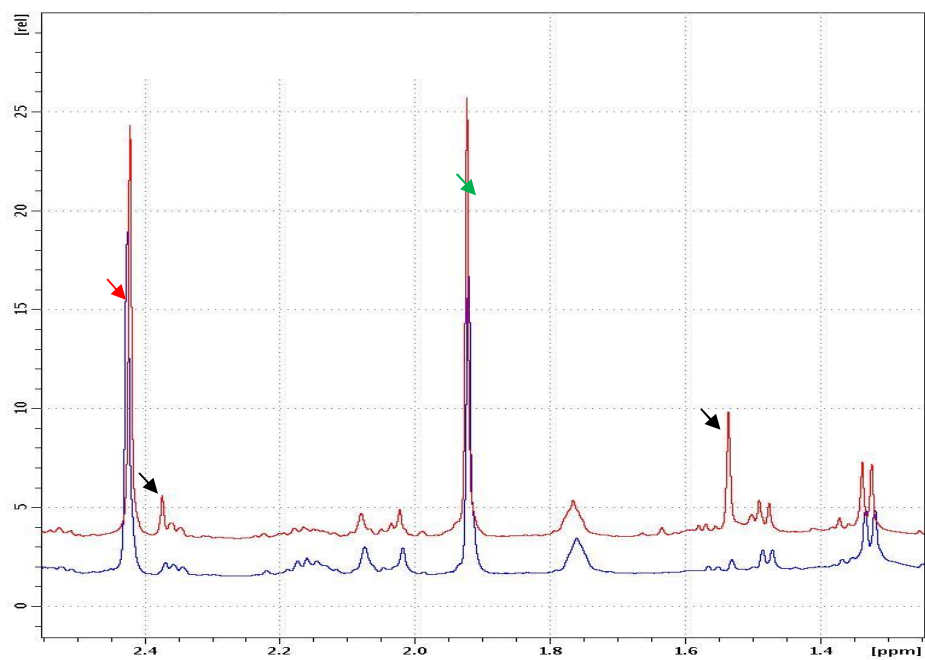
Assigning NMR peaks can be challenging, especially in spectra with overlapped peaks and crowded regions. Many approaches have been proposed to facilitate the identification of NMR peaks, of which the most common are; spiking with reference compounds and computational methods. Spiking with reference compounds is a common way to identify metabolites, where NMR samples are spiked with a small volume of a respective metabolite. Basically the metabolite can be identified by matching the observed spectra to the reference

spectra. This technique is used as evidence for the presence and absence of the metabolite. It is also useful for confirming the assignment of peaks in ambiguous regions.

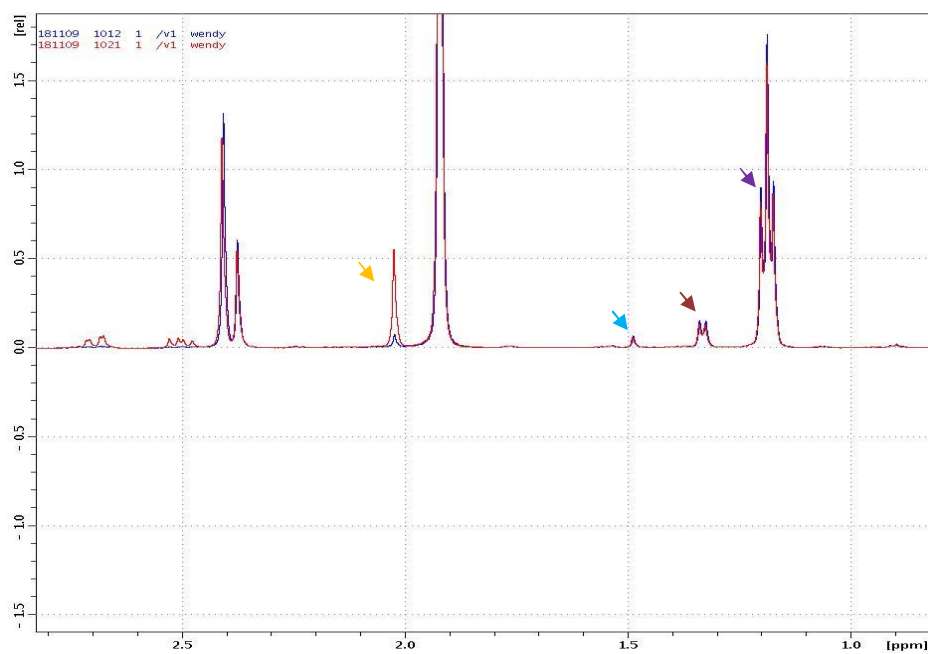
NMR peaks in this study were assigned by spiking NMR samples with metabolite reference and by comparing the chemical shift obtained from the spectra with the chemical shift from the database. Figure 3.3 shows two examples of NMR spiking in order to facilitate the identification of metabolite. NMR spectra are collected after both or more respective metabolites were put in NMR tubes and observed by NMR. TSP was added as a chemical shift reference. For example, the pyruvate (Figure 3.3a) molecule has two resonances in proton NMR; at 2.37 ppm and 1.47 ppm. In water, pyruvate is in equilibrium between $\text{CH}_3\text{COCOO}^-$ and the hydrated form, $\text{CH}_3\text{C}(\text{OH})_2\text{COO}^-$. The two signals are coming from the two CH_3 groups in these two forms. Because in water, pyruvate is present as an equilibrium mixture of pyruvate plus the hydrate, it is necessary to correct for this in the calculation of pyruvate concentration. This can be done either by adding together the intensities of the two methyl signals, or by measuring the ratio of pyruvate to pyruvate hydrate at equilibrium, and using this to correct the concentration obtained by using only one of the two peaks. The peak for the hydrate is sometimes hidden by other signals and is thus difficult to measure accurately. We therefore measured the ratio of pyruvate to hydrate at equilibrium (1:0.58) and multiplied the concentration of pyruvate obtained from the pyruvate peak by 1.58 to obtain the total concentration of [pyruvate + hydrate] in the cell. Since the glutamate peak (triplet) has a similar chemical shift as pyruvate (at 2.37 ppm), this assignment confirmed the presence of pyruvate. For acetyl aspartate, only one peak is identified even though this molecule has several other signals. Figure 3.3(b) showed that the signal comes at the right place but it is possible that the signal observed is something else with a very similar shift.

Oxaloacetate is an important intermediate in the citric acid cycle and gluconeogenesis. In the citric acid cycle, oxaloacetate is formed by the oxidation of malate and reacts with acetyl-CoA to form citrate while in gluconeogenesis, oxaloacetate is formed by the

carboxylation of pyruvate. To prove that pyruvate is the metabolite present in the NMR spectrum from the experiment and not oxaloacetate, NMR spiking was carried out. Oxaloacetate was added to the samples and the spectrum is presented in Figure 3.4. It is clear that the oxaloacetate peak is at different place from pyruvate, proving that pyruvate and oxaloacetate are not identical. The chemical shift of oxaloacetate is not identical to that found in databases, but the values in databases are not identical anyway due to different experimental conditions or referencing. NMR is thus able to distinguish between pyruvate and oxaloacetate. These spectra also show that pyruvate and succinate can be clearly distinguished. In Figure 3.3(a), pyruvate is indicated by the arrow at 2.37 ppm, while succinate is the intense peak at 2.42 ppm.



(a)



(b)

Figure 3.3: Analysis of spiked samples by 1D NMR of (a) pyruvate- arrows in black; acetate- arrows in green; succinate- arrows in red and (b) acetyl aspartate- arrows in orange; ethanol- arrow in purple; lactate- arrows in brown; pyruvate- arrows in blue. Untreated spectra are shown in blue and spiked spectra are overlaid in red.

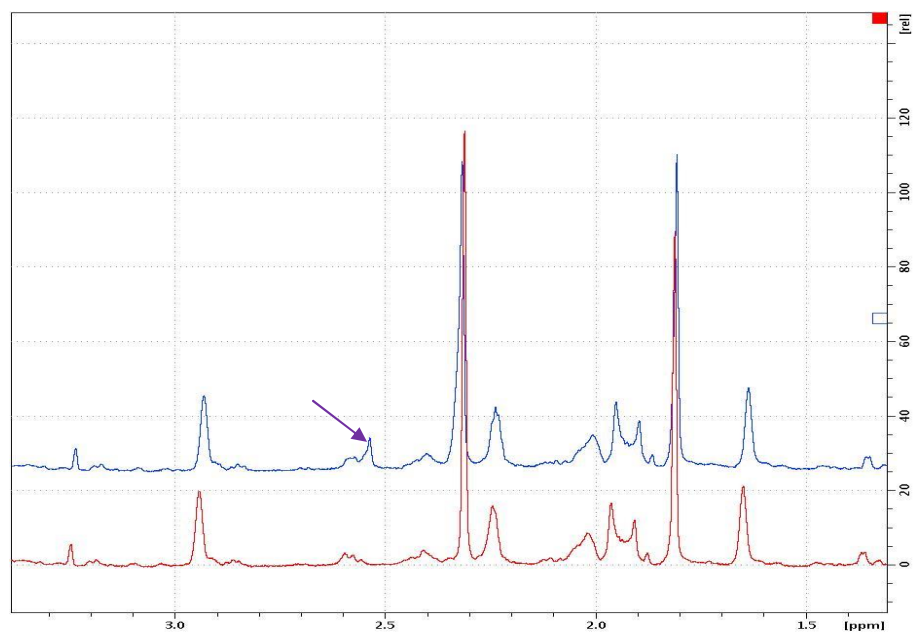


Figure 3.4: Analysis of spiked sample by 1D NMR of oxaloacetate – arrows in purple.
Untreated spectra are shown in red and spiked spectra are overlaid in blue.

3.6 Discussion

In this study, *E. coli* was used as a model organism to understand more about changes in metabolism during oxygen stress, and more generally to investigate how much can be understood about system-wide regulation of metabolic processes. Metabolic measurements have been carried out under steady-state conditions, and it needs information of both extracellular and intracellular metabolites. Extracellular metabolites were quantified in the cell-free supernatant by centrifugation at a low temperature while intracellular metabolite detection needs a faster quenching technique to arrest the metabolism.

Spura *et al.* (2009) have shown that a quenching solution with 0.8% (w/v) salt concentration gives reproducible results with highest detection of metabolite concentration. The cold methanol quenching method showed leakage of intracellular metabolites (Bolten *et al.*, 2007; Faijes *et al.*, 2007; Maharjan and Ferenci, 2003; Wittmann *et al.*, 2004) due to the inherent differences in cell wall structure and membrane composition in these organisms. Therefore, Spura *et al.* (2009) proposed that ethanol should be used, because it should damage the cell membrane less, and the concentration of alcohol was reduced to prevent damage and retain the cell integrity before the cell extraction was performed. Ethanol was also shown to produce an efficient quenching with the xanthan-producing organism *Xanthomonas campestris*, where it quenches rapidly and produced polymer-free supernatants of better quality than methanol (Gonzalez *et al.*, 1997). The concentration of salt in the cooling medium should be adjusted to minimise the risk of the cell membrane breaking due to osmotic shock. The concentration proposed by Spura *et al.* (2009) is close to isotonic and was found to produce the least leakage. Metabolites were extracted using a cold methanol method. During this step, freeze-thaw processes were performed six times as suggested by Theobald *et al.* (1993) to achieve a complete metabolite extraction. Both samples then were analyzed using NMR (section 2.4.4.2). Basically, the optimal extraction method is depending on the targeted metabolites. For example, boiling ethanol was used as an extracting agent for study of amino acid pools and pathway intermediates by Gonzalez *et*

al. (1997) while perchloric acid was used to extract acid-stable metabolites (Buchholz *et al.*, 2001; Chassagnole *et al.*, 2002b).

Previous studies have demonstrated that quenching of *S. cerevisiae* cells with cold methanol damages the cell integrity which permits leakage of the metabolites (Villas-Boas *et al.*, 2005a). The use of saline quenching solution was proved to reduce leakage of metabolites (Bolten *et al.*, 2007). The quenching method of Spura *et al.* (2009) has been tested and leads to no detectable leakage from cells. It also produces no detectable metabolism after sampling. The method was modified slightly, because of large random errors in initial trials. For example, the cells (after transferring to the quenching solution) are stirred all the time (to let the cells cool homogeneously and prevent damage by freezing), and the quenching solution is precooled to -35°C, to give more rapid quenching. Using this method, the temperature of the culture is reduced to 0°C in 1-2 seconds, which should be short enough that metabolism is stopped almost completely. It is possible that metabolism can continue even at 0°C, and hence it is important to separate cells and supernatant, and get the cells into LN₂, as quickly as possible after quenching.

The efficiency of the quenching method can be checked by comparing quenched and unquenched cells. Succinate was found in a significantly higher concentration in unquenched samples where no succinate was present in quenched cells. The results suggest that the unquenched cells become anaerobic during the centrifugation step, because succinate is a typical metabolite under anaerobic conditions, and is produced because after sampling the cells are still close to 37°C and only cool gradually during the centrifugation. One should be aware that during extraction metabolite levels were not changed by enzymatic or chemical conversion, and they were not destroyed during extraction.

During anaerobic respiration, succinate is produced from the reduction of fumarate by fumarate reductase, when the citric acid cycle (CAC) is repressed and the metabolic flow in

the C4 section of the CAC is reversed. Studies by Vemuri *et al.* (2002) proved that fumarate reductase activity was increased at both oxygen transfer rates as fermentations became increasingly oxygen limited. Under oxygen limitation, FNR protein (regulator of fumarate and nitrate reduction) triggers the expression of fumarate. Apart from succinate, acetate is another metabolite that appeared high in unquenched cells. This verifies that the metabolism is not stopped properly in the unquenched cells, thus will affect the measurement of intracellular metabolites.

Metabolomics, analytical platforms such as NMR, GCMS or LCMS, are able to measure many metabolites in biological samples but various error sources can contribute to the error of measurement of each metabolite analysed. These variations might have been caused by the different sampling/quenching techniques, and the different analysis procedures applied. Measurement error can be defined as an error related to the repeated analysis of the same sample. Different metabolites may have measurement errors that correlate with each other. The initial data on using the unchanged Spura *et al.* (2009) method exhibited large errors, of the order of 40% (data not shown). After refinement of the procedure, the error for quenching is still big (13%), but acceptable. The results indicate that overall the method is robust and reliable. Each experimental condition was independently repeated three times to make sure to prevent inaccuracy while doing the experiment. The high turnover of intracellular metabolites highlights the need for reliable and reproducible quenching techniques for microbial metabolomics.

Apart from having better quenching and extraction techniques, how the measurement of intracellular concentration is carried out is of utmost importance since an accurate measurement will give valuable information on the metabolic reaction inside the cells. Initially, a calculation method was attempted using one of the metabolites present inside the cell as an internal standard to provide a simple yet better method to calculate the intracellular metabolite concentration. The only concerns of this approach would be finding a stable standard, which is not going to change inside the cell. Not much information on the

stability of the concentration of glutamate can be found at the moment. Measurements based on cell volume are the most common method used but quite challenging as information on the total cell volume of *E. coli* is still inconsistent. Many researchers have been carried out to determine the total cell volume; often by using coulter counter measurements or by electron microscopy (Kubitschek, 1969). This method is much more promising since a lot of scientific report can be found on the cell volume of *E. coli*. Analysis on the concentration of intracellular metabolites calculated from these methods shows that the relative concentrations are fairly constant but that the ratios at the 0 min timepoint is bigger than at other timepoints, suggesting that the concentration of glutamate is not stable inside the cells. This argument made us to decide to choose measurement based on cell volume to present the data of concentration of intracellular metabolite. This measurement will provide much information on the metabolism of *E. coli* during the transition from anaerobic to aerobic in the next chapter.

CHAPTER 4

ANALYSIS OF *E. COLI*

METABOLITES AT DIFFERENT LEVELS OF OXYGENATION

4.0 Analysis of *E. coli* metabolites at different levels of oxygenation

4.1 Introduction

The *Escherichia coli* system has been studied extensively, especially its physiology, genetics and metabolism. This metabolically versatile bacterium is able to grow in the presence or absence of oxygen. When oxygen is available, aerobic respiration allows the complete oxidation of glucose and generates maximal energy in the form of energy-carrying molecules (ATP). In the absence of oxygen, two separate pathways can occur; anaerobic and fermentation, depending on the electron acceptor present. For anaerobic respiration, nitrate, sulphate or fumarate can act as a terminal electron acceptor, while in fermentation, NADH gets reoxidised by the metabolites of the pathway, which are then secreted into the medium to maintain the redox balance. The energy produced by anaerobic respiration is less than that achieved by aerobic respiration, but is greater than that produced by fermentation (Partridge *et al.*, 2006). The major factor that controls the switching between these metabolic modes is oxygen availability. The change from anaerobic to aerobic or microaerobic metabolism can be very rapid and leads to alterations in the rate, route and efficiency of pathways of electron flow (Sawers, 1999).

Under aerobic conditions, *E. coli* synthesizes two main cytochrome oxidases, cytochrome *bo* and cytochrome *bd-I*, as major terminal electron acceptors in the electron transport chain. Cytochrome *bo* is synthesized maximally under conditions of high oxygen availability, and is regarded as a proton-pumping oxidase (Poole *et al.*, 1994), where it catalyses the two-electron oxidation of ubiquinol within the membrane and the four-electron reduction of molecular oxygen to water. Cytochrome *bd* in comparison is prominent under microaerobic conditions and does not function as a proton pump. There is a cytochrome *bd-II* but this is largely uncharacterised (Poole and Cook, 2000).

In response to lower oxygen concentrations, the role of pyruvate dehydrogenase complex (PDHC), which oxidises pyruvate to acetyl-CoA and CO₂, is replaced by pyruvate formate lyase (PFL), which converts pyruvate to acetyl-CoA and formate (Murarka *et al.*, 2010). This change is regulated by the FNR and ArcBA systems. FNR is a direct oxygen sensor while ArcBA senses oxygen availability indirectly by monitoring the redox state of the quinone pool (Georgellis *et al.*, 2001).

The steady-state metabolism of *E. coli* under anaerobic and aerobic conditions is well understood. Partridge *et al.* have characterised the changes during the transition from anaerobic to aerobic (2006) and aerobic to microaerobic (2007) at the transcriptome level. However, the change at the metabolome level is still not analysed. The objective of this chapter is to characterise the metabolite changes of *E. coli* at different level of oxygen and analyse the metabolites during the transition from anaerobic to aerobic.

4.2 Results

4.2.1 Metabolic profile of cells grown under anaerobic and aerobic steady-state culture

The chemostat is the most suitable method of analysing cells under steady-state conditions. It has been widely used in transcriptomic, proteomic and metabolomic studies (Hayes *et al.*, 2002; Hoskisson and Hobbs, 2005; Partridge *et al.*, 2006). The importance of chemostat cultures resides in the fact that they allow growth of microorganisms under constant and well-defined conditions. In particular, the results from chemostat cultures can be compared readily between different laboratories, compared to the same studies using batch cultures (Piper *et al.*, 2002). In the present work, we use chemostat cultures of *E. coli* MG1655 with NMR analysis to compare the metabolic profiles of anaerobic and aerobic chemostat cultures grown in steady-state conditions. Steady-state cultures provide reproducible

starting points, with growth rate, medium composition, pH value and aeration of the culture controlled (Hoskisson and Hobbs, 2005). Glucose (20 mM) was used as the carbon source and the dilution rate chosen was 0.2 h^{-1} . Thus, cultures have the potential to respond to changes in O_2 availability without changes in growth rate.

To compare the metabolic profiles of cells growth under aerobic and anaerobic conditions, extracellular and intracellular samples from steady-state cultures were collected rapidly and quenched before being analysed using NMR. During aerobic metabolism, pyruvate (the end product of glycolysis) is completely oxidised by the pyruvate dehydrogenase complex (PDHC) to yield acetyl-CoA, CO_2 and water. The other carbon atoms are converted ultimately to cell mass, implying that the cell does not need to produce secreted over metabolites in order to achieve redox balance. The role of PDHC is replaced by pyruvate formate lyase (PFL) under anaerobic conditions, where pyruvate is converted to acetate, ethanol, formate and succinate (Figure 4.1). This process prevents the build-up of NADH in the cytoplasm and provides NAD^+ to be used in glycolysis again.

Figure 4.2 shows NMR spectra of extracellular (Figure 4.2a) and intracellular (Figure 4.2b) extracts from cells grown under aerobic conditions. In the extracellular extract, the largest signals are from water (reduced by presaturation), the NTA buffer, and added TSP. Secreted metabolites are present at very low concentrations. None of the glucose added to the medium is detected, meaning that the cells have taken up all the glucose in the medium. In the intracellular extract, there are a large number of peaks, as expected. Many of these are derived from TCA cycle intermediates like α -ketoglutarate, fumarate and oxaloacetate. There are again no signals detected from glucose, showing that the glucose is fully oxidised by glycolysis and the TCA cycle to produce water and carbon dioxide.

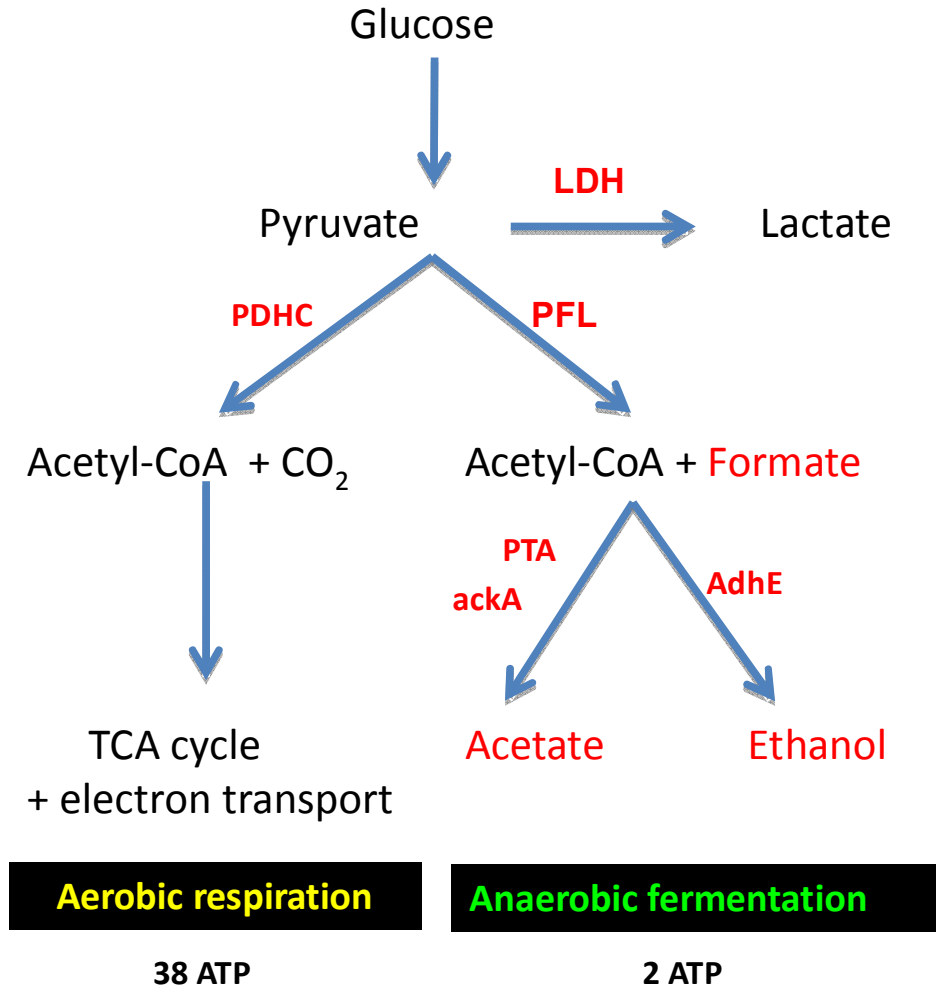
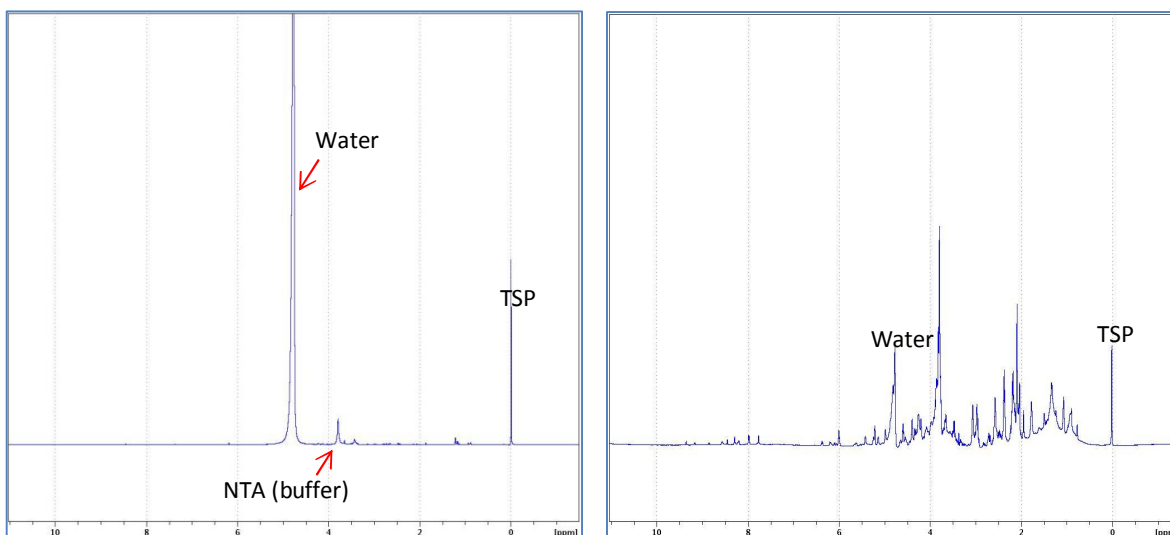


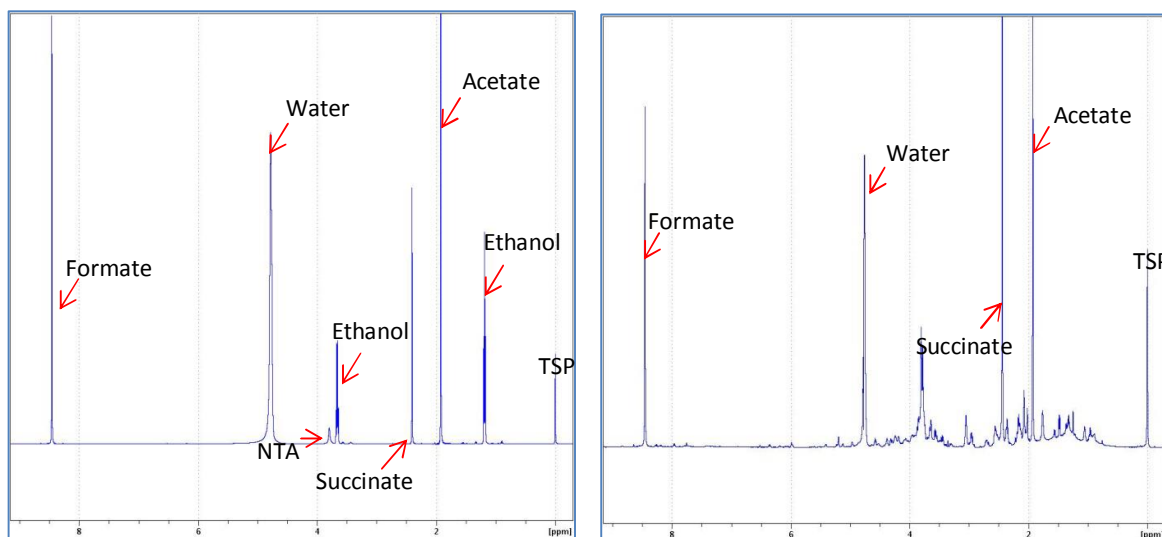
Figure 4.1: Schematic pathways of glucose metabolism. The glucose molecule is broken down into pyruvate during glycolysis. In the presence of oxygen, pyruvate enters the TCA cycle to produce more energy in the form of ATP than can be obtained from any anaerobic pathway. When no oxygen or alternative electron acceptor are present, fermentation pathways are important and are the sole source of ATP for some anaerobic bacteria. Anaerobic cells need to produce NAD⁺ to maintain redox balance, which they do by fermentation of pyruvate to produce ethanol, or reduction to lactate. Anaerobic respiration leaves a lot of energy in the ethanol or lactate molecules that the cell cannot use and must secrete. (LDH: lactate dehydrogenase; PDHC: pyruvate dehydrogenase complex; PFL: pyruvate formate lyase; AdhE: aldehyde dehydrogenase; PTA: phosphotransacetylase).



(a)

(b)

Figure 4.2: NMR spectra of (a) extracellular and (b) intracellular metabolites of *E. coli* WT MG1655 grown under **aerobic** steady state.



(a)

(b)

Figure 4.3: NMR spectra of (a) extracellular and (b) intracellular metabolites of *E. coli* WT MG1655 grown under **anaerobic** steady state.

In comparison, NMR spectra of extracellular and intracellular extracts from cells grown under anaerobic conditions are presented in Figure 4.3 (a) and (b). Both spectra show the presence of acetate, succinate and formate. Ethanol is only present in extracellular extracts but not in intracellular extracts since ethanol inside the cells is volatile and is evaporated during the extraction process (section 2.4.3). These results show that aerobically grown cells are able to use all their carbon source for growth, but anaerobically grown cells oxidise NADH to maintain a redox balance through the production of these overflow metabolites. The large number of metabolites present in the NMR spectra of intracellular extracts make the spectra difficult to integrate and quantify compared to NMR spectra of extracellular extracts.

The concentrations of extracellular and intracellular metabolites of the anaerobic steady-state grown cultures were measured (Table 4.1). No measurement of metabolite concentrations can be done for aerobically grown extracellular extracts since glucose is fully oxidised to carbon dioxide and water. For cells grown under anaerobic conditions, acetate, succinate and formate were detected in both extracellular and intracellular extracts, of which formate has the highest concentration (63 mM extracellular; 96 mM intracellular), followed by acetate (25 mM extracellular; 44 mM intracellular), ethanol (16 mM; which can be detected only extracellular) and succinate (6 mM extracellular; 47 mM intracellular).

Table 4.1: Concentration of extracellular and intracellular metabolites for cells grown under anaerobic condition.

Cells grown under anaerobic conditions	Concentration (mM)	
	Extracellular	Intracellular
Ethanol	16	-
Acetate	25	44
Succinate	6	47
Formate	63	96

4.2.2 Steady-state metabolite analysis at different level of oxygenation

Oxygen plays an important role in the regulation of various cellular processes. The availability of oxygen is the major factor that determines which metabolic modes (aerobic respiration, anaerobic respiration and fermentation) will be adopted by the organism. Alexeeva *et al.* (2002) defined 100% aerobiosis as the minimal oxygen input rate that results in undetectable secretion of the fermentation product acetate. Figures 4.2 and 4.3 show that aerobic cells secrete no acetate, whereas anaerobic cells secrete a large amount of acetate. This aerobiosis scale only applies to carbon-limited cultures as used in this study. The specific rate of acetate production (q_{acetate}) increases to a maximum under anaerobic conditions, when the amount of oxygen supplied to cultures decreases (0% aerobiosis). The microaerobic range lies between these limits (0-100% aerobiosis), which is defined by a linear decrease in q_{acetate} as the oxygen transfer rate increases (Figure 4.4).

To determine at what level of oxygenation the *E. coli* start to experience microaerobic conditions, the metabolism of *E. coli* was analysed at different levels of oxygenation. Previously 5.4% dissolved oxygen (25.7% air) has been used as a standard microaerobic condition (Trotter *et al.*, 2011), based on the data in Figure 4.4. However, transcriptomic and proteomic results (Partridge *et al.*, 2006) suggested that this may not be properly microaerobic, possibly because the periplasm of *E. coli* contains cytochrome *bd*, which has a very high affinity to oxygen, and may reduce it all before it can reach the cytoplasm. *E. coli* wild-type strain (MG1655) was used throughout this study. Cells were grown in chemostat cultures under glucose-limited conditions at a constant dilution rate of 0.2 h^{-1} at variable oxygen supply rates. Oxygen supply was controlled by varying the percentage of oxygen in a gas mixture of air and N_2 while stirring the culture at a constant speed (400 rpm). A culture was grown at 0% air to steady state, and sampled. The proportion of air was then increased to 5%, cells were allowed to come to steady state (24 hr), and sampled. Samples were taken at 5%, 10%, 15%, 20%, 40%, 60% and 80% air. In order to check whether this gradual

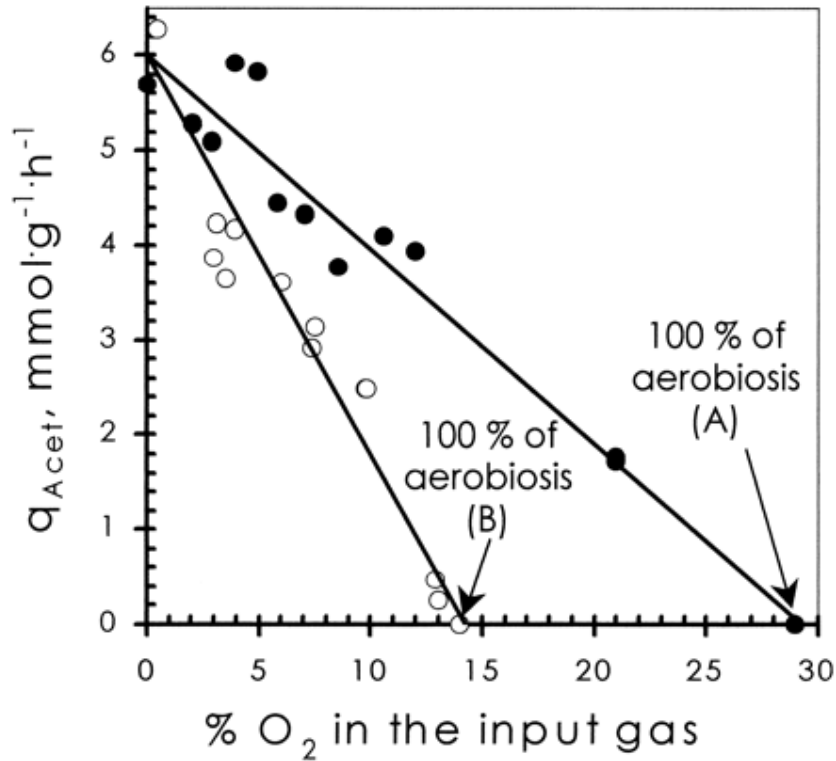


Figure 4.4: Effect of oxygen supply on steady-state acetate production rate (q_{acetate}) at two different stirring rates. Acetate shows a linear decrease in production when fermentative metabolism is replaced by aerobic metabolism. Fully respiratory catabolism could be achieved by varying either the oxygen concentration in the inflowing gas or the stirring rate (adapted from Alexeeva *et al.* 2002).

increase in oxygenation produced acclimatisation, fresh cell cultures were also grown to different oxygenations and compared. No significant differences were observed depending on the process, and results for the same oxygenation levels from different cultures were therefore pooled. The cells were harvested using the unquenched method as described in section 2.4.2.3.

Table 4.2 summarises the concentration of formate and acetate in WT *E. coli* at different levels of oxygenation. Since formate and acetate are the major products of fermentation, only these two metabolites were measured in this study as it is easier to integrate the NMR peaks in order to obtain reproducible data. Examination of formate and acetate in intracellular samples by proton NMR showed the level of acetate and formate decreased significantly after 40% air and nearly disappeared at 60 and 80%. There is not much difference in the concentration of metabolites between 0, 5 and 10% air. From this result, it can be concluded that cells need more than 40% air in order to experience aerobic conditions, presumably because of the action of periplasmic cytochromes in absorbing ambient oxygen. This result will be useful in future studies aimed at characterising changes during microaerobic growth.

Air (%)	0%	5%	10%	15%	20%	40%	60%	80%
Formate	0.20	0.22	0.24	0.26	0.14	0.18	0.03	0.03
Acetate	0.14	0.28	0.25	0.47	0.34	0.29	0.04	0.05

Table 4.2: Summary of metabolite concentrations of formate and acetate at different level of oxygenation. Concentrations are in arbitrary units.

4.2.3 Metabolite changes during transition from anaerobic to aerobic growth

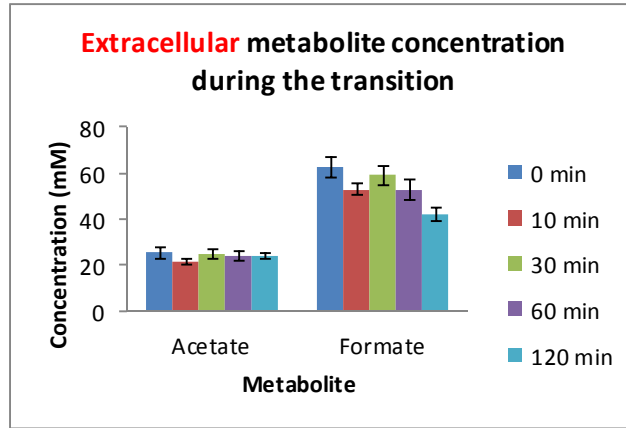
4.2.3.1 Extracellular metabolite

There is not much information on transcriptome dynamics and metabolic profiling of *E. coli* during adaptation to changes in oxygen availability. Earlier reports on the effects of oxygen on transcription in *E. coli* have compared separate aerobic and anaerobic cultures, regularly grown as batch cultures (Constantinidou *et al.*, 2006; Salmon *et al.*, 2005). Partridge *et al.* have characterised the changes during the transition from anaerobic to aerobic (2006) and aerobic to microaerobic (2007) at the transcriptome level. Recently, Trotter *et al.* (2011) reported the changes of *E. coli* from aerobic to microaerobic at metabolome level, focusing on extracellular metabolites. Here the adaptation process was investigated by determining the changes in metabolites when anaerobic steady-state cultures were perturbed by the introduction of air. Transition was followed at 10, 30, 60 and 120 minutes by looking at the metabolite profile by NMR. The metabolite changes resulting from introduction of air to the anaerobic steady-state cultures were monitored by looking at the extracellular and intracellular ^1H NMR profile. For this study, it was very important to quench the metabolism as rapidly as possible after sampling, because of the fast rate of pyruvate turnover in cells. The method described in Chapter 3 (section 3.2) was therefore used.

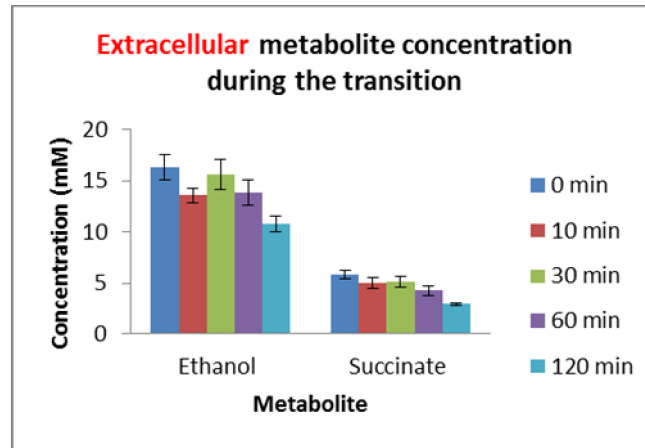
Changes in extracellular metabolite concentrations are shown in Figure 4.5, and listed in Table 4.3. The 10-minute time point is consistently low for all metabolites, although this could be an artifact. Different metabolites have very different profiles. The group of overflow metabolites (acetate, formate, succinate and ethanol) is secreted by anaerobic cells to maintain redox balance and is not produced by aerobic cells. The concentrations of formate, succinate and ethanol drop steadily after introduction of air. If cells stop secreting these overflow metabolites immediately on introduction of air, then we would expect that

their concentrations in extracellular medium will decrease by $20\% \text{ hr}^{-1}$ because of washout by fresh medium.

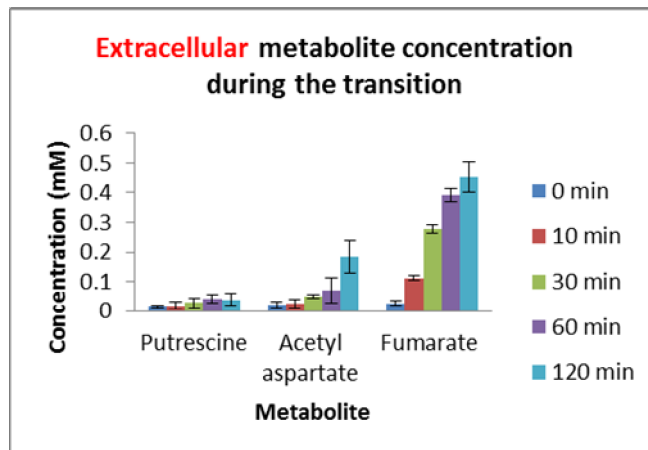
This behaviour can be observed in Figure 4.6 (a), (b) and (c), implying that they are not secreted once the transition to aerobic growth has begun. For ethanol, it should go down faster than $20\% \text{ hr}^{-1}$ because of evaporation during growth in the chemostat. However, the decrease in ethanol is in fact very close to $20\% \text{ hr}^{-1}$. This result suggests that the cells are still producing ethanol. However, some other metabolites like acetate (Figure 4.7a) are almost steady at the same level, suggesting that acetate is still being secreted by aerobic cells, roughly at constant rate. Fumarate (Figure 4.7b) increases from a small initial level, implying that it is not produced by anaerobic cells but is produced by aerobic cells. The same behaviour is also seen for a small number of other metabolites, in particular putrescine and a signal which best matches the frequency of acetyl aspartate, based on metabolomics databases and spiking (Figure 3.3). Pyruvate and lactate show unusual behaviour, with transient secretion by the culture. As can be seen in Figure 4.7c, pyruvate was undetectable in the anaerobic steady-state culture and increased initially but then decreased. This indicates that it is produced immediately after the transition to aerobic growth but is taken up again once the cells are adjusted to aerobic growth. This behaviour is observed because PFL is expected to be destroyed during the transition to aerobic growth but it will take some time for PDHC to be induced (see discussion). Lactate (Figure 4.7d) showed a similar profile as pyruvate, where the metabolite level increases initially but decreases again at 120 min. Lactate is secreted as a fermentation product under anaerobic condition under control of lactate dehydrogenase promoter (*ldhA*). Studies done by Bartosiak-Jentys *et al.* (2012) suggested that *ldhA* promoter is less active under fully fermentative anaerobic conditions than under oxygen limitation but is inactive under fully aerobic condition. This may explain the up and down pattern of lactate secretion.



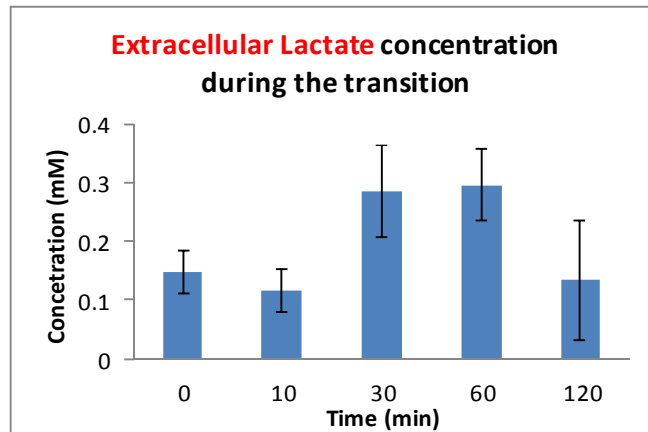
(a): Acetate and Formate



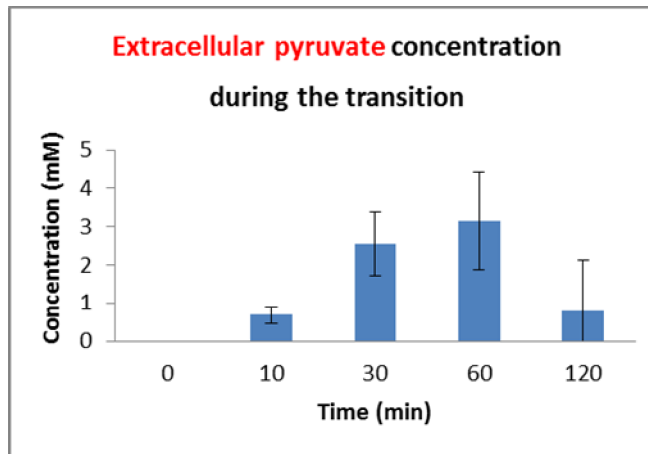
(b): Ethanol and Succinate



(d): Putrescine, Acetyl aspartate and Fumarate



(d) Lactate

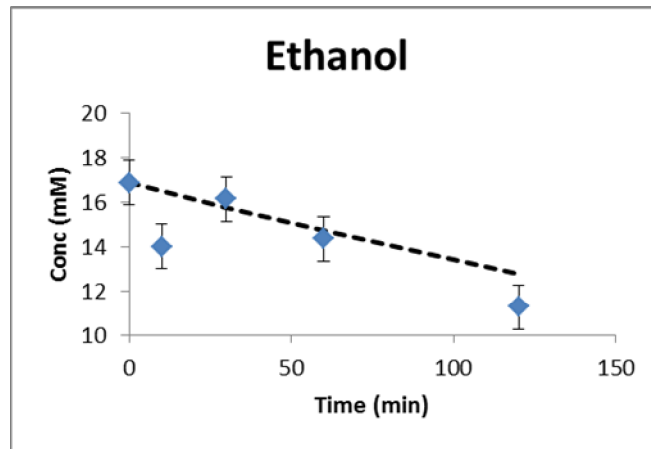


(e) Pyruvate

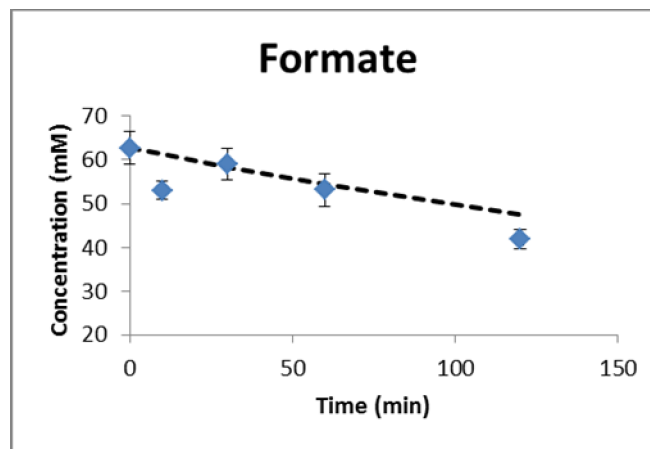
Figure 4.5: Metabolite concentrations of extracellular metabolites: (a) acetate and formate; (b) ethanol and succinate; (c) putrescine, acetyl aspartate and fumarate; (d) lactate; (e) pyruvate during the transition from anaerobic to aerobic. These data were obtained from three independent cultures. Error bars show the standard deviation.

Time after transition	Ethanol (mM)	Acetate (mM)	Formate (mM)	Succinate (mM)	Lactate (mM)	Putrescine (mM)	Acetyl aspartate (mM)	Fumarate (mM)	Pyruvate (mM)
0 min	16.4	25.4	62.7	5.8	0.15	0.02	0.02	0.03	0.00
10 min	13.6	21.8	53.1	5.0	0.12	0.02	0.02	0.11	0.69
30 min	15.7	25.2	59.0	5.1	0.29	0.03	0.05	0.28	2.54
60 min	13.9	24.1	53.1	4.3	0.30	0.04	0.07	0.39	3.15
120 min	10.8	24.3	42.0	2.8	0.13	0.04	0.18	0.45	0.78

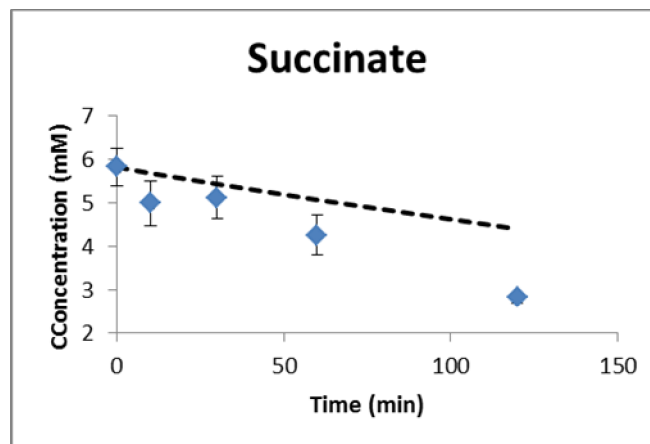
Table 4.3: Summary of extracellular metabolite concentrations during the transition from anaerobic to aerobic.



(a)

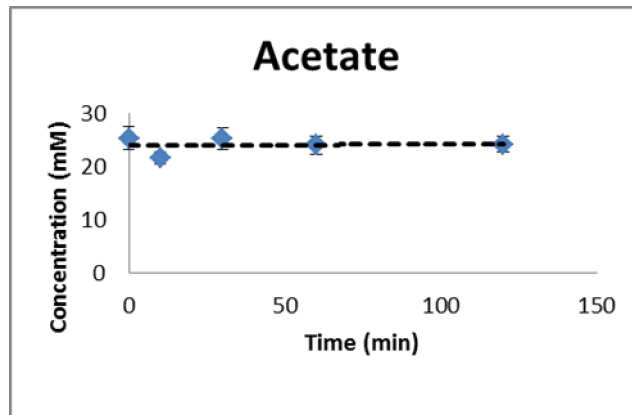


(b)

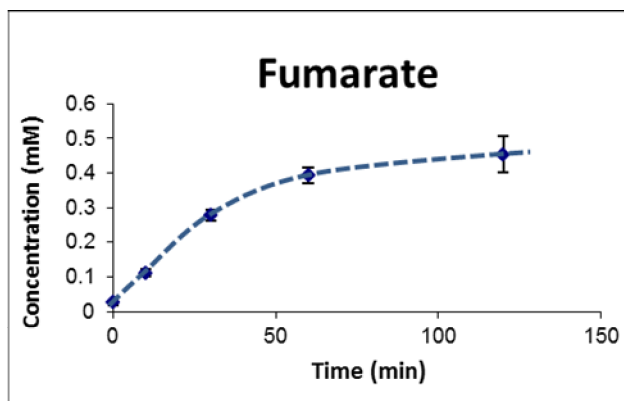


(c)

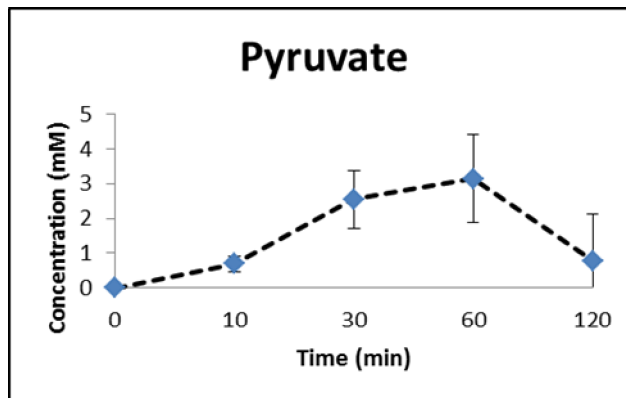
Figure 4.6: Extracellular metabolites that **decrease** at $20\% \text{ h}^{-1}$; (a) ethanol, (b) formate and (c) succinate. The dashed line shows the behaviour expected for a decrease of $20\% \text{ hr}^{-1}$.



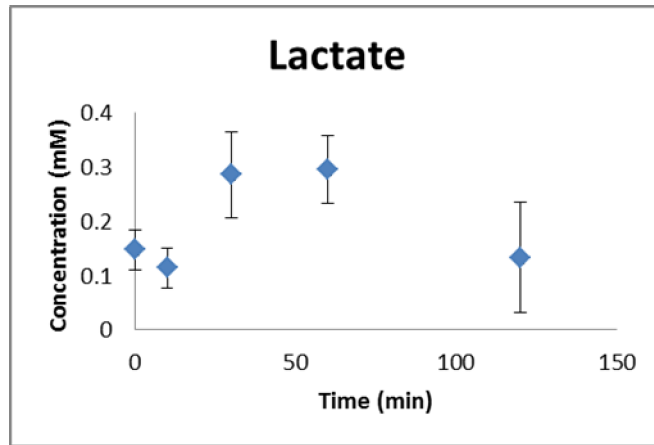
(a)



(b)



(c)



(d)

Figure 4.7: Extracellular metabolites that **do not decrease** at $20\% \text{ h}^{-1}$; (a) acetate; (b) fumarate, (c) pyruvate and (d) lactate. The dashed lines are merely a guide for the eye: in Fig 4.8a the line has a constant value.

A two-tailed t test analysis was performed to check whether the above data is consistent with the concentration decreasing at the same rate as medium replacement. For ethanol, formate and succinate, this test has proved that the data are consistent with the concentration decreasing at 20% % hr⁻¹ (the calculation t value is less than t statistic; so the null hypothesis cannot be rejected) (Table 4.4). Therefore these data are consistent with results reported by Trotter *et al.* (2011). However, acetate production was maintained as the t statistic value is higher than the calculation t.

Calculation	Ethanol	Formate	Succinate	Acetate
t statistic	2.16	2.16	2.16	2.16
calculation t	1.75	1.97	1.64	60.31

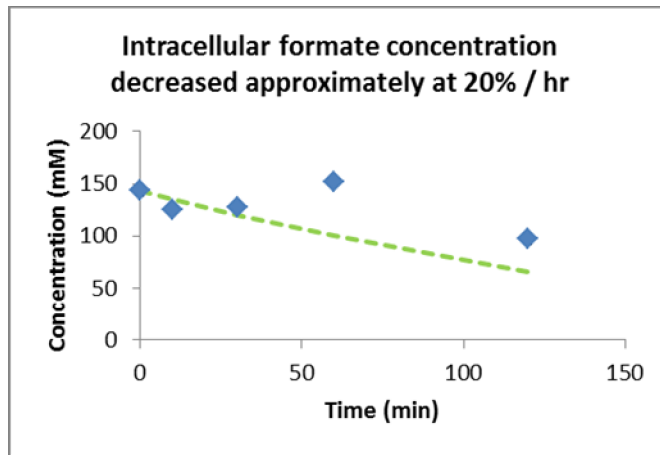
Table 4.4: A two-tailed t test ($p = 0.05$). This test was performed to calculate the significance of data decreasing at 20% h⁻¹. Calculation of t statistic was done by using this formula;

$$t = (\text{slope} - \text{target slope}) / \text{error in slope}$$

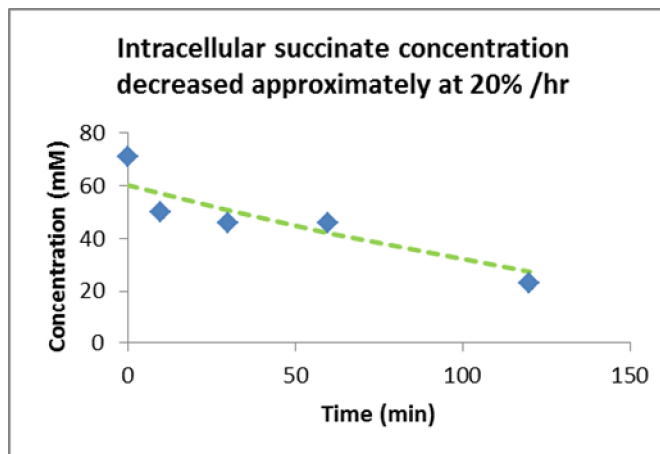
4.2.3.2 Intracellular metabolite

Intracellular metabolite concentration can be measured based on one of two methods: relative to an internal standard of known concentration, or based on cell volume. Measuring intracellular metabolite concentration is challenging compared to extracellular metabolites since no internal standard can be used directly in order to perform the measurement. Previously, TSP was used as an internal standard for both extracellular and intracellular metabolites, but this gives no absolute value for the intracellular concentration without further information. As discussed in section 3.4 and 3.6, measurement based on cell volume was chosen to present the intracellular metabolite concentration data. This well-established method presents a more consistent result compared to the other method based on internal standard. Information on the stability of the concentration of the internal standard is lacking, which indicated that we cannot use that method to measure the metabolite concentration. The measurement was used to calculate an intracellular concentration as described in section 3.4.2.

Similar to extracellular spectra, formate is dominating the intracellular extracts with the highest concentration, 96 mM. It was concluded above that the extracellular metabolite profile was consistent with immediate cessation of secretion of succinate and formate on introduction of oxygen. We may therefore expect that intracellular concentrations of formate and succinate would decrease rapidly on introduction of oxygen. As shown in Figure 4.8, the concentrations of these two metabolites do indeed decrease at approximately 20% hr^{-1} after the start of the transition to aerobic growth. The concentration of intracellular ethanol cannot be determined because it is lost during the extraction process.



(a) Formate

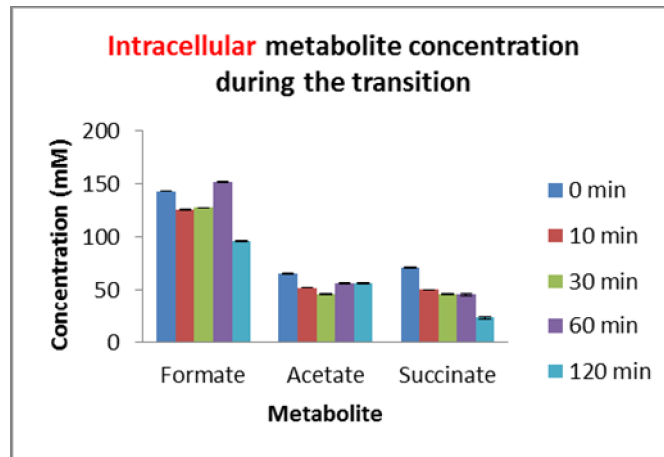


(b) Succinate

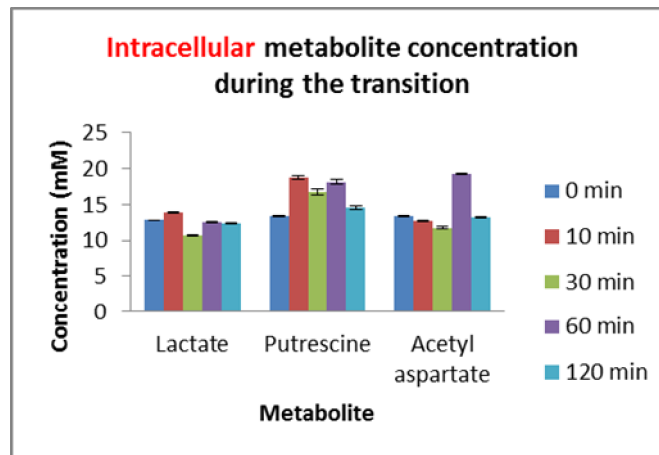
Figure 4.8: Intracellular metabolites that **decrease** at approximately $20\% \text{ hr}^{-1}$; **(a) formate**; **(b) succinate**. The green curve shows the behaviour expected for a decrease of $20\% \text{ hr}^{-1}$.

The concentration of intracellular acetate does appear to drop slightly after start of the transition, but then remains approximately steady. This is again consistent with the observations of extracellular acetate, which remained roughly constant, suggesting continued production of intracellular acetate. The concentrations of intracellular putrescine and acetyl aspartate, and probably also of fumarate, remain constant during the transition. This is by contrast to the extracellular concentrations, which increase. This is discussed below.

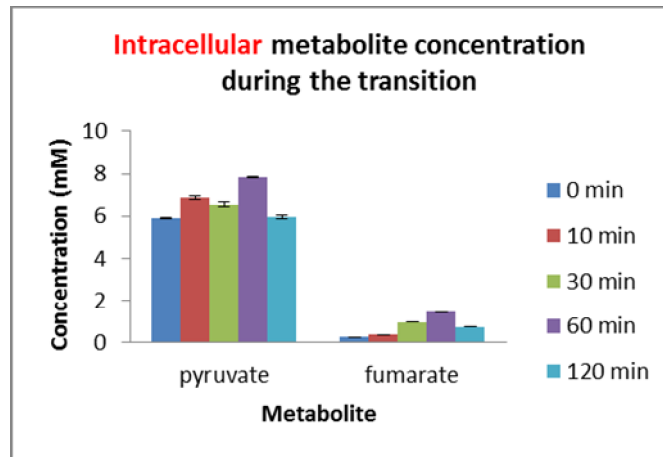
The most interesting result is that the concentration of pyruvate remains approximately constant across the time period. Considering the very large changes in fluxes through metabolic pathways, this result is a surprise. As oxygen is introduced, we expect PFL to be inhibited instantly, stopping metabolism of pyruvate by this route. Although PDHC is expressed even under anaerobic conditions (Trotter *et al* 2011), it is at low levels, and a change to aerobiosis leads to a marked upregulation of PDHC expression over approximately the first 30 minutes (Partridge *et al.* 2006). Thus, transcriptomic data implies that PDHC should be present only at low levels under anaerobic conditions, and would rise to typical aerobic levels 30-60 minutes after the introduction of oxygen. In turn, this implies that for the first 30 minutes, the pyruvate produced continuously by glycolysis should have almost no route to further metabolism and should rise to very high concentrations in the cell. An analysis of gene activity in the cell after transition to aerobic conditions found a pattern of gene expression consistent with PdhR being inhibited by high concentrations of pyruvate (Trotter *et al.*, 2011). In addition, the rise and subsequent fall of pyruvate concentration outside the cell over the first 2 hours after transition implies very significant amounts of secretion of pyruvate from the cells: the obvious cause being a high level of pyruvate inside the cell. Thus, a large number of results imply that the concentration of pyruvate inside the cell should rise to very high levels (of the order of 500 mM) soon after introduction of oxygen. However, the results shown in Figure 4.9c show this not to be the case. There are several possible explanations of this discrepancy. These are discussed below. However first it was thought sensible to check whether pyruvate levels are in fact high using an assay for pyruvate.



(a): Formate, Acetate and Succinate



(b): Lactate, Putrescine and Acetyl aspartate



(c): Pyruvate and Fumarate

Figure 4.9: Metabolite concentration of intracellular metabolites; (a) formate, acetate and succinate; (b) lactate, putrescine and acetyl aspartate; (c) pyruvate and fumarate during the transition from anaerobic to aerobic. These data resulted from three replicates.

4.2.4 Pyruvate assay

This experiment was performed to measure the pyruvate concentration inside the cell during the transition from anaerobic to aerobic, because it is not clear how extracellular pyruvate can increase significantly and then decrease if the intracellular concentration apparently remains very low. Pyruvate concentration was measured by rapid quenching followed by use of a kit. This pyruvate assay kit (BioAssay System) used a single Working Reagent that combines pyruvate oxidase and hydrogen peroxide determination in one step. The principle of the kit is that pyruvate is oxidised by pyruvate oxidase via enzyme reactions to generate acetate, carbon dioxide and hydrogen peroxide (H_2O_2). H_2O_2 then reacts with the Dye Reagent to form the colour. The colour intensity of the reaction was measured at 570 nm, which is directly proportional to pyruvate concentration in the sample. The OD of the samples was plotted against pyruvate standard curves (Figure 4.10a) and the pyruvate concentration was calculated. Figure 4.10b shows that the level of pyruvate is highest at 0 min (12 mM) and decreases after the introduction of air to 6 mM at 120 min. This result compares reasonably well with the result from NMR (Figure 4.11). Table 4.5 summarises the intracellular pyruvate concentration from the assay during the transition. The significance of this result is discussed in Section 4.3.

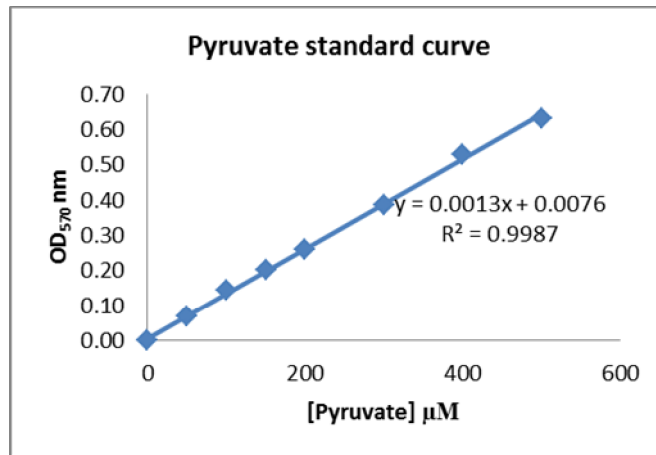


Figure 4.10a: Pyruvate standard curve

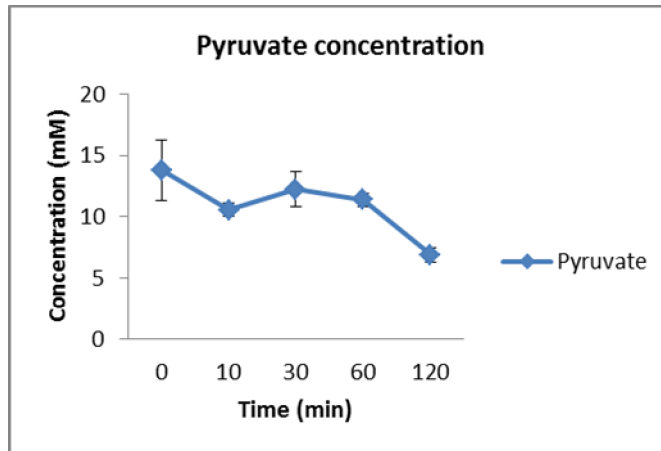


Figure 4.10b: Pyruvate assay on WT intracellular extracts on transition from anaerobic to aerobic. The cells were assayed at 570 nm and the concentration of pyruvate was measured.

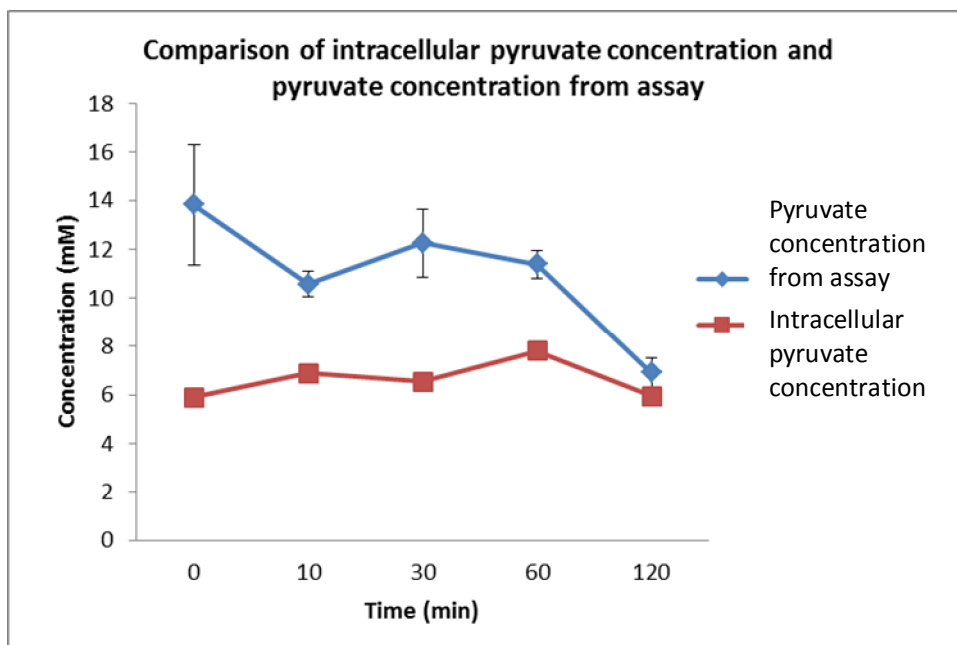


Figure 4.11: Graph comparing the concentration of intracellular pyruvate and the pyruvate concentration obtained from assay.

Time after transition (min)	Pyruvate concentration (mM)
0	13.8
10	10.6
30	12.3
60	11.4
120	6.9

Table 4.5: Pyruvate assay on WT intracellular cells on transition from anaerobic to aerobic.
The cells were assayed at 570 nm and the concentration of pyruvate was measured.

4.2.5 Detection of unknown peak

A possibly significant observation that can be seen by NMR is the presence of an unknown peak after the introduction of air (Figure 4.12). The peak was detected at 30 and 60 min while no peak appears at 0 min. It had disappeared again by 120 minutes. This kind of behaviour is what was expected for pyruvate based on the time dependence of the extracellular pyruvate (a transient rise followed by decay), although with much higher concentration than the unknown peak here, which only reaches about 1 mM maximum. This is the only signal in the intracellular spectra that shows behaviour like this. The peak may therefore provide some clue about changes in metabolism. Further identification of the unknown peak was attempted using HPLC and NMR.

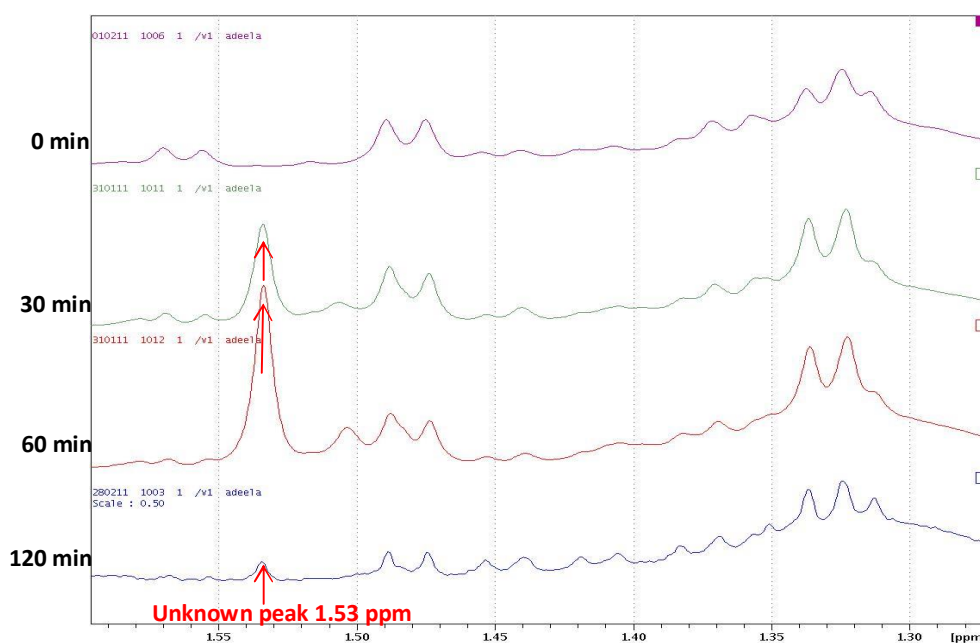


Figure 4.12: Detection of unknown peak at 30 and 60 min after the transition from anaerobic to aerobic. No peak was detected in the 0 min sample, and it had almost disappeared again by 120 minutes.

The chemical shift of the unknown peak varied with the pH of the sample, implying that it may be from a metabolite with a titratable group, such as a carboxylic acid. The chemical shift, together with its lack of observable *J* coupling, implies that it is a methyl signal. A natural abundance ^{13}C HSQC spectrum (Figure 4.13) shows that the attached carbon has a chemical shift of 25.9 ppm, confirming its likely assignment as a methyl group. A long-range HMQC spectrum (Figure 4.14) is ambiguous, but implies that the methyl carbon is 1-2 bonds away from other carbons with chemical shifts of 61.3 and 39.0 ppm.

It would help a lot to get an NMR spectrum of the pure compound. Therefore the 30-minute sample was run down an HPLC column. If this is a low molecular weight carboxylic acid then it may be possible to separate it either using an anion exchange column, or a reverse phase column at low pH where the carboxylic acid should be protonated. Separations were therefore tried using a C-18 column. The unknown peak is quite likely to have no UV absorbance, and so NMR spectra were run on freeze-dried fractions from the column. Spectra acquired at 4, 5 and 6 minutes are shown in Figure 4.15. It can be seen that there is a small degree of purification of the unknown, but not enough to identify the signals from the unknown. The results shown in Figure 4.15 are the best separation achieved. Accordingly, to date it has not been possible to purify the unknown peak to any useful degree.

There are now a number of databases of metabolites, which may be useful for identifying the unknown from the small number of chemical shifts available. The shifts obtained were put through a range of databases, namely Biological Magnetic Resonance Data Bank (BMRB, <http://www.bmrw.wisc.edu/metabolomics/>), Spectral Database for Organic Compounds (SDBS, http://riodb01.ibase.aist.go.jp/sdbs/cgi-bin/cre_index.cgi?lang=eng), COLMAR (<http://spinportal.magnet.fsu.edu/>), the Human Metabolome Database (<http://www.hmdb.ca/>), the Metabolomics Database of Linkoping (MDL, <http://www.liu.se/hu/mdl/main/>), and the PRIME database (<http://prime.psc.riken.jp/>). A number of hits were found, but most were chemically unreasonable. The most promising

results came from using the ACD/Labs software, generously made available by Dr V Paget of ACD/Labs. This software suggested that possible matches might be the types of compounds shown in Figure 4.16a. These compounds share a common structural feature as shown in Figure 4.16b, which is interesting because it could be formed by reaction of pyruvate. It is therefore possible that the unknown is some kind of adduct of pyruvate. One obvious possibility is that the unknown peak could simply be the hydrate of pyruvate, which in water is in equilibrium with the non-hydrated form, as discussed in Chapter 3. This was checked by spiking and shown not to be the case (chemical shift for pyruvate hydrate is 1.47 ppm, and unknown peak is 1.53 ppm). The similarity in shifts does however strengthen the possibility of the unknown being an adduct of pyruvate. This result therefore again provides indirect evidence to suggest that intracellular pyruvate concentrations could be high during the transition and then decrease after the first 60 minutes, in contrast to the intracellular NMR measurements, which suggest a fairly steady decrease.

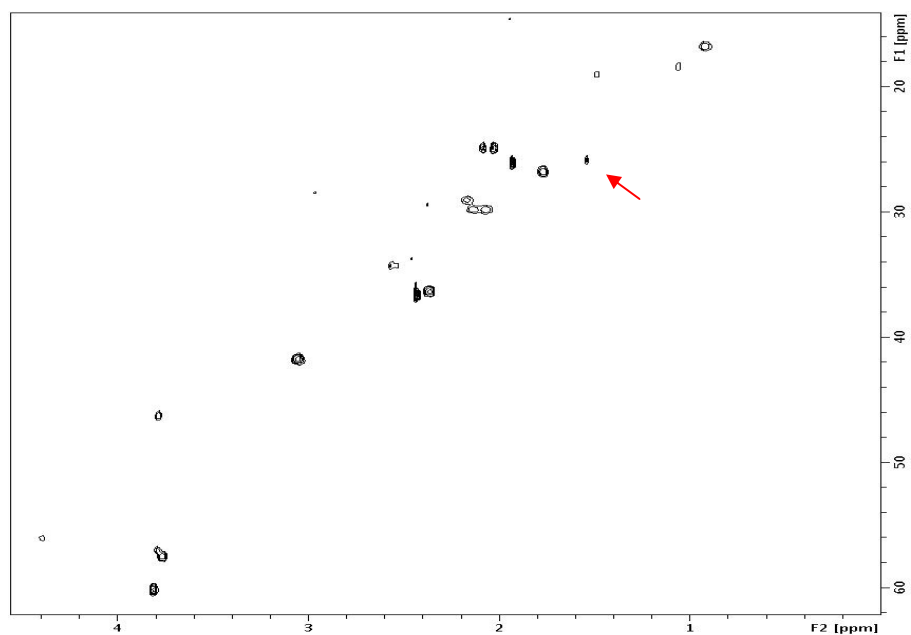


Figure 4.13: A ^{13}C HSQC spectrum of the unknown peak. The correlation for the ^1H signal at 1.53 ppm (shown by an arrow) is at a ^{13}C shift of 25.9 ppm.

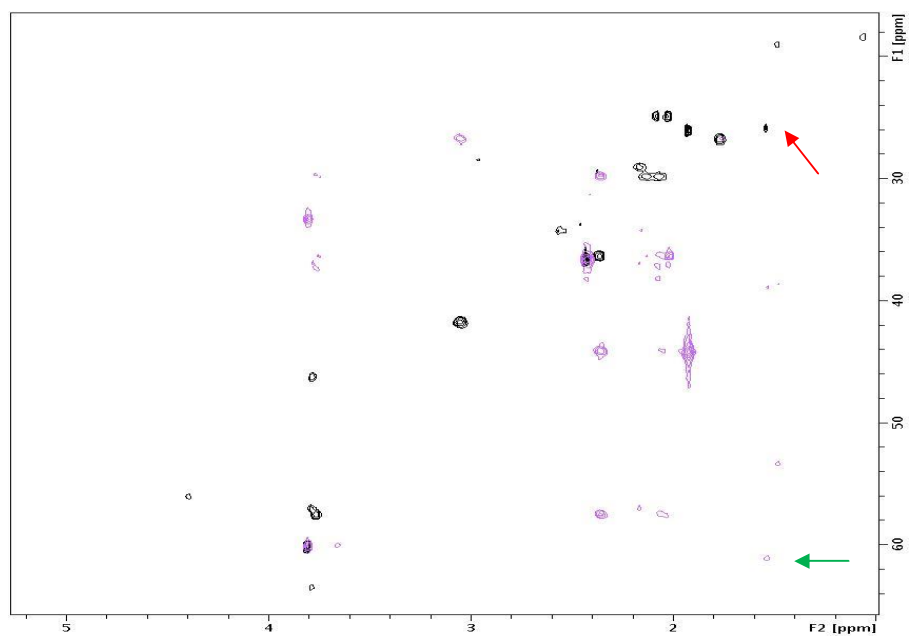


Figure 4.14: A long-range HMQC spectrum of the unknown peak. The spectrum in black is the HSQC spectrum from Fig. 4.13. The spectrum in magenta is the long-range HMQC. The possible long-range correlation is marked by a green arrow.

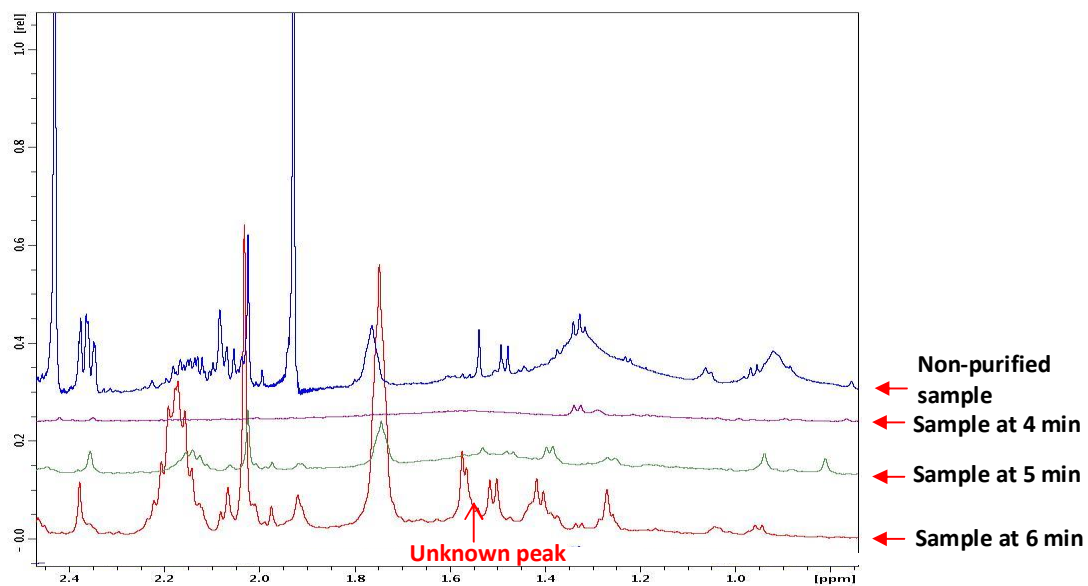


Figure 4.15: NMR spectrum of purified samples at 4, 5 and 6 mins separated by reversed phase chromatography. The purified samples were compared with non-purified sample as shown above.

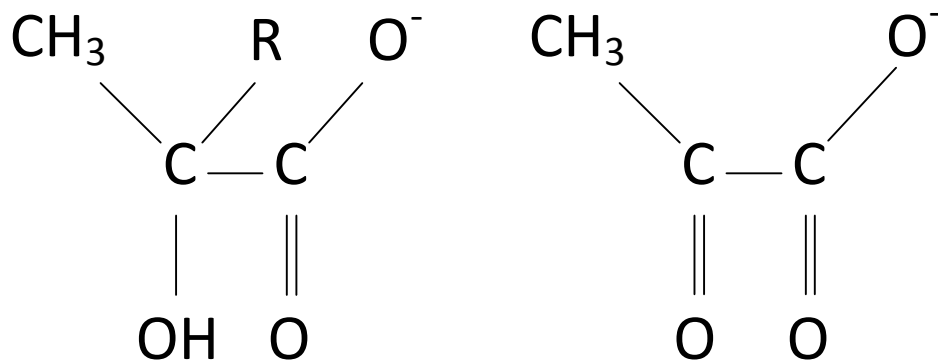


Figure 4.16: (a) Structure of expected compound, (b) Structure of pyruvate

4.3 Discussion

Metabolomics aims to quantify the level of all intermediates of metabolism. Intracellular metabolites of selected pathways have been measured for several decades, mostly by enzymatic assays. The novel feature of metabolomics is the quest for system wide coverage of all metabolites. The increased coverage is facilitated by the recent advances in high-throughput analytics. Metabolomics thus complements genomics, transcriptomics and proteomics in the systems biology approach to studying organisms.

To gain better understanding into the regulation of *E. coli* metabolism, we studied the metabolic profile of *E. coli* at different oxygenation levels using NMR. The bacterial cultures were grown in a glucose-limited chemostat at a dilution rate of 0.2 h^{-1} , where glucose is used as a cell-mass precursor and energy source. This was felt to be a suitable dilution rate because at higher dilution rates (above 0.4 h^{-1}), glucose and acetate concentrations are increased while at low dilution rate, metabolism is oxidative and no formation of acetate occurs (Kayser *et al.* 2005). Steady-state chemostat cultures are an important tool for the study of metabolic changes because chemostats permit the system to be regulated to achieve a desired glucose consumption rate through the selection of dilution rate and also permit collection of metabolite information which represents itself at a steady state. Results in this chapter provide insights into metabolic regulation in *E. coli* as a model during the transition from fermentative to respiratory metabolism.

Almost no metabolite accumulation was observed in the extracellular extracts during aerobic steady state compared to cells grown during anaerobic conditions (Figure 4.2a and Figure 4.3a). When oxygen is available, aerobic respiration allows the complete oxidation of glucose to yield CO_2 , NADH and acetyl-CoA, with the help of pyruvate dehydrogenase complex (PDHC) to generate ATP via electron transport chains. In fermentative metabolism, redox balance is achieved by the formation of the overflow metabolites acetate, ethanol,

formate and succinate (Figure 4.3a) to regenerate the NAD^+ needed for use in glycolysis, as it is not going to be regenerated by electron transport chains, as happens in aerobic respiration. Anaerobic respiration is the incomplete oxidation of glucose and results in less energy production per glucose than aerobic respiration. This makes aerobic respiration the most preferred and productive metabolic mode when compared to anaerobic respiration. A large number of metabolites are present in the intracellular extract as presented in Figure 4.2b. Bennett *et al.* (2009) have observed 103 metabolites that are present in glucose-grown *E. coli* cells, with a total observed intracellular metabolite pool of approximately 300 mM. Glutamate was the most abundant compound, followed by glutathione, fructose-1,6-bisphosphate and ATP. Glutamate is derived from transamination of α -ketoglutarate, together with other products, like pyruvate and oxaloacetate.

In order to understand more about adaptation of *E. coli* to low oxygen levels, the metabolites of this organism were analysed at different levels of oxygenation (section 4.3). The results show a decrease in formate and acetate production above 40% air. Both formate and acetate are major products of fermentative metabolism where pyruvate formate lyase (PFL) converts pyruvate to acetyl-CoA and formate. At higher oxygen concentration, the PFL activity is repressed and pyruvate dehydrogenase complex (PDHC) is activated, hence the aerobic pathway is activated too. A PFL-repair protein, YfiD, plays a major role during microaerobic condition as PFL has been destroyed by the lower amount of oxygen presence in this condition. Transcriptome studies by Partridge *et al* (2007) shows that *yfiD* is expressed maximally under microaerobic condition. Glucose consumed will be fully oxidised to water and carbon dioxide, which explains the decrease in concentration of formate and acetate at higher concentrations.

This study shows that microaerobic condition is fully achieved with a rapid onset between 40 - 60% air. It has previously been observed that under aerobic conditions FNR activity rapidly reduced ~ 15 -fold lower than the anaerobic activity which indicates that the cell membrane has consumed sufficient oxygen to lower oxygen concentrations in the

cytoplasm (Trotter *et al.* 2011). This is consistent with transcriptome analysis on cytochrome *bd* terminal oxidase that has high affinity for oxygen, and is only upregulated under lower oxygen levels but not in anaerobic cultures (Partridge *et al.* 2006, 2007).

The chemostat is working at a replacement rate of 0.2 hr^{-1} . This means that if intracellular metabolism/secretion stops abruptly on introducing air, extracellular metabolite levels should decrease at $20\% \text{ hr}^{-1}$. This behaviour can be observed for formate and succinate, and approximately for ethanol, implying that they are not secreted once the transition to aerobic growth has begun.

Formate is produced by PFL, and is a waste product, required for redox balance. It is therefore secreted by the cell. The stopping of formate secretion is therefore expected. Similarly, ethanol is produced by fermentation for redox balance. Succinate is another redox balance compound and is secreted during anaerobic growth. During early adaptation to aerobic conditions the *dctA* transcript (which encodes the C4-dicarboxylic acid transporter that transports succinate) increased 2-fold (Partridge *et al.* 2006), in agreement with the expectation that succinate could be taken up by the cell from the medium to be used again to feed the Krebs cycle. This may explain why the concentration of extracellular succinate appears to decrease by more than $20\%/hr$ (Figure 4.6c).

As can be seen in Figure 4.7a, the level of acetate remains stable, suggesting that acetate is being produced by the cells throughout the transition. Transcriptomic analysis showed that *poxB* transcripts were increased 2-5 fold at 15 and 60 min after the transition, which is consistent with the above results that acetate is generated in the presence of oxygen (Partridge *et al.* 2006). *poxB* is a gene that encodes pyruvate oxidase, which converts pyruvate to acetate and CO_2 .

A small number of extracellular metabolite signals increase during the transition, in particular putrescine, acetyl aspartate and fumarate. Their concentrations are low, but significant. Surprisingly, the intracellular concentrations of these metabolites does not alter during the transition. Thus, it is not likely that the extracellular concentrations increase simply because the intracellular concentrations increase. Putrescine functions to bind to DNA and help to package it in the bacterial chromosome. During gene expression, putrescine is released from DNA. Thus, the secretion of putrescine from cells during the transition may be a consequence of increased gene transcription: although the concentration of intracellular putrescine does not change much, the amount of free putrescine (ie, not bound to DNA) may change significantly. The increase of fumarate during the transition may be related to the role of fumarate in anaerobic growth: fumarate is reduced to succinate in order to regenerate NAD^+ , and the succinate is secreted. When the cells start to grow aerobically, this pathway is no longer needed. Acetyl aspartate is not a known metabolite of *E. coli* (based on the EcoCyc *E. coli* database, www.ecocyc.org). It is therefore likely that this metabolite is not in fact acetyl aspartate, but we have not been able to identify a more likely candidate.

The most interesting observation is the concentration of pyruvate. Extracellular pyruvate rises for the first hour of the transition and then decreases again. However, intracellular pyruvate is approximately constant in the NMR spectra, despite several indirect experimental results that suggest that it should increase to about 500 mM. Possible explanations for this behaviour include:

- a) NMR spectra only detect mobile molecules. If the pyruvate is somehow made immobile, for example by packaging into vesicles, polymerisation, or binding to some storage molecule, then it would not be seen. This explanation seems inherently unlikely: firstly because no such storage system is known (nor is one observed by transmission electron microscopy of these cells, as shown in Chapter 5), and secondly because even if such a system operated one would expect a transient

increase in pyruvate concentration to be visible by NMR. The fact that the pyruvate assay did not detect any increase in pyruvate inside the cell makes this idea even less likely. If pyruvate were involved in some sort of storage, then one would expect this to be in equilibrium with free pyruvate, so that removal of pyruvate by the assay should lead to release of pyruvate and thus a steady increase in observable pyruvate.

- b) Pyruvate could be secreted directly from the cell without going first into the cytoplasm. The most obvious way in which this could occur is that the enzymes involved in glycolysis could associate to the cell membrane and function to secrete pyruvate directly through a channel. It is remarkable that no pyruvate transporter in *E. coli* has been identified, but it would be surprising if such a channel did not exist. Precedents for such behaviour do exist, and are discussed in more detail in the next chapter.

Because (a) seems so unlikely, and there are no other obvious explanations that we can think of, it is possible that (b) is the true explanation. If so, this would be a very interesting observation, being a striking metabolic change, with a good explanation (ie, to keep the intracellular concentrations of metabolites roughly constant and to prevent pyruvate concentrations building up to excessive levels), and an unusual phenomenon, particularly in bacteria. Therefore, further experiments were carried out to test the hypothesis that glycolytic enzymes associate with the cell membrane on introduction of air, leading to direct secretion of pyruvate. These experiments are described in the next chapter.

CHAPTER 5

METABOLITE CHANELLING

5.0 Metabolite channelling

5.1 Introduction

The previous chapter showed that although extracellular pyruvate rises and then falls significantly during the transition of *E. coli* from anaerobic to aerobic growth, the intracellular concentrations are essentially unchanged, despite an expectation that levels of pyruvate could rise to as high as 500 mM because of loss of the activity of pyruvate formate lyase before the activity of the PDH complex is sufficient to deal with the flux through the glycolytic pathway. Thus the cells appear to work very hard to maintain homeostasis. The hypothesis to be investigated in this chapter is that a complex of glycolytic enzymes moves from a cytoplasmic location (where it is located during anaerobic growth) to the cell membrane, in order to be able to pump pyruvate directly out of the cell. In the present study, we investigated the movement of the pyruvate kinase enzyme pykF during the transition, whether it remained located in the cytoplasm or moved to the cell membrane. Possible movement of pykF following the transition from anaerobic to aerobic growth was investigated in three ways: first, by assaying pyruvate kinase activity in cytoplasmic and membrane fractions; second, by labelling chromosomal pykF with green fluorescent protein (GFP) and using fluorescence microscopy; and third, by labelling chromosomal pykF with a FLAG-tag and using immunohistology to determine the location of pykF.

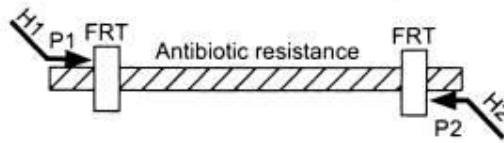
Modification of chromosomal genes is not simple. A recently developed powerful technique for efficient *in vivo* genetic manipulation of bacteria, termed recombineering (recombination-mediated genetic engineering), has the advantage of using short homologous DNA. It is mediated by bacteriophage-based recombination systems such as the Red system, RecET or others. The system was first described in *E. coli* (Datsenko and Wanner, 2000), but has since successfully been applied to other bacteria, for example, *Salmonella* (Husseiny and Hensel, 2005), *Shigella* (Beloin *et al.*, 2003), *Serratia* (Rossi *et al.*,

2003) and *Yersinia* (Derbise *et al.*, 2003). It is now widely used for a variety of purposes: the construction of chromosomal gene knockouts, deletions, insertions and point mutations. Briefly, recombineering is performed by introducing linear DNA substrates containing the desired change and short homologies to the target DNA into cells expressing the phage-encoded recombination enzymes. These enzymes recombine the linear DNA at the target, yielding recombinant molecules.

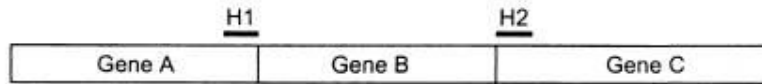
Normally, linear DNA introduced into *E. coli* is degraded by the powerful RecBCD nuclease. Linear DNA recombination systems in *E. coli* were developed by finding ways to inhibit the intracellular exonucleases. In the Red system, the Gam protein inhibits the RecBCD nuclease and prevents it from attacking the linear DNA fragments, and Exo (a 5'-to-3' exonuclease) and Bet (a single-strand DNA binding protein) generate recombination activity for the linear DNA. The length of the homologous region used for homologous recombination can be as short as 35-50 bp (Poteete, 2001; Court *et al.*, 2002). Zhang *et al.* (1998) showed that RecET recombinase could be used to disrupt plasmid-borne genes with linear DNA fragments. Other researchers (Datsenko and Wanner, 2000; Yu *et al.*, 2000) have made use of the advantages of the phage lambda Red (*gam*, *bet*, *exo*) that promotes a greatly enhanced rate of recombination when using linear DNA. Datsenko and Wanner (2000) used Red-mediated recombination for efficient deletion of specific genomic segments in *E. coli*, by replacing a chromosomal target with a linear DNA fragment that carries a selectable antibiotic resistance gene flanked by 50-nucleotide (nt) extensions that are homologous to selected sequences in the bacterial chromosome (Figure 5.1). Linear DNA is required for Red-mediated recombination. This can be either a linear double-stranded DNA (dsDNA) generated by PCR or a short single-stranded DNA (ssDNA) oligonucleotide carrying homology to the target (Court *et al.* 2002).

In yeast, genes can be directly disrupted by transformation with double-stranded DNA (dsDNA) fragments, created with PCR, that encode a selectable marker and have only about 50 bp of flanking DNA that are homologous to the chromosome region of interest. However,

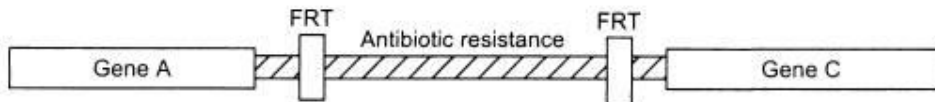
Step 1. PCR amplify FRT-flanked resistance gene



Step 2. Transform strain expressing λ Red recombinase



Step 3. Select antibiotic-resistant transformants



Step 4. Eliminate resistance cassette using a FLP expression plasmid

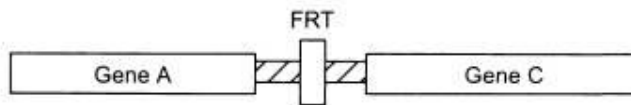


Figure 5.1: A simple gene disruption strategy. H1 and H2 refer to the homology extensions or to priming sites (Adapted from Datsenko and Wanner, 2000).

in *E. coli*, intracellular exonucleases, such as RecBCD, degrade linear DNA (Yu *et al.*, 2000) and inhibit recombination with the PCR products.

Here we describe an adaptation of the lambda Red-based methodology for use with *E. coli*, in which chromosomal single gene deletions were generated using a 2-step PCR product containing 40-nucleotide flanking regions that are homologous to the target sequence. Pyruvate kinase is the key enzyme in this study as it catalyses the transfer of phosphate group from PEP to ADP generating pyruvate and ATP in the final stage of the glycolytic pathway. There are two isoenzymes of pyruvate kinase; PykF and PykA. PykA contributes little to pyruvate kinase activity and the specific activity is much lower compared to PykF (Garrido-Pertierra and Cooper, 1983; Ponce *et al.*, 1995). Therefore pykF was targeted in this study.

5.2 Results

5.2.1 Pyruvate kinase (PK) enzyme assay

An experiment was carried out to look at the pyruvate kinase activity of *E. coli* during the transition from anaerobic to aerobic, by assaying supernatant and pellet samples at 0, 10, 60 and 120 min. PK activity was measured by rapid quenching and sonicating followed by use of a kit (Pyruvate kinase assay kit, Abcam). In the assay, the reaction between PEP and ADP is catalysed by PK to generate pyruvate and ATP. The generated pyruvate is oxidised by pyruvate oxidase via enzyme reactions to generate acetate, carbon dioxide and hydrogen peroxide (H₂O₂). H₂O₂ then reacts with the Dye Reagent to form the colour. The colour intensity of the reaction was measured at 570 nm. Since the increase in color intensity is proportional to the increase in pyruvate amount, the PK activity can be accurately measured. Figure 5.2 shows that the PK activity goes up 10 min after introduction of air for

both pellet and supernatant samples. The graph also shows that the PK activity in supernatant is higher than in the pellet. The hypothesis suggests that PK activity should move to the membrane shortly after introduction of air, and thus that the PK activity in the pellet should become much higher after the introduction of air, and conversely the activity in the soluble fraction should be reduced. However, the results clearly do not show the expected result. There are many possible reasons for this, of which a likely one is that the cell breakage and subsequent washing steps needed to separate the supernatant from the pellet disrupted any membrane complexes formed. In other words, it may be necessary to use a more *in vivo*-like measurement. We therefore decided to tag the PK enzyme with either GFP or 3XFLAG in order to get a clear picture of the location of pyruvate.

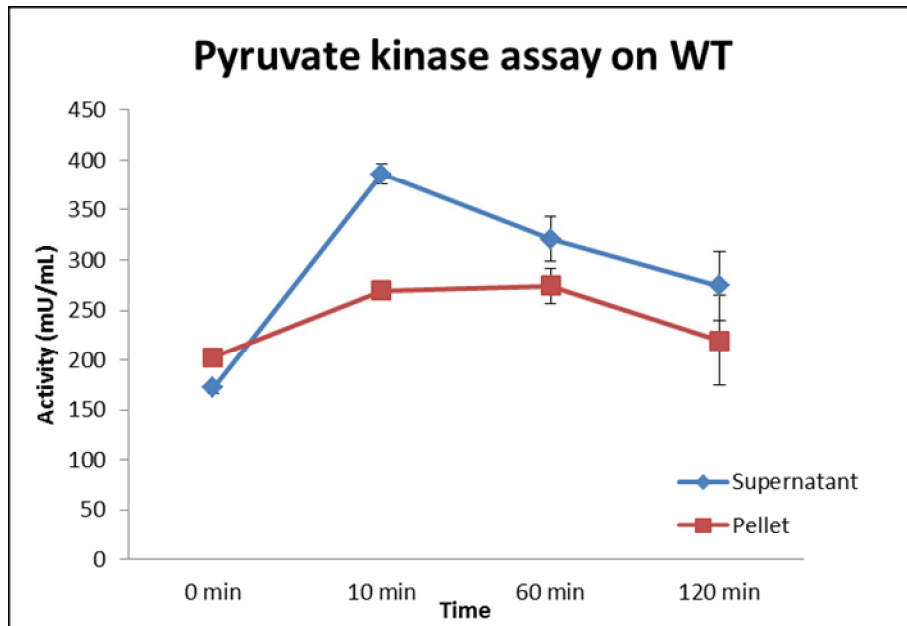


Figure 5.2: Pyruvate kinase assay on WT during the transition from anaerobic to aerobic cells. Both the supernatant and pellet samples were assayed at 570 nm and the concentration of pyruvate was measured at 0, 10, 60 and 120 mins.

5.2.2 Creation of mutants by linear transformation

To investigate the movement of pyruvate through the cell, two mutants (pykF-GFP and pykF-3xFLAG) were constructed by the method of linear transformation (Section 2.6). The *E. coli* strain MG1655 was selected as the parental strain and resulting mutants were created through the insertion of a kanamycin resistance cassette, which not only disrupted the gene of interest but also facilitated mutant isolation as a selectable marker (Kan^R). Constructions of the two different pykF-tag mutants were achieved in collaboration with Dr Matthew Rolfe and Prof Jeff Green at the University of Sheffield. The schematic diagram for creating the fusions is presented as below (Figure 5.3).

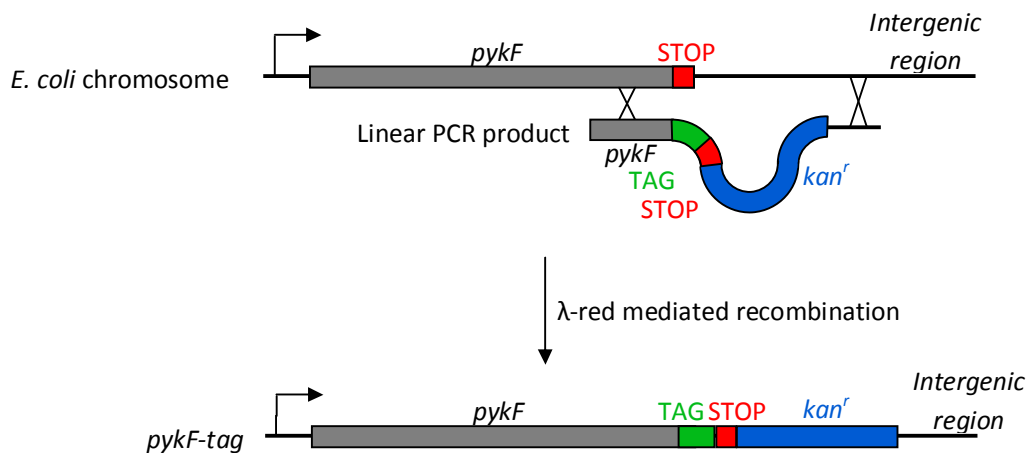


Figure 5.3: Construction of pykF-tag fusions. The linear PCR product is introduced by electroporation into cells induced for the Red recombining functions. The Red functions catalyse the insertion of the cassette at the target site, which is on the bacterial chromosome.

For *pykF*-GFP fusion, oligonucleotide primers (*pykF*-GFP_PCR1F, *pykF*-GFP_PCR1R) were used to amplify (Section 2.6.2) the coding sequence of GFP from a plasmid (pGFPmut3.1), using high fidelity Taq polymerase. The forward primer has a 5' end that is identical to the end of the *pykF* gene (40 bp) while the reverse primer has a 5' end that would amplify the kanamycin resistance cassette from pKD4 (20 bp). The purified PCR products were then used as a forward primer to amplify the *kan* cassette. A 40 bp region of homology was added to the end of the *kan* cassette by *pykF*-GFP_PCR2R, which is homologous to the intergenic region downstream of *pykF*. The respective 2.3 kbp PCR products were purified (Figure 5.4a), treated with *DpnI*, and then transformed into bacteria carrying the Red helper plasmid (Section 2.6.3.2 and 2.6.4). Kanamycin resistant colonies were selected and chromosomal disruption of *pykF* was confirmed by PCR using the primer pair, *pykF*_CheckF and *pykF*_CheckR (Section 2.6.5). Reaction products were analysed by agarose gel electrophoresis (Section 2.5.2) to confirm the region (Figure 5.5).

For *pykF*-3XFLAG fusion, the first PCR reaction was to amplify the kanamycin resistance cassette from pKD4 using primers that add a 3XFLAG tag and stop codon (*pykF*-3XFLAG_PCR1F), and a 40 bp region of homology (using primer *pykF*-3XFLAG_PCR1R) downstream of the cassette. The purified PCR products from PCR 1 were used as a template to add a 40 bp region of homology upstream (using primer *pykF*-3XFLAG_PCR2F) and the downstream end was simply reamplified by using primer *pykF*-3XFLAG_PCR2R. The purified PCR product (1.7 kbp) (Figure 5.4b) was introduced by electroporation into competent cells expressing the lambda-red recombinase from the pKD46 plasmid. Disruption was again confirmed by PCR using the same primer pair, *pykF*_CheckF and *pykF*_CheckR, and analysed by agarose gel electrophoresis (Figure 5.5). A schematic diagram for both *pykF*-GFP and *pykF*-3XFLAG mutants is shown in Figure 5.6 (a) and (b).

P1 phage was used to transduce the constructs into the bacterial chromosome as stable single-copy insertions (section 2.7.2). The presence of a single-copy chromosomal fusion was confirmed by streak testing (section 2.7.3). The constructs were further verified by DNA

sequencing. The sequences were analysed and aligned manually using the Bioedit program (Figure 5.7a for pykF-GFP and Figure 5.7b for pykF-3xFLAG). The results confirmed the presence of the fusion constructs on the chromosome.

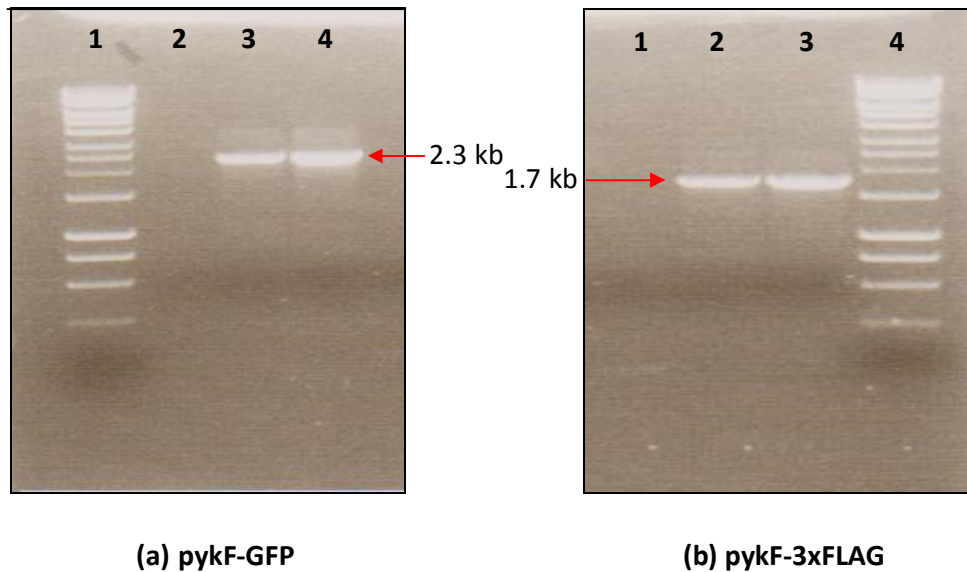


Figure 5.4: PCR purification of (a) pykF-GFP, lane 1: DNA markers; lane 2: Negative control; lane 3-4: pykF-GFP and **(b) pykF-3XFLAG**, lane 1: Negative control; lane 2-3: pykF-3XFLAG; lane 4: DNA markers.

*Primers used to generate (a) pykF-GFP are: pykF-GFP_PCR1F, pykF-GFP_PCR1R and pykF-GFP_PCR2R; and (b) pykF-3xFLAG are: pykF-3XFLAG_PCR1F, pykF-3XFLAG_PCR1R, pykF-3XFLAG_PCR2F and pykF-3XFLAG_PCR2R.

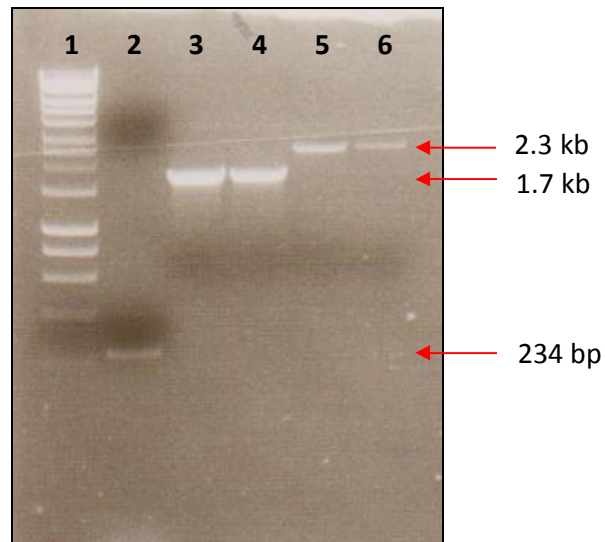


Figure 5.5: PCR verification of *E. coli* mutants. Lane 1: DNA markers; Lane 2: WT (control); Lane 3-4: *pykF*_GFP; Lane 5-6: *pykF*_3XFLAG. Results confirmed the tagging of GFP and 3xFLAG to the *pykF* sequence and insertion of the linear DNA into the chromosome by PCR using the primer pair, *pykF*_CheckF and *pykF*_CheckR.

PCR 1 Incorporate 'forward' 3xFLAG-STOP
& 'reverse' region of homology

PCR 2 Incorporate 'forward' region of
homology (removing
chromosomal stop codon)

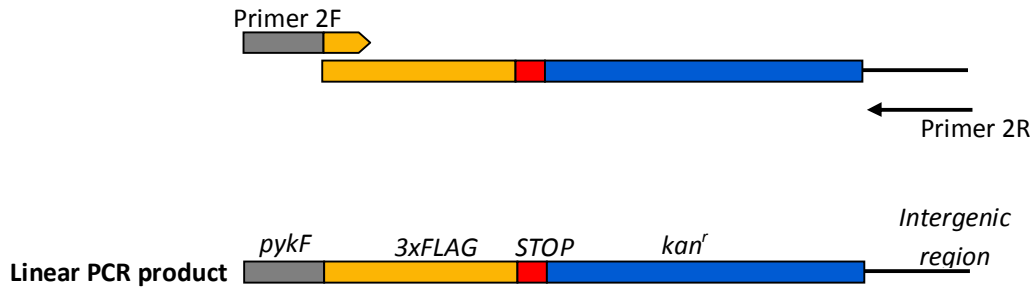
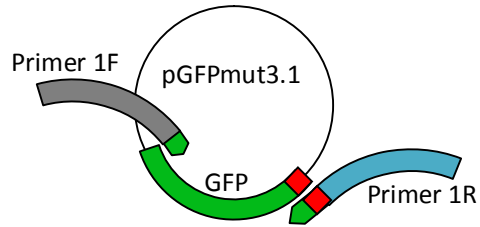
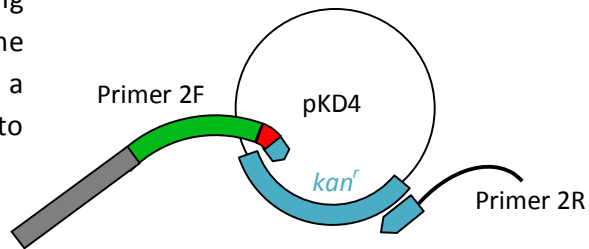


Figure 5.6a: Creating the *pykF*-3xFLAG linear PCR product. A linear PCR product containing the regions of homology, the kanamycin resistance marker, 3xFLAG tag and stop codon was generated using two-step PCR.

PCR 1 Amplify GFP from pGFPmut3.1 adding a 'forward' region of homology to *pykF* (removing chromosomal stop codon) and adding 'reverse' sequence corresponding to *kan^r*



PCR 2 Amplify *kan^r* from pKD4 using product from PCR1 as the forward primer and adding a 'reverse' region of homology to *pykF*



PCR 3 Amplify the whole linear product in a single PCR allowing efficient yields to be obtained

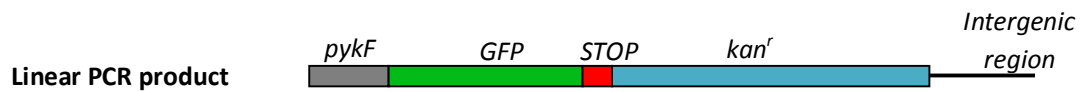
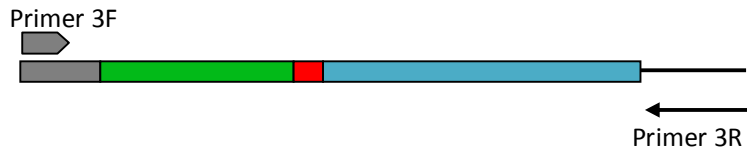
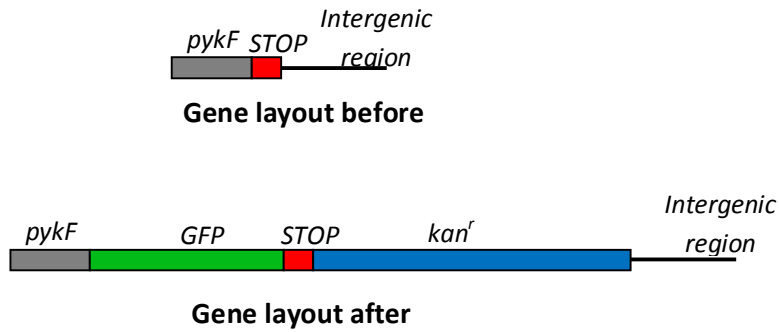


Figure 5.6b: Creating the *pykF*-GFP linear PCR product. A linear PCR product containing the regions of homology, the kanamycin resistance marker, GFP tag and stop codon was generated using two-step PCR.



AGCGGCACTACTAACACCGC ATCTGTTACGTCCTGCGTA AAGGAGAAGAACTTTTCACT
 GGAGTTGTCCCAATTCTTGT TGAATTAGATGGTGATGTTA ATGGGCACAAATTTTCTGTC
 AGTGGAGAGGGTGAAGGTGA TGCAACATACGGAAAACCTTA CCCTTAAATTTATTTGCACT
 ACTGGAAAACCTGTTCC ATGGCCAACACTTGTCACTA CTTTCGGTTATGGTGTTCAA
 TGCTTTCGAGATACCCAGA TCATATGAAACAGCATGACT TTTTCAAGAGTGCCATGCC
 GAAGGTTATGTACAGGAAAG AACTATATTTTTCAAAGATG ACGGGAACATAAGACACGT
 GCTGAAGTCAAGTTTGAAGG TGATACCCTTGTTAATAGAA TCGAGTTAAAAGGTATTGAT
 TTTAAAGAAGATGGAAACAT TCTTGGACACAAATTGGAAT ACAACTATAACTCACACAAT
 GTATACATCATGGCAGACAA ACAAAGAATGGAATCAAAG TTAACCTCAAATTAGACAC
 AACATTGAAGATGGAAAGCGT TCACTAGCAGACCATTATC AACAAAATACTCCAATTGGC
 GATGGCCCTGTCCTTTTACC AGACAACCATTACCTGTCCA CACAATCTGCCCTTTCGAAA
 GATCCCAACGAAAAGAGAGA CCACATGGTCCTTCTTGAGT TTGTAACAGCTGCTGGGATT
 ACACATGGCATGGATGAACT ATACAAATAAAGTGTAGGCTG GAGCTGCTTCGAAGTTCCTA
 TACTTTCTAGAGAATAGGAA CTTCGGA

Figure 5.7a: Manual alignment of DNA sequence of pykF-GFP by using BioEdit software. Sequence in grey represents pykF sequence; green: GFP; red: stop codon and blue: kanamycin resistance cassette.



Gene layout before



Gene layout after

AGCGGCACTACTAACACCGC ATCTGTTACGTCCTGGATT ACAAAGATCACGACGGCGAT
TATAAAGACCATGATATCGA TTATAAAGATGACGACGATA AATAATATTGCTTGTGTAGG
CTGGAGCTGCTTCGAAGTTC CTATACTTTCTAGAGAATAG GAACTTCGGAATAGGAACTT
CGAGATCCCCACGCTGCCG CAAGCACTCAGGGCGCAAGG GCTGCTAAAGGAAGCGGAAC
ACGTAGAAAGCCAGTCCGCA GAGACGGTGCTGACCCCGGA TGAATGTCAACTACTGGGCT
ATCTGGACAAGGGAAAACGC AAGCGCAAAGAGAAAGCAGG TAGCTTGCAGTGGGCTTACA
TGGCGATAGCTAGACTGGGC GGTTTTATGGACAGCAAGCG AACCGGAATTGCCAGCTGGG
GCGCCCTCTGGTAAGGTTGG GAAGCCCTGCAAAGTAAACT GGATGGCTTTCTTGCCGCCA
AGGATCTGATGGCGCAGGGG ATCAAGATCTGATCAAGAGA CAGGATGAGGATCGTTTCGC
ATGATTGAACAAGATGGATT GCACGCAGGTTCTCCGGCCG CTGGGTGGAGAGGCTATTC
GGCTATGACTGGGCACAACA GACAATCGGCTGCTCTGATG CCGCCGTGTTCCGGCTGTCA
GCGCANGGGCGCCCGTTCT TTTGTCAAGACCGACCTGT CCGGTGCCCTGAATGAACTG
CAGGACGAGGCAGCGCGGCT ATCGTGGCTGGCCACGACGG GCGTTCCTTGCGCAGCTGTG
CTCGACGTTGTCACTGAAGC GGAAGGGACTGGCTGCTAT TGGGCGAAGTGNCGGGGCAG
GATCTCCTGTCTACCT TGCTCCTGCCGAGAAAGTAT CCATCATGGCTGANGCAATG
CGGCGGCTGCATACGCTTGA TCCGGCTACCTGCCATTN ACCACCAAGCGAAACATCGC
ATCGAGCGGGCACGTACTCG GATGG

Figure 5.7b: Manual alignment of DNA sequence of pykF-3xFLAG by using BioEdit software. Sequence in grey represent *pykF* sequence; yellow: 3xFLAG tag; red: stop codon; black: a linker and blue: kanamycin resistance cassette.

5.2.3 Functionality of the tags

Functionality of the tags was checked by looking at the constructs under fluorescence microscope (for pykF-GFP) and western blotting, as well as transmission electron microscopy (TEM) (for pykF-3xFLAG).

5.2.3.1 Western blotting

After verification by PCR amplification and DNA sequencing, the functionality of 3xFLAG tag was analysed by Western blotting. Whole cell extracts were separated by SDS-PAGE and proteins transferred to nitrocellulose membranes, which were then probed with primary antibody specific to the tag (section 2.8.2.2). The membranes were then washed and probed with secondary antibody conjugated to horse-radish peroxidase. Figure 5.8 shows the Western blot of the purified constructs that was probed with Anti-FLAG (Sigma). The result clearly indicates a detection of pykf-3xFLAG tag fusion protein with exposures as short as 1 min. Positive control used is pET-21a(FLAG). It is an expressed FLAG tag in *E. coli* and was obtained from Lab F10, University of Sheffield (Lanes 3 and 7). This positive control should give a band, but after several trials, we were unable to observe any band for it. Even though there is no positive control to compare with, we strongly believe that the bands observed were the expected pykF-3xFLAG as it was consistently detected from several trials.

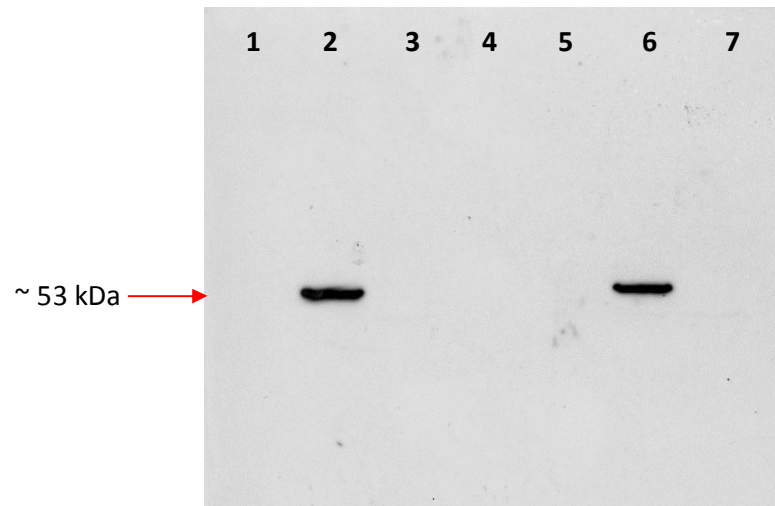


Figure 5.8: Western blot analysis of pykF-3xFLAG construct using Anti-Flag antibody. Lane 1 and 5: Prestained protein marker (Bio-Rad), Lane 2 and 6: pykF-3xFLAG, Lane 3 and 7: positive control {pET21-a(FLAG)}, Lane 4: WT.

5.2.3.2 Fluorescence microscopy (GFP tag)

The green fluorescent protein (GFP) from jellyfish retains its ability to fluoresce *in vivo* when expressed in other organisms, including bacteria (Chalfie *et al.* 1994). GFP has several features that make it an attractive candidate for protein localisation studies in bacteria. Several studies have demonstrated the applications of GFP as a reporter in protein localisation in *E. coli* (Feilmeier *et al.* 2000; Renzette *et al.* 2005). In this study, GFP was used to examine the movement of pykF enzyme inside the cell. To do this, a fusion construct of pykF with GFP was made as described in section 5.2.2. The verified construct was then grown in the chemostat and sampled at 0 and 30 min after the introduction of air. The cells were fixed immediately in paraformaldehyde-glutaraldehyde solution and placed on poly-L-lysine microscope slides (section 2.9). The images were acquired on an Olympus BX61 upright microscope fitted with a 100x (NA 1.4) oil objective with help from Dr Darren Robinson from the Light Microscopy Facility, University of Sheffield. Figure 5.9a shows a fluorescence microscopy image for the 0 min sample while Figure 5.9b shows an image for the 30 min sample. We expected to see that the fluorescence is uniformly distributed on the 0 min cells, while the fluorescence in the 30 min cells will move to the cell membrane.

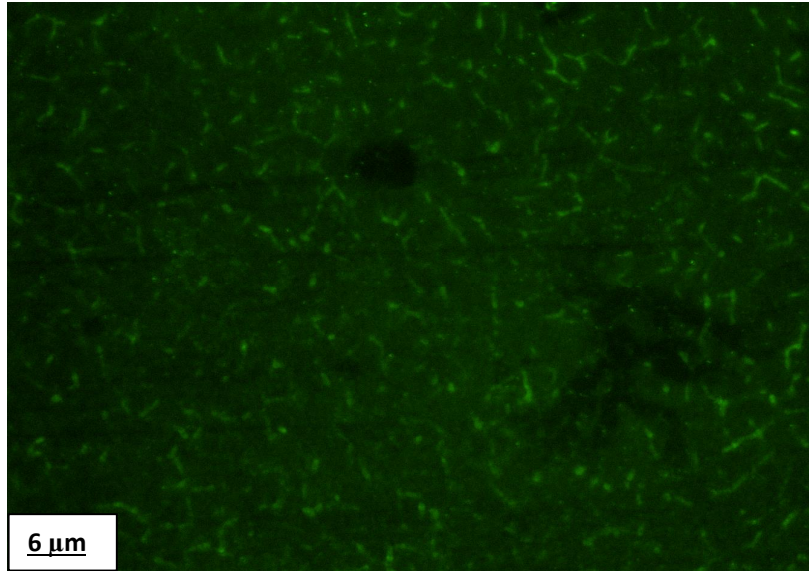


Figure 5.9a: Fluorescence microscopy images of pykF-GFP fusion protein at **0 min.**

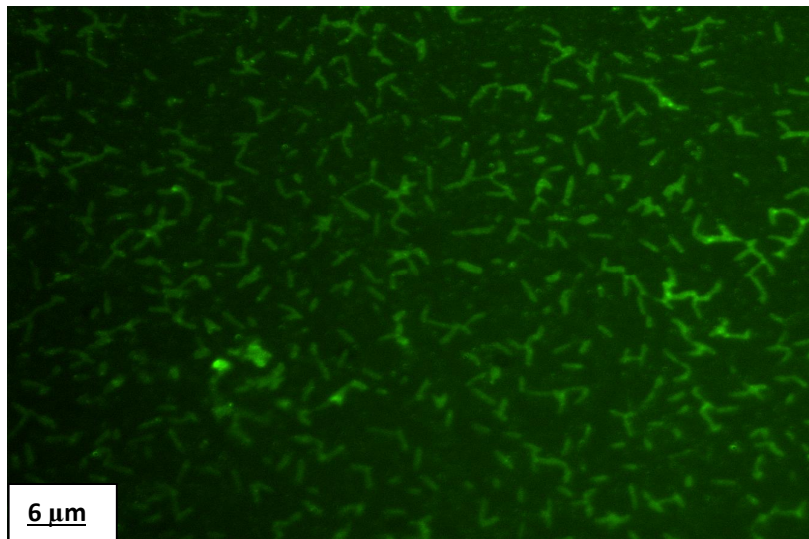


Figure 5.9b: Fluorescence microscopy images of pykF-GFP fusion protein at **30 min.**

The fluorescent *E. coli* cells can be seen clearly, although the intensity of fluorescence is not very great, possibly because pykF is not over-expressed, but is present simply at the same abundance as the chromosomal copy. This leads to rather high background in these images. The disappointing result is that no change in the location of fluorescence can be observed. The optimal resolution obtainable from this microscope is approximately 0.2 μm (200 nm), being limited by the diffraction limit, a consequence of the wavelength of green light. The width of an *E. coli* cell is approximately 1 μm , implying that it should be possible to see a relocalisation of the fluorescence. However, the cell dimensions are close to the resolution of the technique, and it was therefore not unexpected to have no observable effect using this method.

5.2.3.3 Transmission electron microscopy (TEM)

We therefore took advantage of immunogold labeling to visualise the movement of pykF-3xFLAG inside the cells. As in the previous section, cells were grown anaerobically in a chemostat, and then sampled either during anaerobic growth or 30 min after the transition to aerobic growth. The cells were fixed immediately (during the quenching) using paraformaldehyde – glutaraldehyde, and then dried, embedded in resin, and sectioned. The ca. 75 μm thick sections were deposited on formvar coated nickel grids and immunogold labeled with primary anti-FLAG and secondary antibodies conjugated with 10 nm gold particles. Primary anti-FLAG antibody has been used successfully in a non-denaturing application, namely immunoprecipitation (Civiero *et al.* 2012). The fractions were then negatively stained with uranyl acetate and observed directly under TEM.

Figure 5.10 shows TEM images of immunogold labeled samples; (a) and (b) represent 0 min samples and (c) and (d) represent 30 min samples. The nanogold label was observed to be uniformly distributed, mainly within the cytoplasm but also close to the cell and outer membrane, on the 0 min samples (Figure 5.10a and 5.10b), suggesting that the pykF enzyme

is located mainly inside the cells during anaerobic conditions. But pykF was observed to move significantly to the cell membrane during the transition to aerobic growth (Figure 5.10c and 5.10d). Approximately 102 images from the 0 and 30 min samples were analysed and scored based on the location of the gold particles (Table 5.1). The scoring shows that most of the enzyme was located inside the cells during anaerobic conditions (82%), 10% in the cell membrane and 7% in the outer membrane. Thirty minutes after introduction of air, the percentage of gold particles on the cell membrane is increased to 17%, as well as on the outer membrane with the same percentage. This suggests that the enzyme did move to the cell membrane when oxygen is present, though not to such a large extent as expected. Although the observation of nanogold particles in the outer membrane is unexpected, this result does support the hypothesis that the pykF enzyme is associated with cell membrane after the introduction of air.

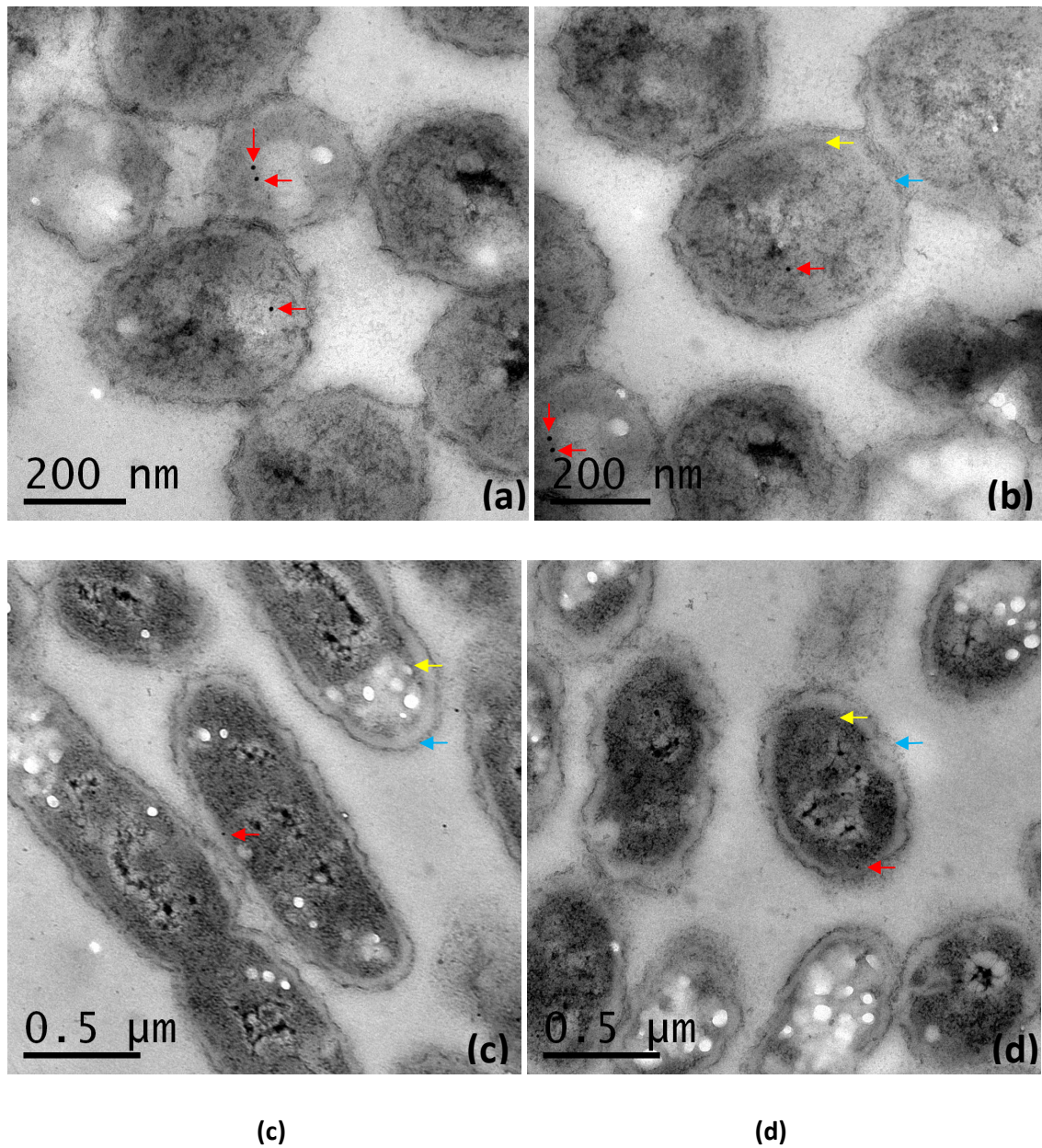


Figure 5.10: Transmission immunogold electron micrographs showing the location of pykF-3xFLAG inside *E. coli* cells. The arrows show immunogold labelling of 0 min (a and b) and 30 min samples (c and d). The sections were labeled with anti-FLAG antibodies coupled to 10 nm nanogold particles, which are observable as intensely black circular particles. The yellow arrow shows a cell membrane and the blue arrow shows an outer membrane. The white circular objects inside the cells are probably artifacts of incomplete penetration of resin (Dr Chris Hill [EM facility], personal communication).

Table 5.1: Percentage of scoring of gold particles in *E. coli* cells

Location	0 min (%)	30 min (%)
Intracellular	82	64
Cell membrane	10	18
Outer membrane	8	18

5.3 Discussion

The most important objective of this chapter is to look at the localisation of the *pykF* gene product inside the cells during the transition from anaerobic to aerobic. Results from the previous chapter (Chapter 4) show that the metabolome doesn't do much during the transition. Trotter *et al.* (2011) has shown that PFL (active under anaerobic conditions) is instantly killed when oxygen is introduced. The increases and decreases of external pyruvate (section 4.2.3.1) are consistent with the immediate loss of PFL and slow increase of PDHC activity as reported by Trotter *et al.* (2011). But our metabolic observation doesn't show a very high level of internal pyruvate. This is a surprise as the growing cells continue to metabolise glucose to pyruvate, thus we expect the concentration of internal pyruvate should be high.

The discrepancy may be explained in several ways. It is possible that the metabolism of pyruvate is so fast that even using the rapid quenching technique, it is metabolised away before it can be seen inside cells. There is however no sign of potential metabolic products of pyruvate, except for the very small rise and fall in the unknown metabolite signal in Chapter 4. There is a possibility that pyruvate is being stored or transported out. Storage granules are not common in bacteria, and there is no sign of such granules in the EM images

obtained (assuming that the white regions in the cells are artifacts and not granules). The hypothesis behind the transport theory is that glycolytic enzymes may relocate to the cell membrane from the cytoplasm. In order to do this, we examined the movement of pykF inside the cells. pykF is an isoenzyme of pyruvate kinase (with pykA), of which pykF is considered the main activity in *E. coli* (Emmerling *et al.* 2002; Siddiquee *et al.* 2004). It is a key enzyme that catalyses the conversion of PEP to pyruvate and ATP. The work started by making two pykF fusions; one with 3xFlag and another one with GFP.

We have adapted recombineering technology to efficiently construct targeted mutations on the chromosome of *E. coli*. It was felt to be important to use chromosomally regulated and synthesised genes, to avoid potential problems from unphysiological concentrations of pykF. This strategy has been shown to promote high efficiency gene replacement with such substrates in *E. coli* K-12. (Murphy, 1998). The mutagenesis process could be simplified by electroporating a PCR product that contains an antibiotic cassette flanked by sequences homologous to the targeted DNA into a strain expressing the lambda red system. The presence of the specific PCR product promotes the deletion of the chromosomally located targeted region via homologous recombination. A two-step strategy of PCR was performed to create pykF-GFP and pykF-3XFLAG fusions. The linear DNA substrate is made by PCR amplification of flanking regions that are homologous to the target sequence. These primers consist of 40 bases of homology to the target region, where the tag is to be inserted, followed by 20 bases to prime the antibiotic cassette. The PCR fragment is introduced via transformation into competent cells that have been induced for the Red system. We encountered considerable difficulty to electroporate the constructs into the bacterial chromosome with the λ Red proteins encoded on a temperature sensitive, ampicillin resistant plasmid pKD46. In the final successful strategy we used SL1344pSIM18, in which pSIM18 is a temperature-sensitive origin (ori101) and compatible with both ColE ori and oriS. This temperature-sensitive origin is useful for removing the pSIM plasmid itself. As shown by Chan *et al.* (2007) the PL promoter in pSIM is controlled by a temperature-sensitive lambda phage cI857 repressor.

Recombination with long (~1 kb) linear dsDNA carrying flanking target homologies requires all three λ Red functions, Gam, Beta and Exo (Murphy, 1998; Zhang *et al.* 1998; Yu *et al.* 2000). The λ Red system has been shown to be efficient to work on short homologies. β protein promotes efficient *in vivo* recombination with ssDNA (Ellis *et al.* 2001). Recombineering requires that the single-strand regions of the incoming linear DNA bound by the Beta protein are annealed to complementary single-strand gaps arising at the replication fork during DNA replication. The Gam protein inhibits the *E. coli* RecBCD and is not absolutely required for recombineering but increases the frequency of dsDNA recombination up to 20-fold (Datta *et al.* 2008). Host DNA polymerases like PolA and DNA ligase play an important role in the recombination process completion (Yu *et al.* 2003).

The pykF fusion constructs were verified by PCR and DNA sequencing analysis. For pykF-3xFlag, it has been detected by Western blot analysis (section 5.2.3.1) with an anti-Flag antibody. Localisation of pykF in *E. coli* during the transition was observed by TEM (section 5.2.3.3). In anaerobic conditions, the nanogold label was distributed uniformly inside the cells but moved to the cell membrane when oxygen is present. There is a significant redistribution of the gold label to both the cell and outer membranes 30 min after introduction of air. The reason why the enzyme moves to the outer membrane is unknown, but this result does support our initial hypothesis and may explain the missing pyruvate. The relocation of pykF to the cell membrane is less dramatic than expected. It is possible that 30 min is too late: transcriptional changes were observed as early as 30 s after the introduction of air, and by 30 min many of the metabolic changes are complete (Trotter *et al.* 2011). This investigation will therefore be extended to look at 2 and 5 min time points to get a clearer picture of the movement of pykF after the transition.

Investigation of the pykF-GFP fusion by fluorescence microscopy did not give much information on the localisation of pykF due to limitations on the microscopy that cannot resolve the GFP very well. The cells were expressing GFP but we cannot see any change in the distribution of the enzyme inside the cells. The cells were initially fixed in 0.2%

glutaraldehyde but we have increased this to 10% to have more rigid cross-linking and cytoplasmic detail. Glutaraldehyde in particular provides a rapid cross-linking but causes high background fluorescence compared to formaldehyde fixation. It is not unexpected to be unable to see any change in the fluorescence. Similarly, the lack of any effect in the enzyme assay was expected because this procedure requires cell disruption and physical separation of the membrane fraction from the cytoplasm, which could easily disrupt any membrane complexes formed.

The potential relocation of pykF (and thus possibly of the entire glycolytic complex) to the cell membrane is a novel and very interesting observation. The existence of a glycolytic metabolon has been postulated for many years but has been a very controversial topic (Srere, 1987; Srere, 2000; Ovádi and Srere, 1992; Knowles, 1991). If such a complex can be clearly demonstrated, and shown to be regulated by oxygen, this would be an important advance in our understanding of bacterial metabolic regulation. In plants, there is reasonably good evidence for a regulatable glycolytic metabolon. ¹³C labelling studies showed that in *Arabidopsis* and potato roots, there is regulatable channelling all the way through from glucose in the cytoplasm to pyruvate within the mitochondrion, as well as colocalisation of glycolytic enzymes to the mitochondrial membrane (Graham *et al.* 2007). Mitochondria are generally believed to be derived from bacterial cells, and thus the mitochondrial membrane is similar to the bacterial cell membrane. Regulatable metabolic pathways have been demonstrated in other systems, for example in purine biosynthesis (An *et al.* 2008). In most of these examples, metabolite channelling is thought to work by the enzymes involved binding to membrane proteins and assembling into a complex on the membrane surface (Williamson, 2011).

CHAPTER 6

GENERAL DISCUSSION AND CONCLUSION

6.0 General Discussion and Conclusion

The work presented here has observed the metabolic changes of *E. coli* during the transition from anaerobic to aerobic conditions. The change at proteomic and transcriptomic levels has been well described (Partridge *et al.* 2006, 2007) but the changes at the metabolome level have not been characterised, as not much information on intracellular and extracellular metabolites is available. Extracellular metabolites are easy to quantify compared to intracellular metabolites, which have a very rapid turnover and sometimes low pool sizes, as well as requiring extraction and quantitation, and being much more varied in number and chemical composition. The concentration of intracellular metabolites is important information, because it is one of the best ways of representing the *in vivo* conditions. A rapid quenching method has been developed based on the method by Spura *et al.* (2009). The method was improved, as discussed in Chapter 3, and the effectiveness of this method has been proved by measuring its reproducibility, which shows that the errors are small from most sources except for quenching (which has acceptable error).

The work described here has raised questions mainly about the regulation of metabolism inside the cells. Surprisingly, not much change can be seen intracellularly even though a big change happened outside the cells (discussed in Chapter 4), and we know (for example from previous transcriptomics and proteomics results) that the major metabolic pathway occurring inside the cells, namely glycolysis, has been perturbed in a major way. The results described in Chapter 4 demonstrate that pyruvate shows a unique profile during the adaptation to oxygen changes (Trotter *et al.* 2011). This highlights the key role of pyruvate as an important key junction in the *E. coli* metabolism and provides useful information about the metabolic activity inside the cells (as discussed in Chapter 1). Pyruvate concentration inside the cells during the transition from anaerobic to aerobic showed a relatively low concentration compared to its concentration outside the cells (after taking into account the different volumes of intracellular and extracellular spaces), and has been further confirmed with a pyruvate assay. If we look at the glycolysis process, pyruvate is

converted to acetyl-CoA and formate during anaerobic conditions. When oxygen is introduced, PFL which catalyses the above reaction is immediately damaged since PFL is extremely sensitive to oxygen (Takahashi *et al.* 1987) but the PDHC does need time to get fully activated to metabolise the pyruvate (Partridge *et al.* 2006). The level of pyruvate is expected to rise very high (of the order of 500 mM) since it cannot be metabolised until PDHC becomes fully functional. Therefore the movement of pyruvate kinase inside the cells was examined.

The role of *pykF* in *E. coli* metabolism remains as an important gene in catalysing the last step in glycolysis, the conversion of PEP to pyruvate and ATP. *pykF* is the best candidate to look at possible metabolite channelling of pyruvate inside the cells during the transition. This has been done by tagging *pykF* with 3xFLAG and GFP. The GFP results did not have sufficient resolution to be useful, but data presented in Chapter 5 shows the nanogold-labeled secondary antibody to the FLAG-tag is distributed evenly on the cells at 0 min but moves to the membrane when oxygen is introduced. This suggests that the glycolytic enzyme is moving to the membrane. The result is so far preliminary and requires further confirmation, but is one of the strongest pieces of experimental evidence yet for metabolite channelling in bacteria.

The approach adopted here has provided new insight into the metabolic adaptations of *E. coli* during the transition from anaerobic to aerobic environment. Although there are major changes to extracellular metabolites during the transition, these are mainly to overmetabolites, which are effectively waste products of anaerobic metabolism. By contrast, the data provided in this thesis suggest that cells are genetically programmed to maintain a remarkably constant level of central metabolites inside the cell. Therefore, understanding the movement of pyruvate may contribute to developmental adaptations by *E. coli* in response to oxygen changes.

The results reported in this thesis raise many questions. The percentage of pyruvate kinase enzyme localised to the cell membrane is significantly higher 30 minutes after introduction of air, but it is far from being 100%: yet we expect that the introduction of air will completely kill the activity of PFL and thus lead to a rapid increase in intracellular pyruvate concentration. Transcriptomic analyses show that gene transcription is altered within 30 s of the introduction of oxygen, and it may therefore be that more dramatic changes in localisation will be observable closer to the start of the transition. Experiments to investigate this question are under way. The results shown here demonstrate that pyruvate kinase is localised to the cell membrane. Is this also true for all of the enzymes within glycolysis? In other words, do all the enzymes within the glycolytic pathway form a single metabolon, or is it limited only to pyruvate kinase? This can be investigated by tagging other enzymes in the same as was done here for *pykF*. What is the signal for the relocalisation of pyruvate kinase? An obvious candidate is the transcription regulator PdhR, which regulates the activity of PDHC depending on the concentration of pyruvate in the cell, and is also linked to the oxygen-sensing regulator FNR (Trotter *et al.* 2011). If glucose metabolism in *E. coli* is a regulatable metabolon, is this also true for other metabolic pathways, such as for example the Krebs cycle?

CHAPTER 7

REFERENCES

7.0 References

Alexeeva, S., Hellingwerf, K.J., and Teixeira de Mattos, M.J. (2002). Quantitative assessment of oxygen availability: perceived aerobiosis and its effect on flux distribution in the respiratory chain of *Escherichia coli*. *Journal of Bacteriology* 184, 1402-1406.

Alsante, K.M., Boutros, P., Couturier, M.A., Friedmann, R.C., Harwood, J.W., Horan, G.J., Jensen, A.J., Liu, Q., Lohr, L.L., Morris, R., Raggon, J.W., Reid, G.L., Santafianos, D.P., Sharp, T.R., Tucker, J.L. and Wilcox, G.E. (2004). Pharmaceutical impurity identification: a case study using a multidisciplinary approach. *Journal of Pharmaceutical Sciences* 93, 2296-2309.

An, S.G., Kumar, R., Sheets, E.D. and Benkovic, S.J. (2008). Reversible compartmentalization of de novo purine biosynthetic complexes in living cells. *Science* 320, 103-106

Andersen, M.R., Nielsen, M.L., and Nielsen, J. (2008). Metabolic model integration of the bibliome, genome, metabolome and reactome of *Aspergillus niger*. *Molecular Systems Biology* 4, 178.

Azaís, T., Hartmeyer, G., Quignard, S., Laurent, G., Tourné-Péteilh, C., Devoisselle, J-M. and Babonneau, F. (2009). Solid-state NMR characterization of drug-model molecules encapsulated in MCM-41 silica. *Pure and Applied Chemistry* 81, 1345-1355.

Barba, I., Garcia-Ramirez, M., Hernandez, C., Alonso, M.A., Masmiquel, L., García-Dorado, D. and Simó, R. (2010). Metabolic fingerprints of proliferative diabetic retinopathy: an ¹H-NMR-based metabonomic approach using vitreous humor. *Biochemistry and Molecular Biology* 9, 4416-4421.

Bartosiak-Jentys, J., Eley, K. and Leak, D.J. (2012). Application of *pheB* as a reporter gene for *Geobacillus* spp., enabling qualitative colony screening and quantitative analysis of promoter strength. *Applied and Environmental Microbiology* 78, 5945-5947.

Bedair, M., and Sumner, L.W. (2008). Current and emerging mass-spectrometry technologies for metabolomics. *Trends in Analytical Chemistry* 27, 238-250.

Beloin, C., Deighan, P., Doyle, M. and Dorman, C. (2003). *Shigella flexneri* 2a strain 2457T expresses three members of the H-NS-like protein family: characterization of the Sfh protein. *Molecular Genetics and Genomics* 270, 66-77.

Bennett, B.D., Kimball, E.H., Gao, M., Osterhout, R., Van Dien, S.J., and Rabinowitz, J.D. (2009). Absolute metabolite concentrations and implied enzyme active site occupancy in *Escherichia coli*. *Nature Chemical Biology* 5, 593-599.

Blattner, F.R., Plunkett, G., Bloch, C.A., Perna, N.T., Burland, V., Riley, M., ColladoVides, J., Glasner, J.D., Rode, C.K., Mayhew, G.F. (1997). The complete genome sequence of *Escherichia coli* K-12. *Science* 277, 1453-1462.

Bolling, C., and Fiehn, O. (2005). Metabolite profiling of *Chlamydomonas reinhardtii* under nutrient deprivation. *Plant Physiology* 139, 1995-2005.

Bolten, C.J., Kiefer, P., Letisse, F., Portais, J.C., and Wittmann, C. (2007). Sampling for metabolome analysis of microorganisms. *Analytical Chemistry* 79, 3843-3849.

Brindle, J.T., Nicholson, J.K., Schofield, P.M., Grainger, D.J. and Holmes, E. (2003). Application of chemometrics to ¹H NMR spectroscopic data to investigate a relationship between human serum metabolic profiles and hypertension. *Analyst* 128 (1), 32-36.

Brown, T.R., Ugurbil, K., and Shulman, R.G. (1977). ³¹P nuclear magnetic resonance measurements of ATPase kinetics in aerobic *Escherichia coli* cells. *Proceedings of the National Academy of Sciences U S A* 74, 5551-5553.

Buchholz, A., Takors, R., and Wandrey, C. (2001). Quantification of intracellular metabolites in *Escherichia coli* K12 using liquid chromatographic-electrospray ionization tandem mass spectrometric techniques. *Analytical Biochemistry* 295, 129-137.

Bundy, J.G., Keun, H.C., Sidhu, J.K., Spurgeon, D.J., Svendsen, C., Kille, P. and Morgan, J. (2007a). Metabolic profile biomarkers of metal contamination in a sentinel terrestrial species are applicable across multiple sites. *Environmental Science Technology* 41, 4458-4464.

Bundy J.G., Papp, B., Harmston, R., Browne, R.A., Clayson, E.M., Burton, N., Reece, R.J., Oliver, S.G. and Brindle, K.M. (2007b). Evaluation of predicted network modules in yeast metabolism using NMR-based metabolite. *Genome Research* 17(4), 510-519.

Buziol, S., Bashir, I., Baumeister, A., Claassen, W., Noisommit-Rizzi, N., Mailinger, W., and Reuss, M. (2002). New bioreactor-coupled rapid stopped-flow sampling technique for measurements of metabolite dynamics on a subsecond time scale. *Biotechnology and Bioengineering* 80, 632-636.

Canelas, A.B., Ras, C., ten Pierick, A., van Dam, J.C., Heijnen, J.J., and Van Gulik, W.M. (2008). Leakage-free rapid quenching technique for yeast metabolomics. *Metabolomics* 4, 226-239.

Carmella, S.G., Han, S.M., Villalta, P.W., and Hecht, S.S. (2005). Analysis of total 4-(methylnitrosamino)-1-(3-pyridyl)-1-butanol in smokers' blood. *Cancer Epidemiology, Biomarkers and Prevention* 14, 2669-2672.

Chalfie, M., Tu, Y., Euskirchen, G., Ward, W.W. and Prasher, D.C. (1994). Green fluorescent protein as a marker for gene expression. *Science* 263, 802-805.

Chan, W., Costantino, N., Li, R.X., Lee, S.C., Su, Q., Melvin, D., Court, D.L., and Liu, P.T. (2007). A recombineering based approach for high-throughput conditional knockout targeting vector construction. *Nucleic Acids Research* 35:e64.

Chassagnole, C., Letisse, F., Diano, A., and Lindley, N.D. (2002a). Carbon flux analysis in a pantothenate overproducing *Corynebacterium glutamicum* strain. *Molecular Biology Reports* 29, 129-134.

Chassagnole, C., Noisommit-Rizzi, N., Schmid, J.W., Mauch, K., and Reuss, M. (2002b). Dynamic modeling of the central carbon metabolism of *Escherichia coli*. *Biotechnology and Bioengineering* 79, 53-73.

Chassagnole, C., Rais, B., Quentin, E., Fell, D.A., and Mazat, J.P. (2001). An integrated study of threonine-pathway enzyme kinetics in *Escherichia coli*. *Journal of Biochemistry* 356, 415-423.

Churchward, G., Estiva, E. and Bremer, H. (1981). Growth-rate dependent control of chromosome replication initiation in *Escherichia coli*. *Journal of Bacteriology* 145, 1232-1238.

Civiero, L., Vancaenenbroeck, R., Belluzzi, E., Beilina, A., Lobbestael, E., Reyniers, L., Gao, F., Micetic, I., De Maeyer, M., Bubacco, L., Baekelandt, V., Cookson, M.R., Greggio, E. and Taymans, J.M. (2012). Biochemical characterization of highly purified leucine-rich repeat kinases 1 and 2 demonstrates formation of homodimers. *PLoS One* 7, e43472.

Coates, M.E. (1975). The influence of the gut microflora on the nutrition of its host. *Bibliotheca Nutritio et Dieta* 22, 101-108.

Constantinou, M.A., Papakonstantinou, E., Benaki, D., Spraul, M., Shulpis, K., Koupparis, M.A. and Mikros, E. (2004). Application of nuclear magnetic resonance spectroscopy

combined with principal component analysis in detecting inborn errors of metabolism using blood spots: A metabonomic approach. *Analytica Chimica Acta* 511, 303-312.

Constantinidou, C., Hobman, J.L., Griffiths, L., Patel, M.D., Penn, C.W., Cole, J.A., and Overton, T.W. (2006). A reassessment of the FNR regulon and transcriptomic analysis of the effects of nitrate, nitrite, NarXL, and NarQP as *Escherichia coli* K12 adapts from aerobic to anaerobic growth. *Journal of Biological Chemistry* 281, 4802-4815.

Court, D.L., Sawitzke, J.A. and Thomason, L.C. (2002). Genetic engineering using homologous recombination. *Annual Review of Genetics* 36, 361-388.

Craven, C.J., and Waltho, J.P. (1995). The action of time-domain convolution filters for solvent suppression. *Journal of Magnetic Resonance* 106, 40-46.

Cunningham, D.S., Liu, Z., Domagalski, N., Koepsel, R., Ataii, M.M. and Domach, M.M. (2009). Pyruvate kinase-deficient *Escherichia coli* exhibits increased plasmid copy number and cyclic AMP. *Journal of Bacteriology* 191(9), 3041-3049.

Datsenko, K.A., and Wanner, B.L. (2000). One-step inactivation of chromosomal genes in *Escherichia coli* K-12 using PCR products. *Proceedings of National Academy of Science USA* 97, 6640-6645.

Datta, S., Costantino, N., Zhou, X. and Court, D.L. (2008). Identification and analysis of recombineering functions from Gram-negative and Gram-positive bacteria and their phages. *Proceedings of National Academy of Science USA* 105, 1626-1631.

de Koning, W., and van Dam, K. (1992). A method for the determination of changes of glycolytic metabolites in yeast on a subsecond time scale using extraction at neutral pH. *Analytical Biochemistry* 204, 118-123.

Derbise, A., Lesic, B., Dacheux, D., Ghigo, J.M. and Carniel, E. (2003). A rapid and simple method for inactivating chromosomal genes in *Yersinia*. *FEMS Immunology and Medical Microbiology* 38, 113-116.

Dettmer, K., Aronov, P.A., and Hammock, B.D. (2007). Mass spectrometry-based metabolomics. *Mass Spectrometry Reviews* 26, 51-78.

Dobson, P.D., Smallbone, K., Jameson, D., Simeonidis, E., Lanthaler, K., Pir, P., Lu, C.A., Swainston, N., Dunn, W.B., Fisher, P., et al. (2010). Further developments towards a genome-scale metabolic model of yeast. *BMC System Biology* 4:145

Domon, B., and Aebersold, R. (2006). Review - Mass spectrometry and protein analysis. *Science* 312, 212-217.

Dumas, M.E., Barton, R.H., Toye, A., Cloarec, O., Blancher, C., Rothwell, A., Fearnside, J., Tatoud, R., Blanc, V., Lindon, J.C. (2006). Metabolic profiling reveals a contribution of gut microbiota to fatty liver phenotype in insulin-resistant mice. *Proceedings of the National Academy of Sciences U S A* 103, 12511-12516.

Durot, M., Bourguignon, P.Y. and Schachter, V. (2009). Genome-scale models of bacterial metabolism: reconstruction and applications. *FEMS Microbiology Review* 33, 164-190.

Dwivedi, P., Puzon, G., Tam, M., Langais, D., Jackson, S., Siems, W.F., Schultz, A.J., Xun, L., Woods, A. and Hill Jr., H.H. (2010). Metabolic profiling of *Escherichia coli* by ion mobility-mass spectrometry with MALDI ion source. *Journal of Mass Spectrometry* 45, 1383-1393.

Ehrmann, K., Pataky, K., Stettler, M., Wurm, F.M., Brugger, J., Besse, P.A., and Popovic, R. (2007). NMR spectroscopy and perfusion of mammalian cells using surface microprobes. *Lab Chip* 7, 381-383.

Eisenberg, R.C. and Dobrogosz, W.J. (1967). Gluconate metabolism in *Escherichia coli*. *Journal of Bacteriology* 93, 941-949.

Ellis, H.M., Yu, D., Ditzio, T. and Court, D.L. (2001). High efficiency mutagenesis, repair and engineering of chromosomal DNA using single-stranded oligonucleotides. *Proceedings of National Academy of Science USA* 98, 6742-6746.

Emmerling, M., Dauner, M., Ponti, A., Fiaux, J., Hochuli, M., Szyperski, T., Wüthrich, K., Bailey, J.E. and Saber, U. (2002). Metabolix flux responses to pyruvate kinase knockout in *Escherichia coli*. *Journal of Bacteriology* 184, 152-164.

Evans, C.G.T., Herbert, D. and Tempest, D.W. (1970). The continuous culture of microorganisms 2. Construction of a chemostat. In: *Methods in Microbiology*, vol 2, Academic London, edited by Norris, J.R. and Ribbons, D.W. pp 277-327.

Faijes, M., Mars, A.E., and Smid, E.J. (2007). Comparison of quenching and extraction methodologies for metabolome analysis of *Lactobacillus plantarum*. *Microbial Cell Factories* 6:27.

Feilmeier, B.J., Iseminger, G., Schroeder, D., Webber, H. and Phillips, G.J. (2000). Green fluorescent protein functions as a reporter for protein localization in *Escherichia coli*. *Journal of Bacteriology* 182, 4068-4076.

Fiehn, O. (2002). Metabolomics--the link between genotypes and phenotypes. *Plant Molecular Biology* 48, 155-171.

Fischer, E., and Sauer, U. (2003). Metabolic flux profiling of *Escherichia coli* mutants in central carbon metabolism using GC-MS. *European Journal of Biochemistry* 270, 880-891.

Flores, N., de Anda, R., Flores, S., Escalante, A., Hernandez, G., Martinez, A., Ramirez, O.T., Gosset, G., and Bolivar, F. (2004). Role of pyruvate oxidase in *Escherichia coli* strains lacking

the phosphoenolpyruvate: carbohydrate phosphotransferase system. *Journal of Molecular Microbiology and Biotechnology* 8, 209-221.

Gaines, G.L., Smith, L., and Neidle, E.L. (1996). Novel nuclear magnetic resonance spectroscopy methods demonstrate preferential carbon source utilization by *Acinetobacter calcoaceticus*. *Journal of Bacteriology* 178, 6833-6841.

Garrido-Pertierra, A. and Cooper, R.A. (1983). Evidence for two distinct pyruvate kinase genes in *Escherichia coli* K-12. *FEBS Letters* 162, 420-422.

Georgellis, D., Kwon, O., and Lin, E.C.C. (1999). Amplification of signaling activity of the arc two-component system of *Escherichia coli* by anaerobic metabolites - an in vitro study with different protein modules. *Journal of Biological Chemistry* 274, 35950-35954.

Georgellis, D., Kwon, O., and Lin, E.C.C. (2001). Quinones as the redox signal for the Arc two-component system of bacteria. *Science* 292, 2314-2316.

Gerosa, L. and Sauer, U. (2011). Regulation and control of metabolic fluxes in microbes. *Current Opinion in Biotechnology* 22, 1-10.

Gonthier, M.P., VERNY, M.A., Besson, C., Remesy, C. and Scalbert, A. (2003). Chlorogenic acid bioavailability largely depends on its metabolism by the gut microflora in rats. *Journal of Nutrition* 133, 1853-1859.

Gonzalez, B., Francois, J., and Renaud, M. (1997). A rapid and reliable method for metabolite extraction in yeast using boiling buffered ethanol. *Yeast* 13, 1347-1355.

Goodacre, R., Vaidyanathan, S., Dunn, W.B., Harrigan, G.G., and Kell, D.B. (2004). Metabolomics by numbers: acquiring and understanding global metabolite data. *Trends in Biotechnology* 22, 245-252.

Graham, J.W.A., Williams, T.C.R., Morgan, M., Fernie, A.R., Ratcliffe, R.G. and Sweetlove, L.J. (2007). Glycolytic enzymes associate dynamically with mitochondria in response to respiratory demand and support substrate channeling. *Plant Cell* 19, 3723-3738.

Grainger, D.J. (2006). Metabolic profiling in heart disease. *Heart and Metabolism* 32, 22-25.

Green, J., and Paget, M.S. (2004). Bacterial redox sensors. *Nature Reviews Microbiology* 2, 954-966.

Griffin, J.L. (2003). Metabonomics: NMR spectroscopy and pattern recognition analysis of body fluids and tissues for characterisation of xenobiotic toxicity and disease diagnosis. *Current Opinion in Chemical Biology* 7, 648-654.

Griffin, J.L. and Shockcor, J.P. (2004). Metabolic profiles of cancer cells. *Nature Reviews Cancer* 4, 551-561.

Guest, J.R., Quall, M.A., Davé, E., Cassey, B. and Attwood, M.M. (1996). Regulatory and other aspects of pyruvate dehydrogenase complex synthesis in *Escherichia coli*. In *Biochemistry and Physiology of Thiamin Diphosphate Enzymes*, pp. 326-333. Edited by Bisswanger, H. and Schellenberger, A. Prien: Intemann.

Hajjaj, H., Blanc, P.J., Goma, G., and Francois, J. (1998). Sampling techniques and comparative extraction procedures for quantitative determination of intra- and extracellular metabolites in filamentous fungi. *FEMS Microbiology Letters* 164, 195-200.

Halket, J.M., Waterman, D., Przyborowska, A.M., Patel, R.K., Fraser, P.D. and Bramley, P.M. (2005). Chemical derivatization and mass spectral libraries in metabolic profiling by GC/MS and LC/MS/MS. *Journal of Experimental Botany* 56, 219-243.

Hayes, A., Zhang, N.S., Wu, J., Butler, P.R., Hauser, N.C., Hoheisel, J.D., Lim, F.L., Sharrocks, A.D., and Oliver, S.G. (2002). Hybridization array technology coupled with chemostat

culture: Tools to interrogate gene expression in *Saccharomyces cerevisiae*. *Methods* 26, 281-290.

Heinken, A., Sahoo, S., Fleming, R.M.T and Thiele, I. (2013). Systems-level characterization of a host-microbe metabolic symbiosis in the mammalian gut. *Gut Microbes* 4, 28-40.

Hellerstein, M.K. (2004). New stable isotope-mass spectrometric techniques for measuring fluxes through intact metabolic pathways in mammalian systems: introduction of moving pictures into functional genomics and biochemical phenotyping. *Metabolic Engineering* 6, 85-100.

Hiller, J., Franco-Lara, E., Papaioannou, V., and Weuster-Botz, D. (2007). Fast sampling and quenching procedures for microbial metabolic profiling. *Biotechnology Letters* 29, 1161-1167.

Holms, H. (1996). Flux analysis and control of the central metabolic pathways in *Escherichia coli*. *FEMS Microbiology Review* 19, 85-116.

Holmes, E., Foxall, P.J., Spraul, M., Farrant, R.D., Nicholson, J.K. and Lindon, J.C. (1997). 750 MHz ^1H NMR spectroscopy characterisation of the complex metabolic pattern of urine patients with inborn errors of metabolism: 2-Hydroxyglutaric aciduria and maple syrup urine disease. *Journal of Pharmaceutical and Biomedical Analysis* 15, 1647-1659.

Holmes, E., Tsang, T., Jeffrey, T.J., Leweke, M., Koethe, D., Gerth, C., Nolden, B., Gross, S., Schreiber, D., Nicholson, J. and Bahn, S. (2006). Metabolic profiling of CSF: evidence that early intervention may impact on disease progression and outcome in schizophrenia. *PLoS Medicine* 3, e327.

Hooper, L.V., and Gordon, J.I. (2001). Commensal host-bacterial relationships in the gut. *Science* 292, 1115-1118.

Hore, P.J. (1989). Nuclear magnetic resonance. Solvent suppression. *Methods in Enzymology* 176, 64-77.

Hoskisson, P.A., and Hobbs, G. (2005). Continuous culture--making a comeback? *Microbiology* 151, 3153-3159.

Husseiny, M.I. and Hensel, M. (2005). Rapid method for the construction of *Salmonella enterica* serovar Typhimurium vaccine carrier strains. *Infection and Immunity* 73, 1598-1605.

Isern, N.G., Xue, J., Rao, J.V., Cort, J.R. and Ahring, B.K. (2013). Novel monosaccharide fermentation products in *Caldicellulosiruptor saccharolyticus* identified using NMR spectroscopy. *Biotechnology for Biofuels* 6, 47-57.

Iuchi, S. and Lin, E.C. (1988). arcA (dye) regulatory gene in *Escherichia coli* mediating repression of enzymes in anaerobic pathways. *Proceedings of National Academy of Science USA* 85(6), 1888-1892.

Iversen, J.J.L. (1981). A rapid sampling valve with minimal dead space for laboratory scale fermenters. *Biotechnology and Bioengineering* 23, 437-440.

Jackson, A.U., Werner, S.R., Talaty, N., Song, Y., Campbell, K., Cooks, R.G., and Morgan, J.A. (2008). Targeted metabolomic analysis of *Escherichia coli* by desorption electrospray ionization and extractive electrospray ionization mass spectrometry. *Analytical Biochemistry* 375, 272-281.

Jung, J., Park, M., Park, H.J., Shim, S.B., Cho, Y.H., Kim, J., Lee, H-S., Ryu, D.H., Choi, D. and Hwang, G-S. (2011). ¹H NMR-based metabolic profiling of naproxen-induced toxicity in rats. *Toxicology Letters* 200, 1-7.

Jurica, M.S., Mesecar, A., Heath, P.J., Shi, W., Nowak, T., and Stoddard, B.L. (1998). The allosteric regulation of pyruvate kinase by fructose-1,6-bisphosphate. *Structure* 6, 195-210.

Kaderbhai, N.N., Broadhurst, D.I., Ellis, D.I., Goodacre, R., and Kell, D.B. (2003). Functional genomics via metabolic footprinting: monitoring metabolite secretion by *Escherichia coli* tryptophan metabolism mutants using FT-IR and direct injection electrospray mass spectrometry. *Comparative and Functional Genomics* 4, 376-391.

Kaper, J.B., Nataro, J.P., and Mobley, H.L. (2004). Pathogenic *Escherichia coli*. *Nature Reviews Microbiology* 2, 123-140.

Kayser, A., Weber, J., Hecht, V., and Rinas, U. (2005). Metabolic flux analysis of *Escherichia coli* in glucose-limited continuous culture. I. Growth-rate-dependent metabolic efficiency at steady state. *Microbiology* 151, 693-706.

Keseler, I.M., Collado-Vides, J., Gama-Castro, S., Ingraham, J., Paley, S., Paulsen, I.T., Peralta-Gil, M., and Karp, P.D. (2005). EcoCyc: a comprehensive database resource for *Escherichia coli*. *Nucleic Acids Research* 33, 334-337.

Khoo, S.H. and Al-Rubeai, M. (2009). Detailed understanding of enhanced specific antibody productivity in NS0 myeloma cells. *Biotechnology and Bioengineering* 102, 188-199.

Kiley, P.J., and Beinert, H. (1998). Oxygen sensing by the global regulator, FNR: the role of the iron-sulfur cluster. *FEMS Microbiology Reviews* 22, 341-352.

Kind, T., Tolstikov, V., Fiehn, O., and Weiss, R.H. (2007). A comprehensive urinary metabolomic approach for identifying kidney cancer. *Analytical Biochemistry* 363, 185-195.

Kivero, A.D., Bocharov, E.V., Doroshenko, V.G., Sobol, A.G., Dubinnyi, M.A. and Arseniev, A.S. (2008). 2D [¹H, ¹³C] NMR study of carbon fluxes during glucose utilisation by *Escherichia coli* MG1655. *Applied Biochemistry and Microbiology* 44, 151-157.

Knowles, J.R. (1991). Calmer waters in the channel. *Journal of Theoretical Biology* 152:53-55

Kosek, M., Bern, C., and Guerrant, R.L. (2003). The global burden of diarrhoeal disease, as estimated from studies published between 1992 and 2000. *Bulletin of the World Health Organization* 81, 197-204.

Kovárová-Kovar, K. and Egli, T. (1998). Growth kinetics of suspended microbial cells: from single-substrate-controlled growth to mixed-substrate kinetics. *Microbiology and Molecular Biology Reviews* 62(3), 646-666.

Kubitschek, H.E. (1969). Growth during the bacterial cell cycle: analysis of cell size distribution. *Journal of Biophysics* 9, 792-809.

Laemmli, U.K (1970). Cleavage of structural proteins during the assembly of the head of bacteriophage T4. *Nature* 227, 680-685.

Lang, V.J., Leystralantz, C., and Cook, R.A. (1987). Characterization of the specific pyruvate transport-system in *Escherichia coli* K-12. *Journal of Bacteriology* 169, 380-385.

Lange, H.C., Eman, M., van Zuijlen, G., Visser, D., van Dam, J.C., Frank, J., Teixeira de Mattos, M.J. and Heijnen, J.J. (2001). Improved rapid sampling for in vivo kinetics of intracellular metabolites in *Saccharomyces cerevisiae*. *Biotechnology and Bioengineering* 75, 406-415.

Letisse, F. and Lindley, N.D. (2000). An intracellular metabolite quantification technique applicable to polysaccharide-producing bacteria. *Biotechnology Letters* 22, 1673-1677.

Lin, E.C.C., and Iuchi, S. (1991). Regulation of gene-expression in fermentative and respiratory systems in *Escherichia coli* and related bacteria. *Annual Review of Genetics* 25, 361-387.

Lin, C.Y., Viant, M.R. and Tjeerdema, R.S. (2006). Metabolomics: methodologies and applications in the environmental sciences. *Journal of Pesticide Sciences* 169, 637-645.

Lindon, J.C. and Nicholson, J.K. (1997). Recent advances in high-resolution NMR spectroscopic methods in bioanalytical chemistry. *Trends in Analytical Chemistry* *16*, 190-200.

Lindon, J.C., Nicholson, J.K. and Everett, J.R. (1999). NMR spectroscopy of biofluids. *Annual Reports on NMR Spectroscopy* *38*, 1-88.

Lindon, J.C., Nicholson, J.K., Holmes, E., and Everett, J.R. (2000). Metabonomics: Metabolic processes studied by NMR spectroscopy of biofluids. *Concepts in Magnetic Resonance* *12*, 289-320.

Lindon, J.C., and Ferrige, A.G. (1980). Digitization and data-Processing in fourier-transform NMR. *Progress in Nuclear Magnetic Resonance Spectroscopy* *14*, 27-66.

Loferer-Krossbacher, M., Klima, J. and Psenner, R. (1998). Determination of bacterial cell dry mass by transmission electron microscopy and densitometric image analysis. *Applied of Environmental Microbiology* *64*, 688-694.

Lowry, O.H., Carter, J., Ward, J.B., and Glaser, L. (1971). The effect of carbon and nitrogen sources on the level of metabolic intermediates in *Escherichia coli*. *Journal of Biological Chemistry* *246*, 6511-6521.

Lupp, C., and Finlay, B.B. (2005). Intestinal microbiota. *Current Biology* *15*, R235-236.

Magnus, J.B., Hollwedel, D., Oldiges, M., and Takors, R. (2006). Monitoring and modeling of the reaction dynamics in the valine/leucine synthesis pathway in *Corynebacterium glutamicum*. *Biotechnology Progress* *22*, 1071-1083.

Maharjan, R.P., and Ferenci, T. (2003). Global metabolite analysis: the influence of extraction methodology on metabolome profiles of *Escherichia coli*. *Analytical Biochemistry* *313*, 145-154.

Matin, A., and Konings, W.N. (1973). Transport of lactate and succinate by membrane vesicles of *Escherichia coli*, *Bacillus subtilis* and a *Pseudomonas* species. *European Journal of Biochemistry* 34, 58-67.

Melchiorson, C.R., Jensen, N.B., Christensen, B., Vaeber Jokumsen, K., and Villadsen, J. (2001). Dynamics of pyruvate metabolism in *Lactococcus lactis*. *Biotechnology and Bioengineering* 74, 271-279.

Miller, J.H. (1972). Experiments in molecular biology. *Cold Spring Harbor Laboratory*. Cold Spring Harbor, New York.

Misra, D. and Bajpai, U. (2009). Metabolite characterisation in serum samples from normal healthy human subjects by ^1H and ^{13}C NMR spectroscopy. *Bulletin of the Chemical Society of Ethiopia* 23, 211-221.

Monod, J. (1950). La Technique De Culture Continue Theorie Et Applications. *Ann I Pasteur Paris* 79, 390-410.

Moses, V., and Sharp, P.B. (1972). Intermediary metabolite levels in *Escherichia coli*. *Journal of General Microbiology* 71, 181-190.

Murarka, A., Clomburg, J.M., Moran, S., Shanks, J.V., and Gonzalez, R. (2010). Metabolic analysis of wild-type *Escherichia coli* and a pyruvate dehydrogenase complex (PDHC)-deficient derivative reveals the role of PDHC in the fermentative metabolism of glucose. *Journal of Biological Chemistry* 285, 31548-31558.

Murphy, K.C. (1998). Use of bacteriophage λ recombination functions to promote gene replacement in *Escherichia coli*. *Journal of Bacteriology* 180, 2063-2071.

Nataro, J.P., and Kaper, J.B. (1998). Diarrheagenic *Escherichia coli*. *Clinical Microbiology Reviews* 11, 142-201.

Neidhart, F.C. and Umbarger, H.E. (1996). Chemical composition of *Escherichia coli*, p. 13-28. In F.C. Neidhart, R. Curtis III, J.L. Ingraham, E.C.C. Lin, K.B. Low, B. Magasanik, W.S. Reznikoff, M. Riley, M. Schaechter and H.E. Umbarger (ed.), *Escherichia coli and Salmonella: cellular and molecular microbiology*, 2nd ed. American Society for Microbiology, Washington, D.C.

Nicholson, J.K., Lindon, J.C., and Holmes, E. (1999). 'Metabonomics': understanding the metabolic responses of living systems to pathophysiological stimuli via multivariate statistical analysis of biological NMR spectroscopic data. *Xenobiotica* 29, 1181-1189.

Nicholson, J.K., and Wilson, I.D. (2003). Understanding 'global' systems biology: Metabonomics and the continuum of metabolism. *Nature Reviews Drug Discovery* 2, 668-676.

Nicholson, J.K., Holmes, E., Kinross, J., Burcelin, R., Gibson, G., Jia, W. and Pettersson, S. (2012). Host-gut microbiota metabolic interactions. *Science* 336, 62-67.

Noble, K., Zhang, J., and Wray, S. (2006). Lipid rafts, the sarcoplasmic reticulum and uterine calcium signalling: an integrated approach. *Journal of Physiology* 570, 29-35.

Novick, A., and Szilard, L. (1950). Description of the chemostat. *Science* 112, 715-716.

Oliveira, A.P., Nielsen, J., and Forster, J. (2005). Modeling *Lactococcus lactis* using a genome-scale flux model. *BMC Microbiology* 5, 39.
Óvádi, J. and Srere, P.A. (1992). Channel your energies. *Trends in Biochemical Sciences* 17, 445-447.

Partridge, J.D., Sanguinetti, G., Dibden, D.P., Roberts, R.E., Poole, R.K., and Green, J. (2007). Transition of *Escherichia coli* from aerobic to micro-aerobic conditions involves fast and slow reacting regulatory components. *The Journal of Biological Chemistry* 282, 11230-11237.

Partridge, J.D., Scott, C., Tang, Y., Poole, R.K., and Green, J. (2006). *Escherichia coli* transcriptome dynamics during the transition from anaerobic to aerobic conditions. The Journal of Biological Chemistry 281, 27806-27815.

Pasch, H., Heinz, L-C., Macko, T. and Hiller, W. (2008). High-temperature gradient HPLC and LC-NMR for the analysis of complex polyolefins. Pure and Applied Chemistry 80, 1747-1762.

Patel, K.N., Patel, J.K., Patel, M.P., Rajput, G.C. and Patel, H.A. (2010). Introduction to hyphenated techniques and their applications in pharmacy. Pharmaceutical Methods 1, 2-13.

Patschkowski, T., Bates, D.M. and Kiley, P.J. (2000). Mechanisms for sensing and responding to oxygen deprivation. In '*Bacterial stress responses*'. Edited by Storz, G. and Hengge-Aronis, R. ASM Press, Washington, pp 61-78.

Pertierra, A.G. and Cooper, R.A. (1977). Pyruvate formation during the catabolism of simple hexose sugars by *Escherichia coli*: studies with pyruvate kinase- negative mutants. Journal of Bacteriology 129, 1208-1214.

Piper, M.D.W., Daran-Lapujade, P., Bro, C., Regenber, B., Knudsen, S., Nielsen, J., and Pronk, J.T. (2002). Reproducibility of oligonucleotide microarray transcriptome analyses - An interlaboratory comparison using chemostat cultures of *Saccharomyces cerevisiae*. Journal of Biological Chemistry 277, 37001-37008.

Ponce, E., Flores, N., Martinez, A., Valle, F., and Bolivar, F. (1995). Cloning of the two pyruvate kinase isoenzyme structural genes from *Escherichia coli*: the relative roles of these enzymes in pyruvate biosynthesis. Journal of Bacteriology 177, 5719-5722.

Ponce, E., Martinez, A., Bolivar, F., and Valle, F. (1998). Stimulation of glucose catabolism through the pentose pathway by the absence of the two pyruvate kinase isoenzymes in *Escherichia coli*. Biotechnology and Bioengineering 58, 292-295.

Poole, R.K., and Cook, G.M. (2000). Redundancy of aerobic respiratory chains in bacteria? Routes, reasons and regulation. *Advances in Microbial Physiology* 43, 165-224.

Poole, R.K., Salmon, I., and Chance, B. (1994). The high-spin cytochrome o' component of the cytochrome bo-type quinol oxidase in membranes from *Escherichia coli* - formation of the primary oxygenated species at low temperatures is characterized by a slow 'on' rate and low dissociation constant. *Microbiology* 140, 1027-1034.

Poteete, A. R. (2001). What makes the bacteriophage lambda Red system useful for genetic engineering: molecular mechanism and biological function. *FEMS Microbiology Letter* 201, 9-14.

Purcell, E.M., Torrey, H.C. and Pound, R.V. (1946). Resonance absorption by nuclear magnetic moments in a solid. *Physic Review* 69, 37-38.

Rabinowitz, J.D., and Kimball, E. (2007). Acidic acetonitrile for cellular metabolome extraction from *Escherichia coli*. *Analytical Chemistry* 79, 6167-6173.

Ralph, E.T., Scott, C., Jordan, P.A., Thomson, A.J., Guest, J.R., and Green, J. (2001). Anaerobic acquisition of [4Fe 4S] clusters by the inactive FNR(C20S) variant and restoration of activity by second-site amino acid substitutions. *Molecular Microbiology* 39, 1199-1211.

Ramautar, R., Somsen, G.W., and de Jong, G.J. (2009). CE-MS in metabolomics. *Electrophoresis* 30, 276-291.

Renzette, N., Gumlaw, N., Nordman, J.T., Krieger, M., Yeh, S.P., Long, E., Centore, R., Boonsombat, R. and Sandler, S.J. (2005). Localization of RecA in *Escherichia coli* K-12 using RecA-GFP. *Molecular Microbiology* 57, 1074-1085.

Robosky, L.C., Reily, M.D., and Avizonis, D. (2007). Improving NMR sensitivity by use of salt-tolerant cryogenically cooled probes. *Analytical and Bioanalytical Chemistry* 387, 529-532.

Rosenblum, E.S., Tjeerdema, R.S. and Viant, M.R. (2006). Effects of temperature on host-pathogen-drug interactions in red abalone, *Haliotis rufescens*, determined by ¹H NMR metabolomics. *Environmental Science Technology* 40, 7077-7084.

Rossi, M.S., Paquelin, A., Ghigo, J.M. and Wandersman, C. (2003). Haemophore-mediated signal transduction across the bacterial cell envelope in *Serratia marcescens*: the inducer and the transported substrate are different molecules. *Molecular Microbiology* 48, 1467-1480.

Rui, B., Shen, T., Zhou, H., Liu, J., Chen, J., Pan, X., Liu, H., Wu, J., Zheng, H., and Shi, Y. (2010). A systematic investigation of *Escherichia coli* central carbon metabolism in response to superoxide stress. *BMC System Biology* 4, 122.

Russell, J.B., and Cook, G.M. (1995). Energetics of bacterial growth: balance of anabolic and catabolic reactions. *Microbiology Reviews* 59, 48-62.

Salmon, K.A., Hung, S., Steffen, N.R., Krupp, R., Baldi, P., Hatfield, G.W., and Gunsalus, R.P. (2005). Global gene expression profiling in *Escherichia coli* K12 - effects of oxygen availability and ArcA. *Journal of Biological Chemistry* 280, 15084-15096.

Sauer, U., Hatzimanikatis, V., Bailey, J.E., Hochuli, M., Szyperski, T. and Wüthrich, K. (1997). Metabolic fluxes in riboflavin-produced *Bacillus subtilis*. *Nature Biotechnology* 15, 448-452.

Sauer, U., Lasko, D.R., Fiaux, J., Hochuli, M., Glaser, R., Szyperski, T., Wüthrich, K., and Bailey, J.E. (1999). Metabolic flux ratio analysis of genetic and environmental modulations of *Escherichia coli* central carbon metabolism. *Journal of Bacteriology* 181, 6679-6688.

Sauer, U. (2006). Metabolic networks in motion: 13C-based flux analysis. *Molecular Systems Biology* DOI:10.1038.

Sawers, G. (1999). The aerobic/anaerobic interface. *Current Opinion in Microbiology* 2, 181-187.

Schaefer, U., Boos, W., Takors, R., and Weuster-Botz, D. (1999). Automated sampling device for monitoring intracellular metabolite dynamics. *Analytical Biochemistry* 270, 88-96.

Schaub, J., Schiesling, C., Reuss, M., and Dauner, M. (2006). Integrated sampling procedure for metabolome analysis. *Biotechnology Progress* 22, 1434-1442.

Shockcor, J.P. and Holmes, E. (2002). Metabonomics applications in toxicity screening and disease diagnosis. *Current Topics in Medicinal Chemistry* 2, 35-51.

Siddiquee, K.A., Arauzo-Bravo, M.J., and Shimizu, K. (2004). Effect of a pyruvate kinase (pykF-gene) knockout mutation on the control of gene expression and metabolic fluxes in *Escherichia coli*. *FEMS Microbiology Letters* 235, 25-33.

Simao, E., Remy, E., Thieffry, D., and Chaouiya, C. (2005). Qualitative modelling of regulated metabolic pathways: application to the tryptophan biosynthesis in *E. coli*. *Bioinformatics* 21, 190-196.

Smart, K.F., Aggio, R.B.M., Van Houtte, J.R., and Villas-Boas, S.G. (2010). Analytical platform for metabolome analysis of microbial cells using methyl chloroformate derivatization followed by gas chromatography-mass spectrometry. *Nature Protocol* 5, 1709-1729.

Snoep, J.L., Degraef, M.R., Demattos, M.J.T., and Neijssel, O.M. (1992). Pyruvate catabolism during transient state conditions in chemostat cultures of *Enterococcus faecalis* NCTC 775 - importance of internal pyruvate concentrations and NADH/NAD⁺ ratios. *Journal of General Microbiology* 138, 2015-2020.

Spura, J., Reimer, L.C., Wieloch, P., Schreiber, K., Buchinger, S., and Schomburg, D. (2009). A method for enzyme quenching in microbial metabolome analysis successfully applied to gram-positive and gram-negative bacteria and yeast. *Analytical Biochemistry* 394, 192-201.

Srere, P.A. (1987). Complexes of sequential metabolic enzymes. *Annual Review of Biochemistry* 56, 89-124.

Srere, P.A. (2000). Macromolecular interactions: tracing the roots. *Trends in Biochemical Sciences* 25, 150-153.

Steiner, P., Fussenegger, M., Bailey, J.E., and Sauer, U. (1995). Cloning and expression of the *Zymomonas mobilis* pyruvate kinase gene in *Escherichia coli*. *Gene* 220, 31-38.

Steiner, P., and Sauer, U. (2003). Long-term continuous evolution of acetate resistant *Acetobacter aceti*. *Biotechnology and Bioengineering* 84, 40-44.

Stella, C., Beckwith-Hall, B., Cloarec, O., Holmes, E., Lindon, J., Powell, J., van der Ouderaa, F., Bingham, S., Cross, A. and Nicholson, J. (2006). Susceptibility of human metabolic phenotypes to dietary modulation. *Journal of Proteome Research* 5, 2780-2788.

Sutton, V.R., Mettert, E.L., Beinert, H. and Kiley, P.J. (2004). Kinetic analysis of the oxidative conversion of the $[4\text{Fe-4S}]^{2+}$ cluster of FNR to a $[2\text{Fe-2S}]^{2+}$ cluster. *Journal of Bacteriology* 186, 8018-8025.

Takahashi, N., Takahashi-Abbe, S. and Yamada, T. (1987). Oxygen sensitivity of sugar metabolism and interconversion of pyruvate formate-lyase in intact cells of *Streptococcus mutans* and *Streptococcus sanguis*. *Infection and Immunity* 55, 652-656.

Taymaz-Nikerel, H., de Mey, M., Ras, C., ten Pierick, A., Seifar, R.M., Van Dam, J.C., Heijnen, J.J., and Van Glijik, W.M. (2009). Development and application of a differential

method for reliable metabolome analysis in *Escherichia coli*. *Analytical Biochemistry* 386, 9-19.

Theobald, U., Mailinger, W., Reuss, M., and Rizzi, M. (1993). In vivo analysis of glucose-induced fast changes in yeast adenine nucleotide pool applying a rapid sampling technique. *Analytical Biochemistry* 214, 31-37.

Tiziani, S., Lopes, V. and Gunther, U.L. (2009). Early stage diagnosis of oral cancer using 1H NMR-based metabolomics. *Neoplasia* 11, 269-276.

Tredwell, G.D., Edwards-Jones, B., Leak, D.J. and Bundy, J.G. (2011). Development of Metabolomic sampling procedures for *Pichia pastoris* baseline metabolome data. *PloS one* 6, e16286.

Trotter, E.W., Rolfe, M.D., Hounslow, A.M., Craven, C.J., Williamson, M.P., Sanguinetti, G., Poole, R.K., and Green, J. (2011). Reprogramming of *Escherichia coli* K-12 metabolism during the initial phase of transition from an anaerobic to a micro-aerobic environment. *PloS one* 6, e25501.

Tulpan, D., Léger, S., Belliveau, L., Culf, A. and Čuperlović-Culf, M. (2011). MetaboHunter: an automatic approach for identification of metabolites from ¹H-NMR spectra of complex mixtures. *BMC Bioinformatics* 12, 400-422.

Uden, G., Achebach, S., Holighaus, G., Tran, H.Q., Wackwitz, B., and Zeuner, Y. (2002). Control of FNR function of *Escherichia coli* by O₂ and reducing conditions. *Journal of Molecular Microbiology and Biotechnology* 4, 263-268.

Uden, G., Becker, S., Bongaerts, J., Holighaus, G., Schirawski, J., and Six, S. (1995). O₂-sensing and O₂-dependent gene regulation in facultatively anaerobic bacteria. *Archives of Microbiology* 164, 81-90.

Usuda, Y., Nishio, Y., Iwatani, S., Van Dien, S.J., Imaizumi, A., Shimbo, K., Kageyama, N., Iwahata, D., Miyano, H., and Matsui, K. (2010). Dynamic modeling of *Escherichia coli* metabolic and regulatory systems for amino-acid production. *Journal of Biotechnology* 147, 17-30.

van der Werf, M.J., Overkamp, K.M., Muilwijk, B., Coulier, L. and Hankemeier, T. (2007). Microbial metabolomics: toward a platform with full metabolome coverage. *Analytical Biochemistry* 370, 17-25.

Vemuri, G.N., Eiteman, M.A., and Altman, E. (2002). Succinate production in dual-phase *Escherichia coli* fermentations depends on the time of transition from aerobic to anaerobic conditions. *Journal of Industrial Microbiology and Biotechnology* 28, 325-332.

Viant, M.R., Rosenblum, E.S. and Tjeerdema, R.S. (2003). NMR-based metabolomics: a powerful approach for characterizing the effects of environmental stressors on organism health. *Environmental Science Technology* 37, 4982-4989.

Viant, M.R. (2008). Recent developments in environmental metabolomics. *Molecular BioSystems* 4, 980-986.

Villas-Boas, S.G., and Bruheim, P. (2007). Cold glycerol-saline: the promising quenching solution for accurate intracellular metabolite analysis of microbial cells. *Analytical Biochemistry* 370, 87-97.

Villas-Boas, S.G., Hojer-Pedersen, J., Akesson, M., Smedsgaard, J., and Nielsen, J. (2005a). Global metabolite analysis of yeast: evaluation of sample preparation methods. *Yeast* 22, 1155-1169.

Villas-Boas, S.G., Mas, S., Akesson, M., Smedsgaard, J., and Nielsen, J. (2005b). Mass spectrometry in metabolome analysis. *Mass Spectrometry Reviews* 24, 613-646.

Visser, D., van Zuylen, G.A., van Dam, J.C., Oudshoorn, A., Eman, M.R., Ras, C., van Gulik, W.M., Frank, J., van Dedem, G.W.K., and Heijnen, J.J. (2002). Rapid sampling for analysis of in vivo kinetics using the BioScope: A system for continuous-pulse experiments. *Biotechnology and Bioengineering* 79, 674-681.

von Baum, H., and Marre, R. (2005). Antimicrobial resistance of *Escherichia coli* and therapeutic implications. *International Journal of Medical Microbiology* 295, 503-511.

Weljie, A.M., Newton, J., Mercier, P., Carlson, E., and Slupsky, C.M. (2006). Targeted profiling: quantitative analysis of ¹H NMR metabolomics data. *Analytical Chemistry* 78, 4430-4442.

Weuster-Botz, D. (1997). Sampling tube device for monitoring intracellular metabolite dynamics. *Analytical Biochemistry* 246, 225-233.

Wick, L.M., Quadroni, M., and Egli, T. (2001). Short- and long-term changes in proteome composition and kinetic properties in a culture of *Escherichia coli* during transition from glucose-excess to glucose-limited growth conditions in continuous culture and vice versa. *Environmental Microbiology* 3, 588-599.

Williamson, M.P. (2011). How Proteins Work, Garland Science, Chapter 9.4

Wills, C., Martin, T. and Melham, T. (1986). Effect on gluconeogenesis of mutants blocking two mitochondrial transport systems in the yeast *Saccharomyces cerevisiae*. *Archives of Biochemistry and Biophysics* 246, 306-320.

Wilson, I.D., Plumb, R., Granger, J., Major, H., Williams, R. and Lenz, E.M. (2005). HPLC-MS-based methods for the study of metabolomics. *Journal of Chromatography B* 817, 67-76.

Winnike, J.H., Busby, M.G., Watkins, P.B. and O'Connell, T.M. (2009). Effects of a prolonged standardized diet on normalizing the human metabolome. *The American Journal of Clinical Nutrition* *90*, 1496-1501.

Winning, H., Larsen, F.H., Bro, R. and Engelsen, S.B. (2008). Quantitative analysis of NMR spectra with chemometrics. *Journal of Magnetic Resonance* *190*, 26-32.

Wishart, D.S. (2008). Quantitative metabolomics using NMR. *Trends in Analytical Chemistry* *27*, 228-237.

Wishart, D.S., Querengesser, L.M.M., Lefebvre, B.A., Epstein, N.A., Greiner, R., and Newton, J.B. (2001). Magnetic resonance diagnostics: A new technology for high-throughput clinical diagnostics. *Clinical Chemistry* *47*, 1918-1921.

Wishart, D.S., Knox, C., Guo, A.C., Eisner, R., Young, N., Gautam, B., Hau, D.D., Psychogios, N., Dong, E. and Bouatra, S. (2009). HMDB: a knowledgebase for the human metabolome. *Nucleic Acid Research* *37*, D603-D610.

Wishart, D.S., Jewison, T., Guo, A.C., Wilson, M., Knox, C., Liu, Y., Djoumbou, Y., Mandal, R., Aziat, F., Dong, E., Bouatra, S., Sinelnikov, I., Arndt, D., Xia, J., Liu, P., Yallou, F., Bjorn Dahl, T., Perez-Pineiro, R., Eisner, R., Allen, F., Neveu, V., Greiner, R. and Scalbert, A. (2013). HMDB 3.0- The human metabolome database in 2013. *Nucleic Acid Research* *41*, D801-807.

Wittmann, C., Kromer, J.O., Kiefer, P., Binz, T., and Heinzle, E. (2004). Impact of the cold shock phenomenon on quantification of intracellular metabolites in bacteria. *Analytical Biochemistry* *327*, 135-139.

Xie, G., Zhang, S., Zheng, X. and Jia, W. (2013). Metabolomics approaches for characterizing metabolic interactions between host and its commensal microbes. *Electrophoresis* *35*, 1-46

Yang, A.J., Chandswangbhuvana, D., Shu, T., Henschen, A., and Glabe, C.G. (1999). Intracellular accumulation of insoluble, newly synthesized A β n-42 in amyloid precursor protein-transfected cells that have been treated with a A β 1-42. *Journal of Biological Chemistry* 274, 20650-20656.

Yang, Y.T., Bennett, G.N., and San, K.Y. (2001). The effects of feed and intracellular pyruvate levels on the redistribution of metabolic fluxes in *Escherichia coli*. *Metabolic Engineering* 3, 115-123.

Yeom, J., Shin, J-H., Yang, J-Y., Kim, J. and Hwang, G-S. (2013). ¹H NMR based metabolite profiling of planktonic and biofilm cells in *Acinetobacter baumannii* 1656-1662. *PLoS ONE* 6, e57730.

Yu, D., Ellis, H.M., Lee, E.C., Jenkins, N.A. and Copeland, N.G. (2000). An efficient recombination system for chromosome engineering in *Escherichia coli*. *Proceedings of National Academy of Science USA* 97, 5978-5983.

Yu, D., Sawitzke, J.A., Ellis, H. and Court, D.L. (2003). Recombineering with overlapping single-stranded DNA oligonucleotides: testing a recombination intermediate. *Proceedings of National Academy of Science USA* 100, 7207-7212.

Yukihira, D., Miura, D., Saito, K., Takahashi, K., and Wariishi, H. (2010). MALDI-MS-based high-throughput metabolite analysis for intracellular metabolic dynamics. *Analytical Chemistry* 82, 4278-4282.

Zamboni, N., Fendt, S-M., Rühl, M. and Sauer, U. (2009). ¹³C-based metabolic flux analysis. *Nature Protocols* 4, 878-892.

Zhang, Y., Buccholz, F., Muyrers, J.P. and Stewart, A.F. (1998). A new logic for DNA engineering using recombination in *Escherichia coli*. *Nature Biotechnology* 18, 1314-1317.

Zhang, F., Bruschweiler-Li, L. and Brüschweiler, R. (2012). High-resolution homonuclear 2D NMR of carbon-13 enriched metabolites and their mixtures. *Journal of Magnetic Resonances* 225, 10-13.

Zhu, H., Bilgin, M., Bangham, R., Hall, D., Casamayor, A., Bertone, P., Lan, N., Jansen, R., Bidlingmaier, S., Houfek, T., et al. (2001). Global analysis of protein activities using proteome chips. *Science* 293, 2101-2105.

Zhu, J.F., and Shimizu, K. (2005). Effect of a single-gene knockout on the metabolic regulation in *Escherichia coli* for D-lactate production under microaerobic condition. *Metabolic Engineering* 7, 104-115.